NASA CR-170399

Analysis of Pilot Control Strategy

Robert K. Heffley, Gregory D. Hanson, Wayne F. Jewell, and Warren F. Clement

Contract NAS4-2941
April 1983

National Aeronautics and
Space Administration

NASA CR-170399

Analysis of Pilot Control Strategy

Robert K. Heffley, Gregory D. Hanson, Wayne F. Jewell, and Warren F. Clement
Systems Technology, Inc., Mountain View, California 94043

Prepared for
Ames Research Center
Dryden Flight Research Facility
under Contract NAS4-2941

1983

National Aeronautics and
Space Administration
Ames Research Center
Dryden Flight Research Facility
Edwards, California 93523

Use of trade names or names of manufacturers in this report does not constitute an official endorsement of such products or manufacturers, either expressed or implied, by the National Aeronautics and Space Administration.

FOREWORD

This project was sponsored by the National Aeronautics and Space Administration (NASA) Dryden Flight Research Facility (DFRF) at Edwards Air Force Base, California, under Contract NAS4-2941. The NASA contract technical monitor was Ms. Mary F. Shafer. The Systems Technology, Inc., (STI) project engineer was Mr. Robert K. Heffley. The work was accomplished during the period from February 1982 to September 1982.

TABLE OF CONTENTS

TABLE OF CONTENTS (Continued)

TABLE OF CONTENTS (Concluded)

LIST OF FIGURES

LIST OF FIGURES (Continued)

LIST OF FIGURES (Continued)

LIST OF FIGURES (Concluded)

LIST OF TABLES

LIST OF SYMBOLS

a	First-order lag time constant
b_1, b_2	Unknown coefficients to be determined by NIPIP
c	Sensed control action
e	Error
G_N	Neuromuscular system
g	Gravitational constant
h	Height or altitude
h_{baro}	Barometric altitude
h_c	Altitude command
h_o	Initial height during the flare maneuver
h_{ref}	Altitude reference
$\dot{h}$	Sink rate
$\dot{h}_c$	Sink rate command
$\dot{h}_o$	Initial vertical velocity during the flare maneuver
$\dot{h}_{ref}$	Sink rate reference
$\hat{\dot{h}}$	Estimated sink rate
$\ddot{h}$	Vertical acceleration
$\hat{\ddot{h}}$	Estimated vertical acceleration
$\dddot{h}$	Time derivative of vertical acceleration
i	Input
K_1, K_2	Finite difference equation gain
k	Continuous domain ngain
L_{δ_a}	Rolling moment due to aileron
ℓn	Natural logarithm

m	Output
s	Laplace transform
T	Discrete sample period
T_I	Integration time constant
T_L	Lead time constant
T_R	Roll time constant
t	Time
U	Axial velocity
V	Airspeed
V_c	Velocity command
V_{ref}	Predetermined reference speed
V_g	Ground speed
$Y_{c_{()}}$	Controlled element transfer function with respect to ()
$Y_{p_{()}}$	Pilot transfer function with respect to ()
Y_{p_e}	Human pilot
y	Lateral displacement
y_o	Initial lateral displacement
z	z-transform variable
$\dot{\delta}$	Control rate
δ_a	Aileron control
δ_e	Elevator control
δ_{e_s}	Longitudinal stick position
δ_T	Throttle control
ε	Phase plane state

$\dot{\varepsilon}$	Phase plane state rate
ε_c	Flight director command
ε_{GS}	Flight director
ε_{LOC}	Localizer
$\dot{\varepsilon}_{pk}$	Peak state rate
ε_θ	Pitch attitude error
$\dot{\varepsilon}_{td}$	Touchdown state rate
ζ	Closed loop damping ratio
ζ_a	Closed-loop damping ratio
$\hat{\zeta}_a$	Estimated closed-loop damping ratio
ζ_f	Closed-loop damping ratio during flare maneuver
θ	Pitch attitude
θ_c	Pitch attitude command
ξ	Variable of integration
ϕ	Bank angle
ϕ_c	Bank angle command
ϕ_e	Bank angle error
$\phi_{M_{FD}}$	Phase margin
ϕ_{ref}	Bank angle reference
ψ	Heading
$\dot{\psi}$	Turn rate
ψ_c	Heading command
$\dot{\psi}_c$	Turn rate command
ψ_e	Heading error

$\dot{\psi}_e$	Heading rate error
ψ_m	Perceived heading rate
ω_a	Closed-loop natural frequency
$\hat{\omega}_a$	Estimated closed-loop natural frequency
$\omega_{c_{FD}}$	Crossover frequency
ω_f	Undamped natural frequency during flare maneuver
ω_n	Undamped natural frequency

Subscripts

h	height or altitude
$\dot{h}$	Vertical velocity
v	Airspeed
y	Lateral displacement
ε	Phase plane state
θ	Pitch attitude
ϕ	Bank angle
ψ	Heading
$\dot{\psi}$	Heading rate

LIST OF ABBREVIATIONS

AFTI	Advanced Flighter Technology Integration
G/S	Glide slope
ILS	Instrument Landing System
NASA	National Aeronautics and Space Administration
NIPIP	Non-Intrusive Parameter Identification Procedure
SOP	Successive Organization of Perception

SECTION I

INTRODUCTION

A. DEVELOPMENT OF PILOT CONTROL STRATEGY IDENTIFICATION

Pilot control strategy or piloting technique refers to the manner in which the human pilot perceives and processes specific information and manipulates the aircraft controls based on that information in order to perform a given task or maneuver. The principles of manual control theory (Ref. 1) rest on the notion that, given an aircraft and a task to perform, the skilled pilot is an efficient selector and processor of available and essential information (cues), respectively. This leads to control actions by which the pilot executes a task with a defined precision in a timely and stable manner even in the presence of disturbances, interruptions, and the demands of other tasks.

It has been possible over recent years to measure how the human operator performs a task, especially where that task is well defined. For example, the single-axis tracking task with one cue and one controller inherently restricts the basic loop structure. Further, if the controlled element dynamics are essentially stationary, then a spectral treatment of the pilot's cue-control relationship is easily obtainable based on control theory in the frequency domain. In this context classical describing functions of pilot control strategy have been widely and sucessfully applied. Time domain parameter identification based on modern control theory techniques has also received substantial attention. A recent synopsis of pilot modeling approaches can be found in Ref. 2.

The pilot identification process can be generalized in the form shown in Fig. 1. The objective is to structure and quantify the human operator using available measurements of the actual operator stimuli and responses. This can be accomplished in many ways, however, using any number of combinations of the identification techniques listed in Table 1. The

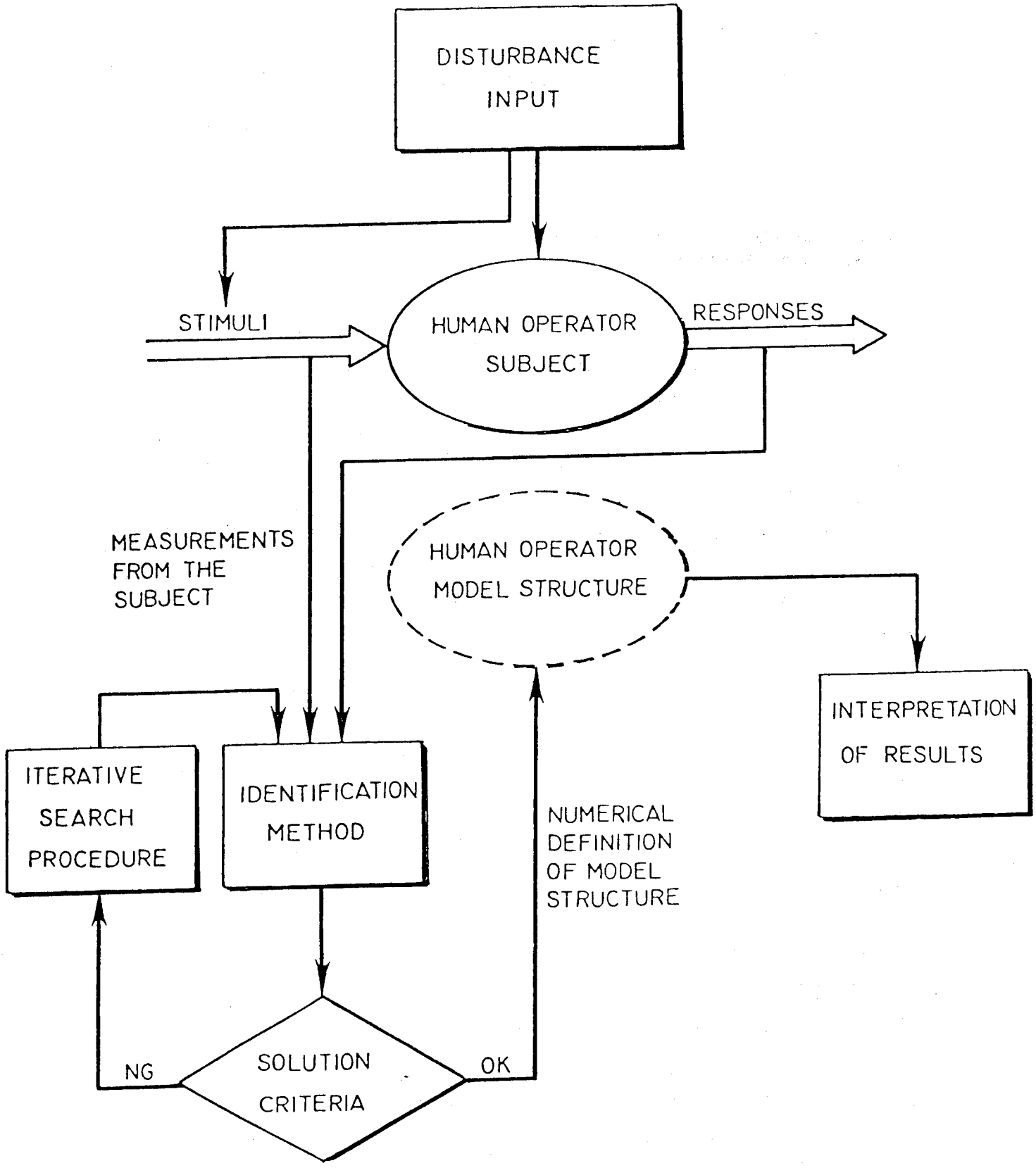

Figure 1. The Pilot Identification Process

TABLE 1

SUMMARY OF IDENTIFICATION TECHNIQUES

IDENTIFICATION METHODS

- Describing function analyzer
- Finite Fourier transform cross-spectral analysis
- Finite Fourier transform input-output analysis
- Cross-correlation analysis
- Response error
- Equation error
- Sampled-data correlation (NIPIP)

DISTURBANCE INPUTS

- Injected test inputs
  - Sum of sine waves
  - Frequency sweep
  - Pseudo-random binary
  - Random
- Existing inputs
  - Deterministic
  - Random (NIPIP)

SOLUTION CRITERIA

- Time domain
  - Maximum likelihood
  - Least squares (NIPIP)
- Frequency domain
  - Weighted least squares

SEARCH PROCEDURES

- Parallel-tangent
- Davidon-Fletcher-Powell-Levenberg
- Newton-Raphson
- Random
- Simplex
- Direct solution (NIPIP)

NIPIP approach presented in this report represents only one set of those techniques, but it is a powerful and relatively uncomplicated process.

Although the computer algorithms of NIPIP are fairly simple, the real challenge lies in developing the assumed form of structure of the pilot control strategy which is to be fitted to the data. This consists of defining a finite difference equation which is linear with respect to unknown parameters. While this is partly an art at this stage, a practical working knowledge of manual control theory is a valuable aid in obtaining successful results.

B. OBJECTIVES OF THIS STUDY

The main objectives of the study described herein were to develop, implement, and demonstrate NIPIP software for NASA Dryden Flight Research Facility. Several examples of existing F-8 digital fly-by-wire flight data were treated to serve as a guide to the pilot control strategy analysis process. Additionally, applications to a future aircraft flight program, the AFTI/F-16, were discussed. Recommendations were then developed regarding a future addition of interactive computer graphics to NIPIP.

SECTION II

IDENTIFICATION OF PILOT CONTROL STRATEGY

The purpose of this section is to provide the reader with a pragmatic perspective for characterizing and identifying pilot control strategy. This process cannot yet be done entirely automatically either through the use of NIPIP or any other parameter identification algorithm. Rather the analyst must apply his or her own skills and experience in discovering and quantifying the particular control strategy employed by the pilot. It is essential to exploit systematically all the resources at hand in this exercise.

A. TASK MODELS AND PILOT MODELS

It is necessary to distinguish the dynamics associated with the execution of a task from those of the pilot, per se. The task model includes the total maneuver specification, command inputs, inanimate parts of the outer or task loop structure, and the overall closed-loop response of the pilot-vehicle combination as well as the effect of any environmental disturbances such as gusts. The pilot model is an element in that chain which includes the cue-control loop structure which we call piloting technique and the perceptual features associated with the pilot. These distinctions are shown in Fig. 2.

It has been found that pilot control strategy identification is usually a multistep process. It is necessary to understand first the overall piloting task then to hypothesize the form or structure of the pilot's control strategy commencing with the exterior pilot control loops and progressing to the interior ones. Indispensable to this progression is a thorough knowledge of the vehicle dynamics. This general analytical procedure will be demonstrated in the several examples to be presented shortly.

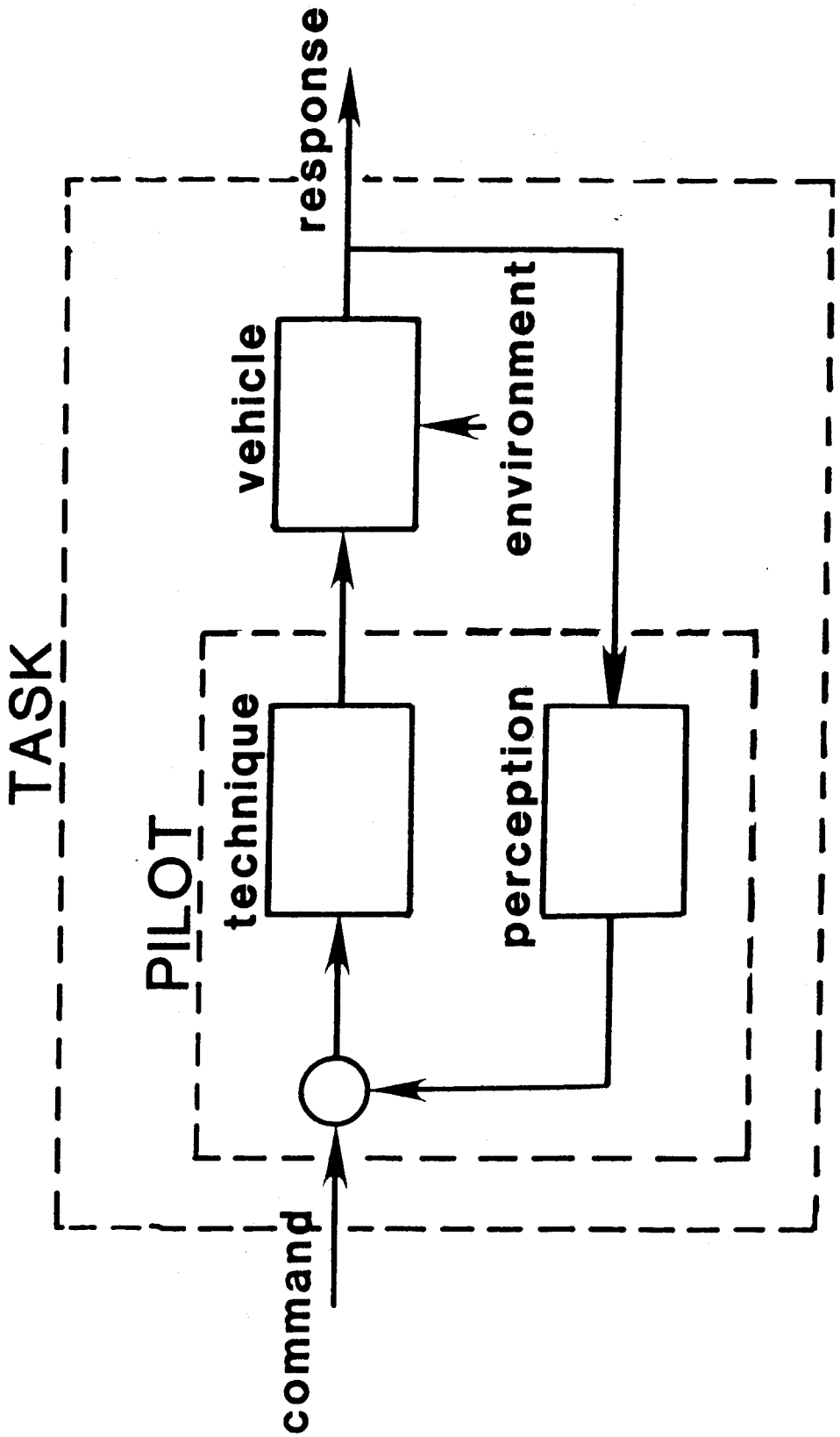

Figure 2. Block Diagram of Pilot-Vehicle-Task System

B. TRACKING TASKS AND DISCRETE MANEUVERS

There are two main kinds of piloting tasks to which NIPIP has been applied: tracking tasks and discrete maneuvers. In general both varieties can be expected to be involved in any piloting situation or flight phase. For example, a landing flare is itself a discrete maneuver, but the pilot's inner-loop regulation of pitch is a kind of tracking task. A change of heading is a discrete maneuver with respect to heading control, but there is also an inner-loop bank-angle tracking task involved in supporting the heading change. However the outer loop is not always a discrete maneuver. For example, tracking an ILS glide slope is an outer-loop tracking task. If flaps are selected upon intersecting the glide slope and initiating the descent, the flap selection could be considered as an "inner loop" discrete task. Clearly each case needs to be considered individually; nevertheless, we shall try to be as general as possible.

In dealing with either tracking tasks or discrete maneuvers, it is useful to concentrate first on the task model. If the task model can be quantified adequately, then the pilot aspects, per se, can be addressed.

C. EXAMPLES OF TRACKING TASKS

Tracking tasks generally involve a fairly self-evident control strategy, at least on a compensatory level. There is normally a well-defined command input-referenced error signal and cockpit controller. For example, maintenance of airspeed involves a predetermined reference speed, V_{ref}, and a prescribed means of adjusting speed, usually either throttle or pitch attitude. Maintaining V_{ref} is normally a fairly long-term job, and it is likely that several oscillations about V_{ref} would be observed during a sampled interval of the task execution. In contrast, a discrete speed change maneuver involves the step application of a new, significantly different value of V_{ref} and the speed transient and the settling to a new speed.

Tracking tasks can be divided into explicit and implicit varieties. The explicit tracking task is one in which the error signal is an obvious presentation. Examples include gunsight pipper errors, regulation about a desired airspeed, heading, course, flight path angle, glide slope, or altitude. Some block diagrams of explicit tracking tasks with undetermined pilot describing functions are shown in Fig. 3.

The implicit tracking tasks are ones in which an outer control loop supplies the command signal, an artificial construct which is itself continually varying. Examples would include the "tracking" of pitch and roll in order to support such outer loop tasks as steady regulation of or discrete changes in altitude or heading. Some block diagrams of implicit tracking tasks with undetermined pilot describing functions are shown in Fig. 4. Such implicit tracking tasks will be addressed in some of the examples to follow.

The pilot may use more characteristic intervals of distance (wavelengths of motion) or time (natural periods of motion) to null the error signal in performing a tracking task than for a discrete maneuver. Consequently tracking tasks are sometimes characterized by lower phase margin (lower closed-loop damping ratio) than are discrete maneuvers. Both types of tasks, however, are characterized by a bandwidth commensurate with the task and vehicle dynamics.

D. DEFINITION OF A DISCRETE MANEUVER

Several examples of discrete maneuvers have been cited, such as commanded changes in heading, altitude, speed, or position. In each case it is the "transitory" nature of a discrete maneuver which distinguishes it from the "steady-state" quality of a tracking task. A simple heading change in cruising flight is a discrete occurrence in terms of the decision to turn, initiation of the command, the turn itself, and the eventual settling on to the new heading. Beyond a certain point, though,

a. Speed

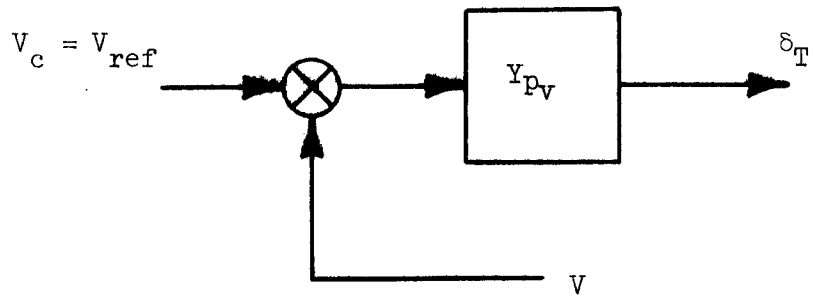

b. Glide Slope Displacement or Flight Director

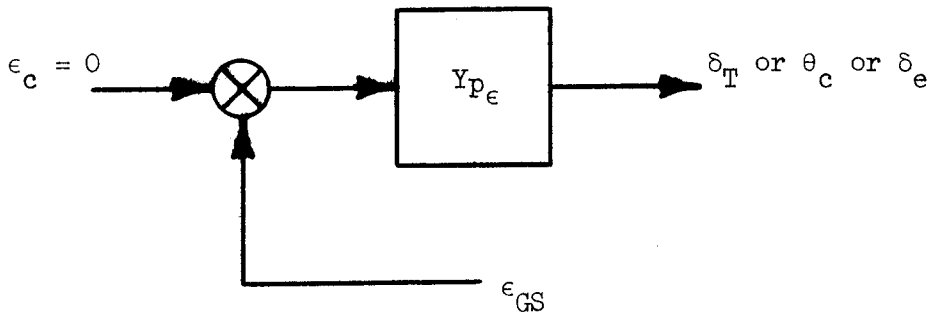

c. Bank Angle

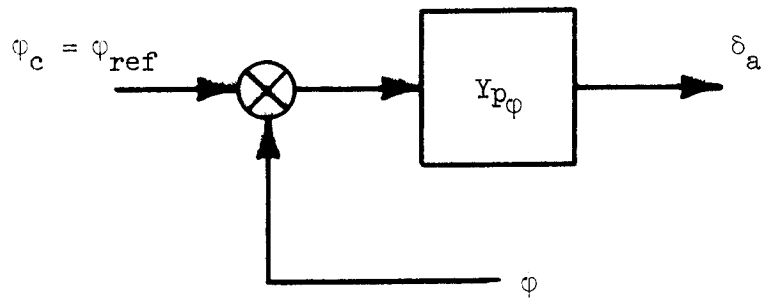

Note: Explicit tracking task commands are a clearly definable cue or instrument quantity

Figure 3. Examples of Explicit Tracking Tasks

a. Height via Pitch Attitude

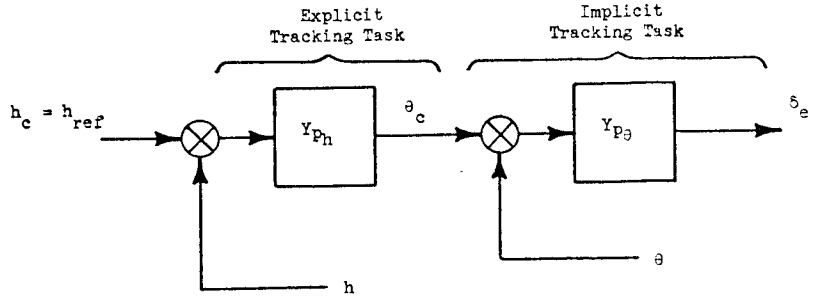

b. Localizer Displacement via Bank Angle

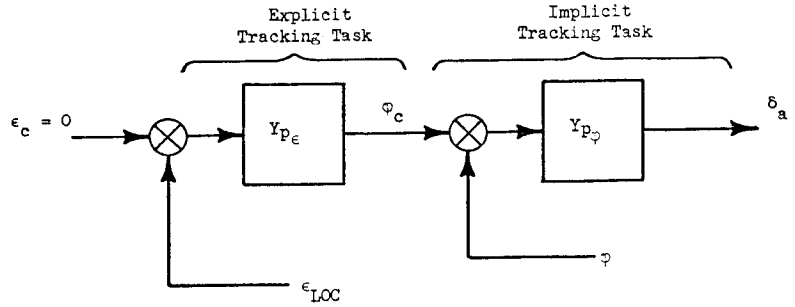

c. Heading or Course Angle via Bank Angle

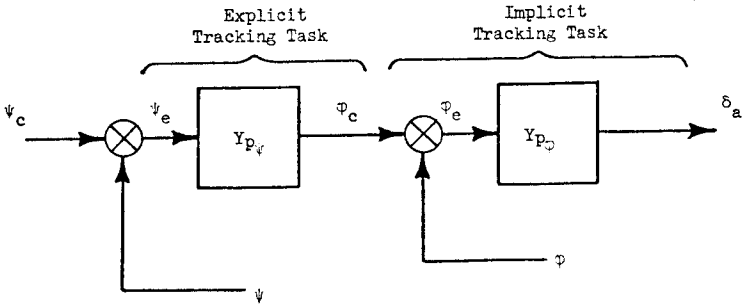

d. Localizer Displacement via Heading and Bank Angle

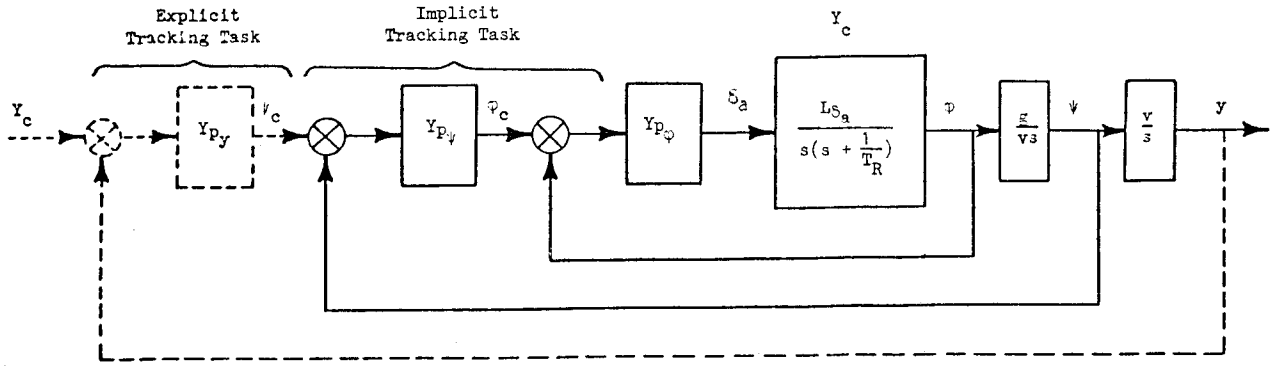

Note: Implicit tracking task commands are based on the control strategy output from an exterior loop, an artificial, pilot-derived relationship not directly measurable.

Figure 4. Examples of Implicit Tracking Tasks

regulation of that new heading becomes equivalent to a steady-state tracking task, and there may not necessarily be a precise boundary separating the short-term discrete task and the longer-term regulatory task.

One useful definition for a discrete maneuver is simply the limited-term transition from one tracking task to another. Thus a heading change would be the transition from holding one heading to holding another, or a decelerating approach to hover would be the transition from holding a steady approach speed to maintaining a steady hover over the landing area.

In the following pages the transitory aspect of the discrete manuever will be quantified in terms of specific mathematical models and the parameters associated with those models.

E. DISCRETE MANEUVER MODELS

A reasonable mathematical model of the discrete maneuver can be obtained by direct transient response analysis methods. That is, a characteristic equation can be evaluated starting with a set of initial conditions and the commands appropriate to the final condition. The first step is to obtain a reasonable estimate of the closed-loop response type. One method by which this can be accomplished is through the use of phase plane analysis. For example, a first-order dominant mode can be distinguished from a second-order one depending upon the relative curvature of the trajectory. (Various texts can be consulted for an in-depth treatment of phase plane analysis, e.g., Refs. 3 or 4.) Reference 5 describes how pilot training manuals can be exploited to obtain estimates of the discrete maneuver dynamics.

F. AN EXAMPLE OF TOOLS FOR ANALYZING DISCRETE MANUEVER TASK DYNAMICS

In the course of analyzing various discrete maneuvers, it has been found that identification of the dominant closed-loop response mode is

useful. However, as the definition of a discrete maneuver implies, the discrete maneuver is transient. The predominant response mode may appear for only a fraction of its effective wavelength, period, or characteristic time interval.

One technique for identifying a mode during a limited interval is to use a phase plane trajectory, i.e., a plot of rate versus displacement of a given state. The particular state to be considered is that of the discrete command. For example, in a heading change maneuver, one would choose to inspect heading rate plotted against heading displacement; for hover position, closure rate versus range; or for altitude change, vertical velocity versus height. Examples of such command-loop phase planes are presented in the following pages.

For a second-order response, the closed-loop damping ratio, ζ, and undamped natural frequency, ω_n, can be found using rigorous parameter identification procedures; however, even simple phase plane estimation methods work well. The sketch in Fig. 5 outlines one technique that has been found particularly useful for a variety of discrete maneuvers. Thus the undamped natural frequency can be extracted from the aspect ratio of the phase plane. A large number of landing maneuvers were so analyzed in Ref. 6.

Here we shall summarize an example of a discrete maneuver which illustrates aspects of the general closed-loop analysis technique.

Consider the landing flare maneuver. First, based on observation of the closed-loop dynamics, the basic response appears to be second order--a damped sinusoid. Figure 6 is a sample of a landing phase-plane which illustrates the second-order-like behavior, at least during the latter portion of the trajectory. Hence a second-order transient response starting with a given height and sink rate should yield a comparable phase plane. If the second-order characteristic equation is assumed to be $\ddot{h} + 2\zeta_f\omega_f\dot{h} + \omega_f^2 h = 0$, then the Laplace transform can be written as

$$\left(s^2 + 2\zeta_f\omega_f s + \omega_f^2\right) h(s) = \left(s + 2\zeta_f\omega_f\right) h_o + \dot{h}_o \qquad (1)$$

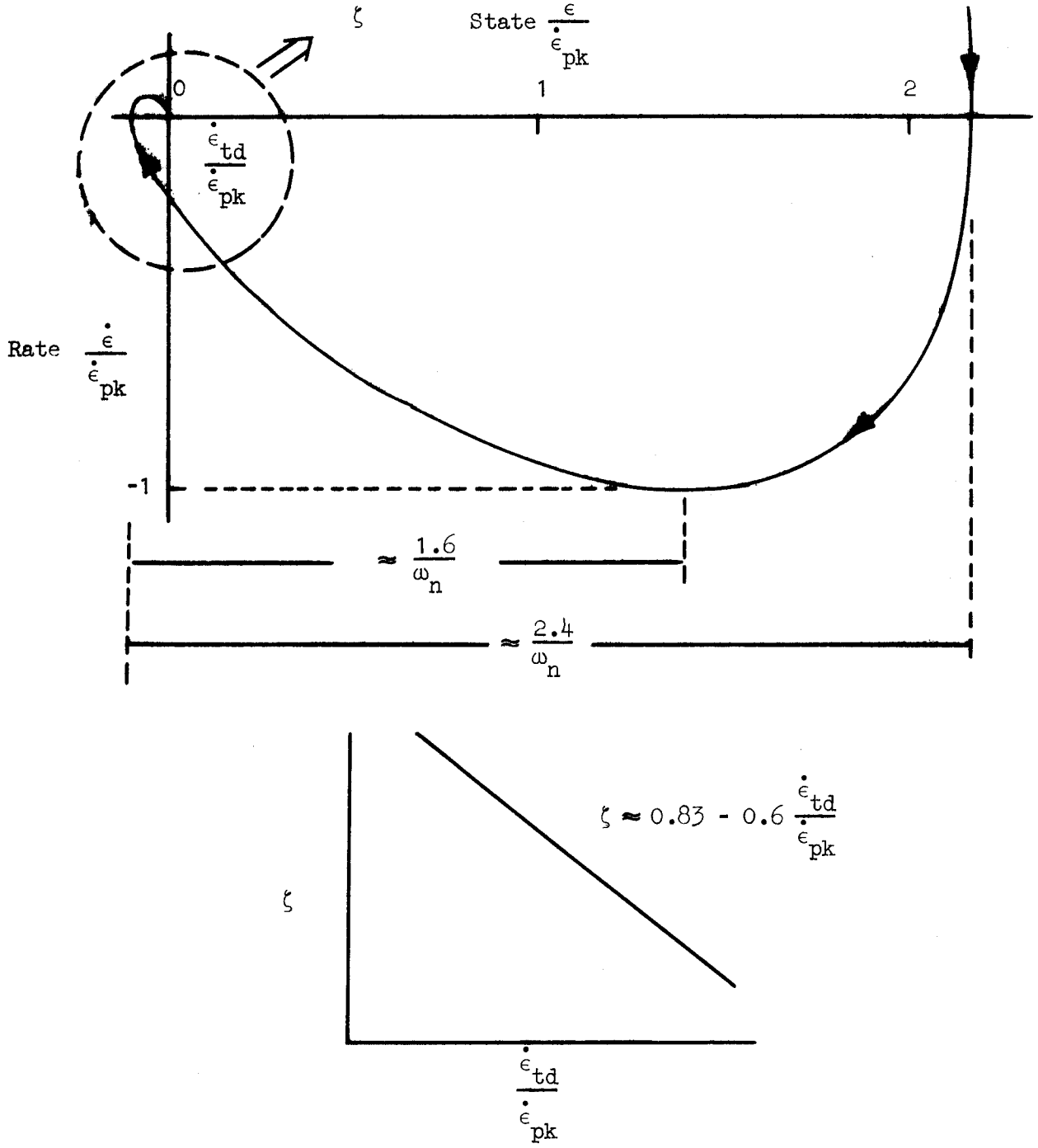

Figure 5. Normalized Phase Plane and Relationships for Extracting Closed-Loop Damping Ratio and Undamped Natural Frequency

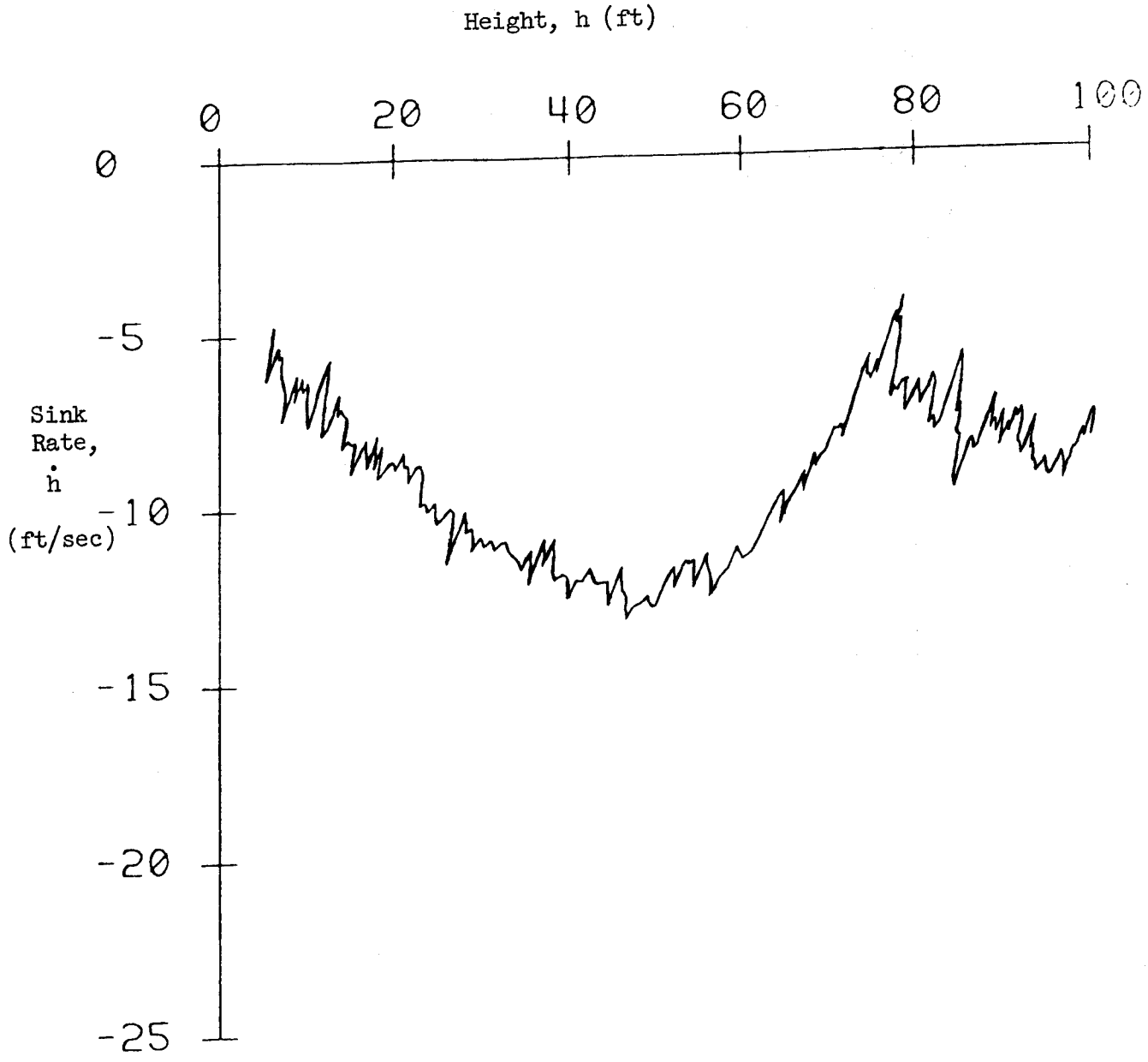

Figure 6. Sample Landing Phase Plane Trajectory

where h_o and $\dot{h}_o$ are the initial height and vertical velocity during the flare maneuver. Thus a family of general solutions could be constructed from the parameters ζ_f and ω_f and particularized using h_o and $\dot{h}_o$. The appropriate command for height would presumably be zero, and this does appear to agree with comparisons of the above model to actual flight data. An example of a DC-10 landing with the matched second-order model parameters is shown in Fig. 7.

For the DC-10 landing flare, it was found in Ref. 6 that a fairly large sample of pilots preferred a closed-loop damping ratio of about 0.7 ± 0.1 and a closed-loop natural frequency of about 0.4 ± 0.1 rad/sec. It should be noted that a closed-loop response with these properties tends to provide consistently good decay of sink rate from a wide range of initial conditions, from off-nominal aircraft flight conditions, or from a variation in flare maneuver aggressiveness.

If the closed-loop response can be evaluated as shown above, then it may be possible to deduce something about the pilot control strategy and the perceptual pathways. In Ref. 6 it was shown that the combined pilot-vehicle system during landing has the general properties of a lag-lead network. Further, using ensemble landing data and knowledge of the aircraft flight path dynamics, one can deduce the use of lead-compensated height variation and the existence of a significant lag or decay in addition to the airframe flight path lag.

A general effective lag-lead pilot-vehicle form for the landing maneuver is shown in Fig. 8. Assumption of such a form can be based on knowledge of the vehicle flight path dynamics and the deduction that the rate feedback or its equivalent must be involved to explain the relatively large amount of closed-loop damping. By expanding the closed-loop characteristic equation for this feedback system, the open-loop parameters T_L and T_I can be related to the closed-loop parameters ζ_f and ω_f in the following manner:

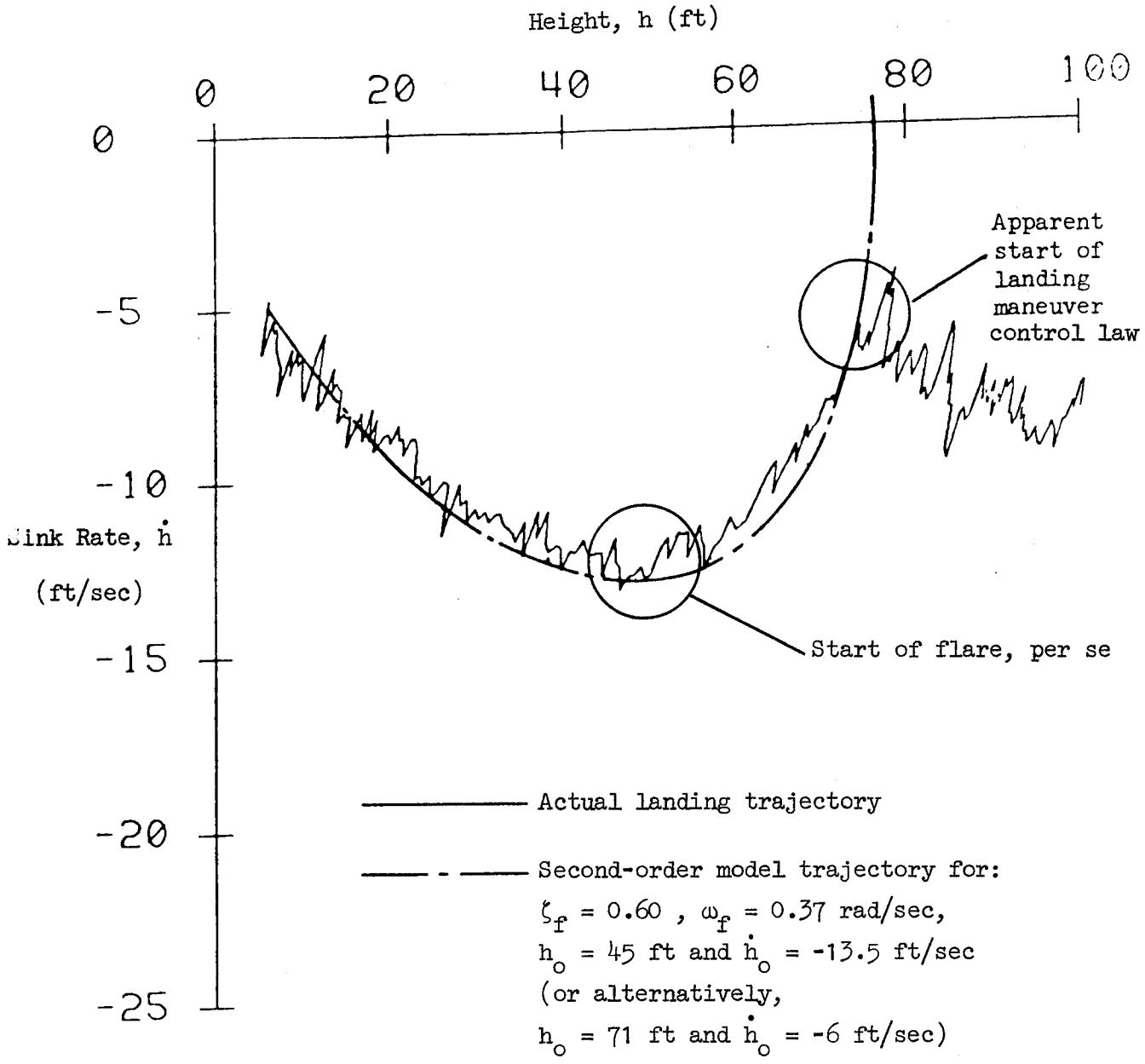

Figure 7. Typical Landing Maneuver Performed in the Actual Aircraft

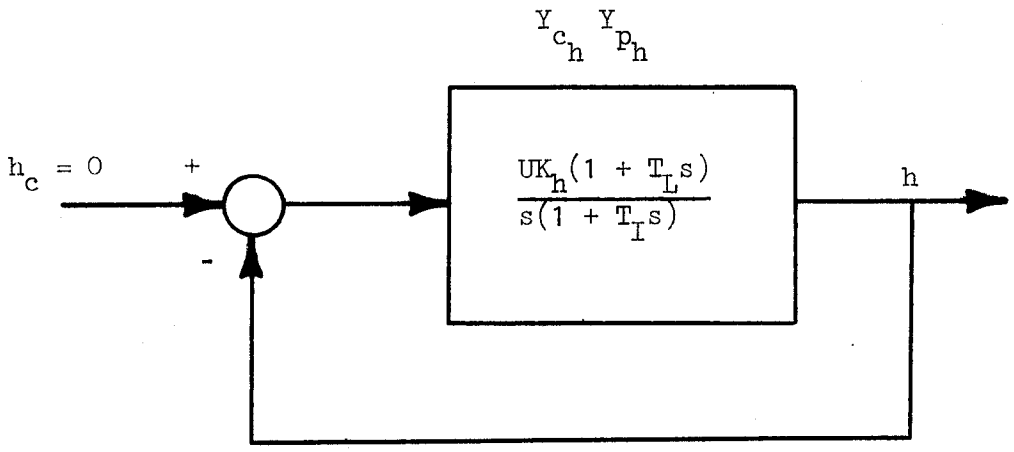

Figure 8. Block Diagram of Equivalent Pilot-Vehicle System for Flare

$$1 + Y_{p_h} Y_{c_h} = s^2 + \frac{1}{T_I}\left(1 + UK_h T_L\right)s + \frac{UK_h}{T_I} = s^2 + 2\zeta_f \omega_f + \omega_f^2 = 0 \tag{2}$$

or

$$2\zeta_f \omega_f = \frac{1}{T_I} + \omega_f^2 \, T_L \tag{3}$$

Hence, if true lead compensation were involved in a fixed amount even for varying pilot gain, there should be a trend in ensemble landing data suggested by the latter equation, namely, ensemble landing data, when plotted in terms of $2\zeta_f\omega_f$ versus ω_f^2, should have a slope equal to T_L and an intercept equal to $1/T_I$ as shown in Fig. 9. Such was shown to be the case in Ref. 6. In fact a more detailed analysis based on this concept was conducted resulting in the suggestion of lead higher than first order (perhaps involving vestibular as well as visual feedback) and the indication of a substantial lag or delay beyond that of just the airframe and closed-loop pitch response. For actual landings, this lag was not detrimental, but for simulator landings it was excessive and could be used to explain the tendency for hard landings. Thus this analysis procedure permitted an assessment of simulator fidelity and even training effectiveness of the simulator through direct comparison of simulator landings with those made in the actual aircraft.

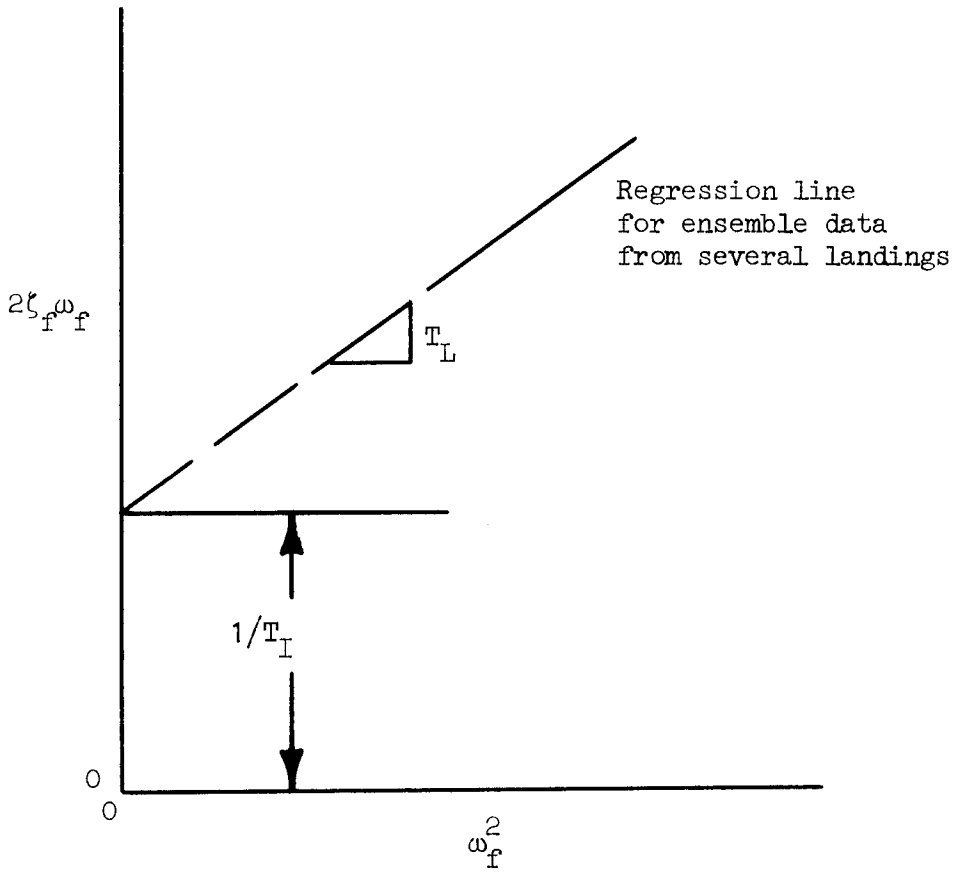

Figure 9. Regression Line Analysis Scheme
for Ensemble Landing Data

SECTION III

APPLICATION OF ANALYSIS TOOLS

It is assumed that the reader has available the NIPIP user's guide (Ref. 7) and is familiar with Section II, Background and Theory of Operation. Therefore the description of procedures which follows will not require lengthy or rigorous treatment. The main goal is to provide some ideas for applying analysis tools either in an exploratory fashion to increase insight and understanding or in a more deliberate data analysis mode in which an accepted model form is refined and finally quantified.

The various features of pilot control strategy that need to be considered and which should be eventually quantified are listed in Table 2. In fact, the specific objective of this section is to discuss how each can be addressed via NIPIP.

A. HYPOTHESIS OF GENERAL LOOP STRUCTURE

Effective quantitative identification of pilot control strategy requires some degree of understanding of the basic flight task or maneuver. A written description may be available from training manuals or flight test reports, or an oral pilot commentary can be useful. References 2 and 5 illustrate how training materials can be literally interpreted, not only to obtain structural descriptions of the essential cues and feedbacks for the task but in some cases to solve directly for pilot control strategy gains.

The chief feature of the general loop structure is the command loop state variable, the cue which forms the outermost feedback control loop.

TABLE 2

QUANTIFIABLE FEATURES OF PILOTING TECHNIQUE

Loop structure in terms of essential cues and feedbacks

Logical switching points or criteria

Loop gains

Loop compensation

Time or spatial dependence

Sampling or discrete control strategy

Successive organization of perception (SOP) stage

Closed-loop pilot-vehicle response

In many tasks the command loop state variable is obvious from the task description:

Task	Command Loop State Variable
Heading change, regulation	Heading, ψ
Altitude change, regulation	Altitude, h
Airspeed change, regulation	Airspeed, V
Straight and level flight	Heading (lateral-directional axes) and altitude (longitudinal axis)

In some tasks, especially those involving outside visual reference, the command loop state variable is less clear. For example, in a visual approach the pilot may be using a complex, ill-defined geometric construct based on his perspective view of the airport area. Nevertheless this could be approximated by a simple glide-slope-like parameter for the purpose of quantifying control strategy. That is to say, we may not know the exact way in which a pilot derives visual or motion state information, but we can assume that the cue is essentially equivalent to the corresponding true state. The perceptual distortion of the true state can always be added to the control law if the distortion is sufficiently known.

Clues to the nature of the loop structure can be obtained from the closed-loop task execution response. For example, active flight path regulation correlated with altitude suggests the presence of an altitude feedback. Further strong damping with respect to altitude would suggest either vertical velocity feedback or its equivalent. Thus candidate loop structure configurations can be developed by deductive reasoning based on manual control theory fundamentals coupled with a mathematical model of the aircraft and the task. This deductive approach has been described in Ref. 8.

It is fair to point out that at some stage of loop structure hypothesizing, the analyst is likely to be faced with a level of ambiguity among candidates. This ambiguity may be resolvable with further data analysis.

B. LOGICAL SWITCHING POINTS OR CRITERIA FOR STRUCTURE ADJUSTMENT

It is normal to encounter changes in the basic task loop structure which are a function of control or state nonlinearities, the pilot switching to other tasks, or a change in the operating environment. Such changes in loop structure cannot be ignored when using an identification scheme such as NIPIP because of the hazard in applying an invalid model form to identify a portion of flight data. This is, in fact, one of the major hurdles to creating a truly automatic pilot control strategy identification scheme.

Some examples of logical switching points are given in Ref. 5 for turns and altitude changes. If a pilot chooses to change heading more than, say, 30 deg, it would be common to observe a steady turn rate limit (or a bank angle limit) until reaching a heading sufficiently close to that desired. Then the pilot would roll out of the turn with a loop closed on heading, per se. Figure 10 summarizes the phase plane of such action.

For the above maneuver the pilot's decision to turn or roll out is represented by a logical switch which transitions the loop structure from a constant bank angle command to a heading feedback as shown in Fig. 11. The decision or switching logic is represented by a function of heading error, designated as $f(\psi_e)$. According to one widely accepted rule of thumb (Ref. 9), that switch in technique would occur when the heading error reaches one third (or one half) the steady bank angle. For example for a 30-deg banked turn, the pilot might begin to roll out 10 deg before the desired new heading. This would then be a guide to identifying the end of the turn maneuver. One would then apply NIPIP first to the steady turn with the bank angle control loop structure shown previously in

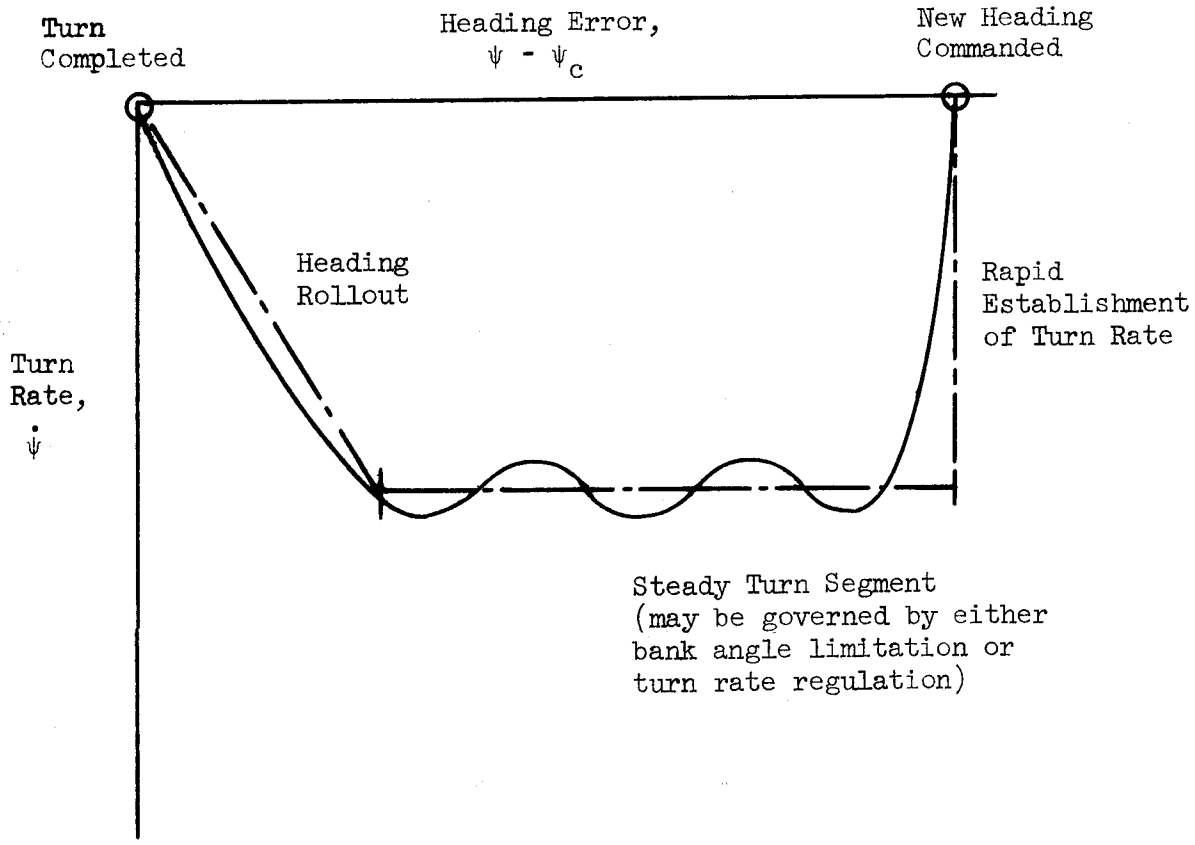

Figure 10. Large Amplitude Heading Change Maneuver

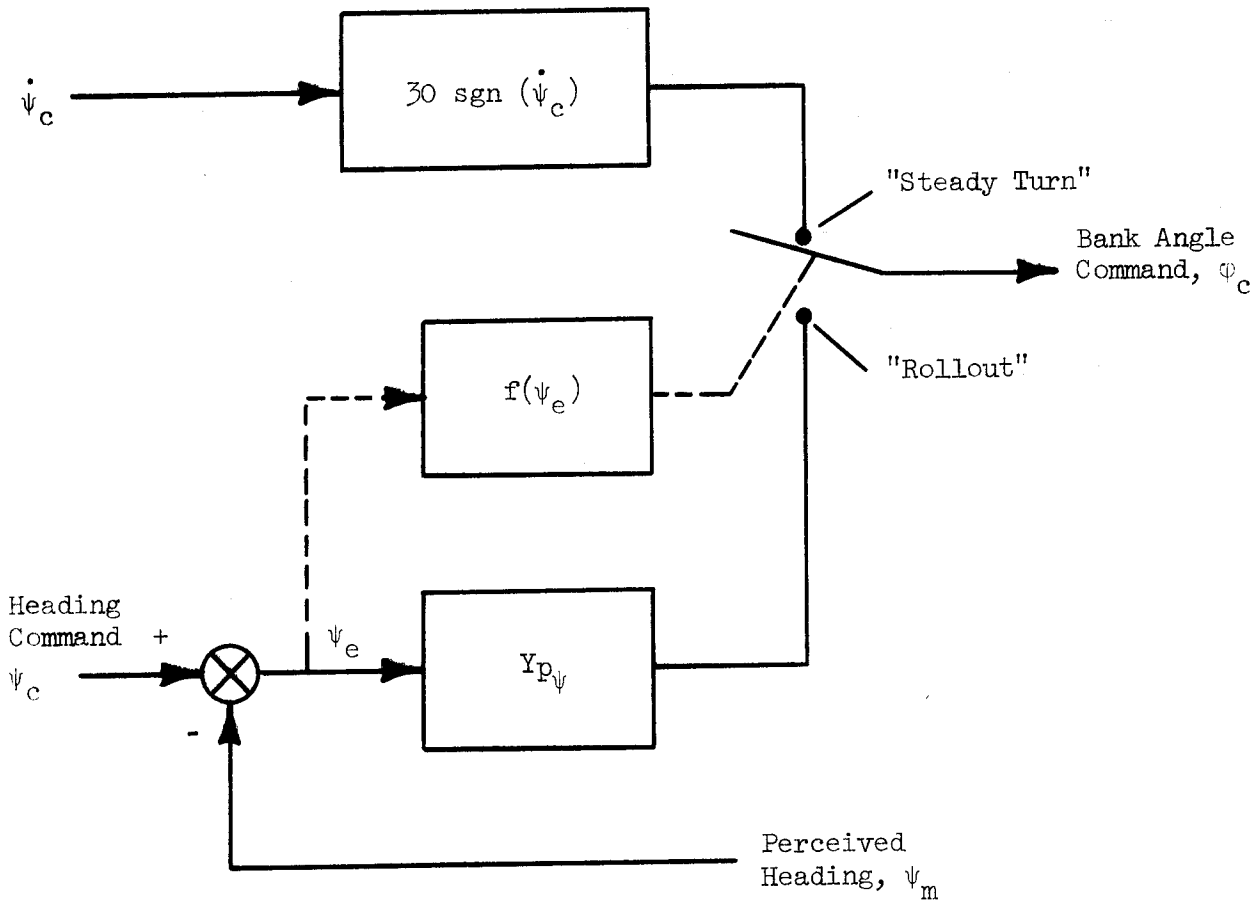

Figure 11. Pilot's Control Loop Structure for Changing Heading with a Constant Bank Angle Command of 30 Degrees

Fig. 3(c) and, second, to the rollout with the loop structure shown in Fig. 12.

Alternatively, if the pilot chooses to change heading by regulating turn rate, as in the case of making a standard rate turn by observing the turn rate needle, the constant 30 deg bank angle command of Fig. 11 would not necessarily apply, especially if the speed were varying substantially. Instead one would apply NIPIP first to the steady turn, with the turn rate control loop structure shown in Fig. 13; then, second, to the rollout with the loop structure shown in Fig. 12.

C. INTERPRETATION OF LOOP GAINS AND COMPENSATION

The identification of pilot gains and compensation can be done fairly explicitly with NIPIP, regardless of whether the hypothetical loop structure for the piloting technique involves nearly periodic sampling operations which can be reflected explicitly in the identification process (see Topic E, following) or nearly continuous operations which can be approximated by a very short sampling interval in the identification process. An example of speed regulation technique via throttle control [Fig. 3(a) herein] was identified using a sampling strategy in Ref. 10, whereas an example of flight director regulation via column control [Fig. 3(b) herein] in the same reference was identified using a continuous control strategy. Usually the unknowns to be solved (the $\hat{c}$ matrix in the user's guide, Ref. 7) can represent continuous feedback gains, or they can be interpreted in terms of effective lead or lag compensation.

In some cases it is desirable to interpret the finite difference equation, as solved by NIPIP, in the continuous domain, because the user may be more familiar with forms of compensation in the continuous domain. For example:

$$\delta(n) = k_1 \delta(n-1) + k_2 \theta(n-1) \qquad (4)$$

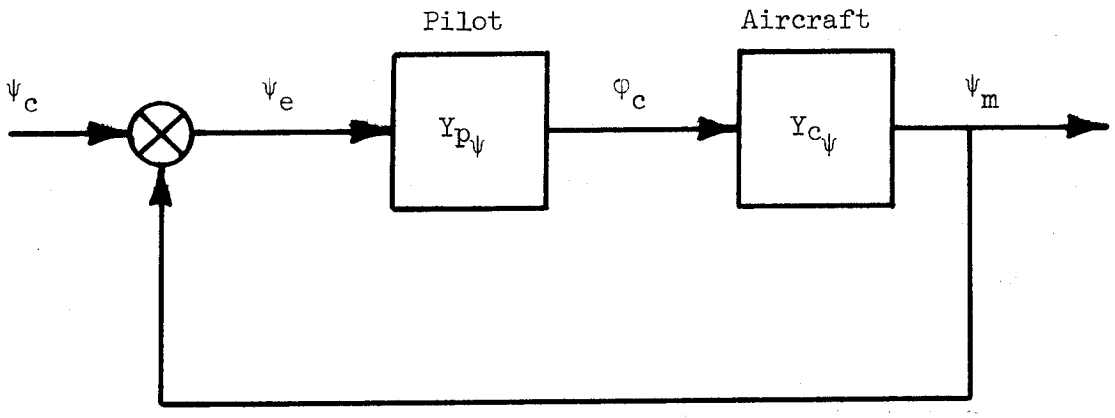

Figure 12. Loop Structure for Rolling Out of a Turn and Holding Heading

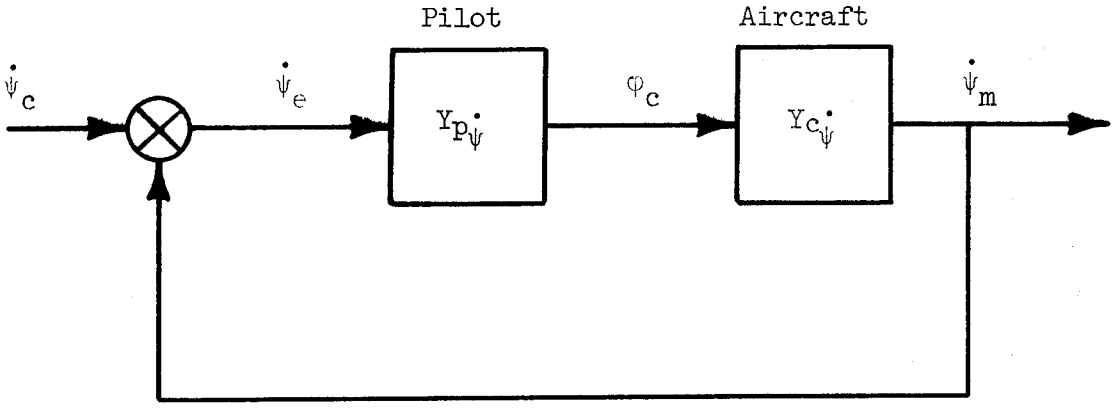

Figure 13. Steady Turning Loop Structure for Turn Rate Regulation

can be legitimately interpreted as a first-order lag if k_1 has a value between zero and one. If translated using an inverse z-transform,

$$\delta(z)\left(1 - e^{-aT}z^{-1}\right) = \theta(z)\, k\left(1 - e^{-aT}\right) z^{-1} \qquad (5)$$

Corresponds to

$$\dot{\delta} = -a\delta - ka\theta \qquad (6)$$

where

$$a = -\frac{1}{T} \ln k_1 \qquad (7)$$

and

$$k = \frac{k_2}{1 - k_1} \qquad (8)$$

These results are not exact, however, since there is not a one-to-one correspondence between the continuous and discrete domains. Several other transformation methods could be applied with about equal accuracy. Table 3 shows a number of such transformations for a first-order lag. Similar sets could be derived for higher order continuous systems.

TABLE 3

EXAMPLES OF FINITE DIFFERENCE EQUATIONS
APPROXIMATING A FIRST-ORDER CONTINUOUS LAG

DIFFERENTIAL EQUATION

$$\dot{x} = -ax + au$$

LAPLACE TRANSFORM

$$\frac{x(s)}{u(s)} = \frac{a}{s + a} = \frac{1}{1 + s/a}$$

FINITE DIFFERENCE EQUATION APPROXIMATIONS

1. Direct z-Transform

$$\frac{x(z)}{u(z)} = \frac{\left(1 - e^{-aT}\right)z^{-1}}{\left(1 - e^{-aT}z^{-1}\right)}$$

or $$x_n = e^{-aT} x_{n-1} + \left(1 - e^{-aT}\right) u_{n-1}$$

2. Tustin Transform

$$\frac{x(z)}{u(z)} = \frac{\frac{a(T/2)}{1 + a(T/2)}\left(1 + z^{-1}\right)}{1 - \frac{1 - a(T/2)}{1 + a(T/2)} z^{-1}}$$

or $$x_n = \frac{1 - a(T/2)}{1 + a(T/s)} x_{n-1} + \frac{a(T/2)}{1 + a(T/2)}\left(u_n + u_{n-1}\right)$$

3. Half-Period Advance

$$\frac{x(z)}{u(z)} = \frac{\left(1 - e^{-a(T/2)}\right) + \left(e^{-a(T/2)} - e^{-aT}\right)z^{-1}}{1 - e^{-aT}z^{-1}}$$

or $$x_n = e^{-aT}x_{n-1} + \left(1 - e^{-a(T/2)}\right) u_n + \left(e^{-a(T/2)} - e^{-aT}\right) u_{n-1}$$

TABLE 3 (Continued)

4. Difference Equation and Adams Second-Order Integration

$$\dot{x}_n = -ax_{n-1} + au_n$$

$$x_n = x_{n-1} + (T/2)\left(3\dot{x}_n - \dot{x}_{n-1}\right)$$

$$\text{or} \quad x_n = \left(1 - a(3T/2)\right)x_{n-1} - a(T/2)x_{n-2} + a(3T/2)u_n - a(T/2)u_{n-1}$$

$$\text{or} \quad \frac{x(z)}{u(z)} = \frac{a(T/2)\left(3 - z^{-1}\right)}{1 - \left(1 - a(3T/2)\right)z^{-1} - a(T/2)\, z^{-2}}$$

5. Difference Equation and Euler Integration

$$\dot{x}_n = -ax_{n-1} + au_n$$

$$x_n = x_{n-1} + T\,\dot{x}_{n-1}$$

$$\text{or} \quad x_n = x_{n-1} - aTx_{n-2} + aTu_{n-1}$$

$$\text{or} \quad \frac{x(z)}{u(z)} = \frac{aTz^{-1}}{1 - z^{-1} + aTz^{-2}}$$

6. Simultaneous Difference Equation and Adams Second-Order Integration

$$\dot{x}_n = -ax_n + au_n$$

$$x_n = x_{n-1} + (T/2)\left(3\dot{x}_n - \dot{x}_{n-1}\right)$$

$$\text{or} \quad x_n = \frac{1 + a(T/2)}{1 + a(3T/2)}\, x_{n-1} + \frac{a(3T/2)}{1 + a(3T/2)}\, u_n - \frac{a(T/2)}{1 + a(3T/2)}\, u_{n-1}$$

TABLE 3 (Continued)

7. Simultaneous Difference Equation and Euler Integration

$$\dot{x}_n = -ax_n + au_n$$

$$x_n = x_{n-1} + T\dot{x}_{n-1}$$

or $$x_n = (1 - aT)x_{n-1} + aTu_{n-1}$$

8. Simultaneous Difference Equation and Trapezoidal Integration

$$\dot{x}_n = -ax_n + au_n$$

$$x_n = x_{n-1} + T/2\ (\dot{x}_n + \dot{x}_{n-1})$$

or $$x_n = \frac{(1 - a(T/2))}{(1 + a(T/2))} x_{n-1} + \frac{a(T/2)}{1 + a(T/2)} (u_n + u_{n-1})$$

NOTE: Same as No. 2, the Tustin Transform

9. Fowler's Method with Half-Period Advance

$$\frac{x(z)}{u(z)} = \frac{(1 - e^{-(aT/2)}) + (e^{-(aT/2)} - e^{-aT})z^{-1}}{1 - e^{-aT}z^{-1}}$$

or $$x_n = e^{-aT}x_{n-1} + (1 - e^{-(aT/2)})u_n + (e^{-(aT/2)} - e^{aT})u_{n-1}$$

TABLE 3 (Concluded)

10. Fowler's Method with z-Transform Substitution

$$x_n = e^{-aT}x_{n-1} + (1 - e^{-aT})u_{n-1}$$

11. Difference Equation and Rectangular Integration

$$\dot{x}_n = -ax_{n-1} + au_n$$

$$x_n = x_{n-1} + T\dot{x}_n$$

or $$x_n = (1 - aT)x_{n-1} + aTu_n$$

12. Modified z-Transform with Full-Period Advance

$$\frac{x(z)}{u(z)} = \frac{(1 - e^{-aT})}{1 - e^{-aT}z^{-1}}$$

or $$x_n = e^{-aT}x_{n-1} + (1 - e^{-aT})u_n$$

13. Difference Equation with Lag Halved and Half-Period Advance

$$\dot{x} = -2ax_{n-1} + 2au$$

$$x_n = e^{-2aT}x_{n-1} + (1 - e^{-aT})u_n + (e^{-aT} - e^{-2aT})u_{n-1}$$

D. TIME OR SPATIAL DEPENDENCE

If a varying control strategy is likely, then at least three means of detection are available. These are:

1. Sequential finite-duration time-averaging windows
2. Sliding time-averaging window
3. Time or spatial variation imbedded in the general control strategy form.

The first of these was demonstrated in Ref. 11 for a flight director tracking task. The three-minute landing approach phase was simply divided into six 30-sec segments. Each of these was sufficiently long to permit reasonable convergence of a NIPIP solution. This showed a steadily increasing pilot gain well beyond the breakout height point (see Fig. 14).

A sliding time window-averaging provides an autoregressive moving average solution. This offers the potential of detecting a time varying strategy (if it exists) in a shorter overall run length after the initial settling time, because it avoids the concatenation of several subsequent settling intervals.

Perhaps the most satisfactory way to handle a time or spatial variation is to imbed it directly in the NIPIP finite difference equation. This is feasible, though, only if a reliable model form can be assumed.

E. SAMPLING OR DISCRETE CONTROL STRATEGY

Often the pilot is assumed to be a continuous controller, and this is sometimes justifiable. It is possible, though, to discern where the pilot is operating more like a sampling or discrete controller and to estimate the parameters of that strategy, e.g., throttle regulation of airpseed in Ref. 10.

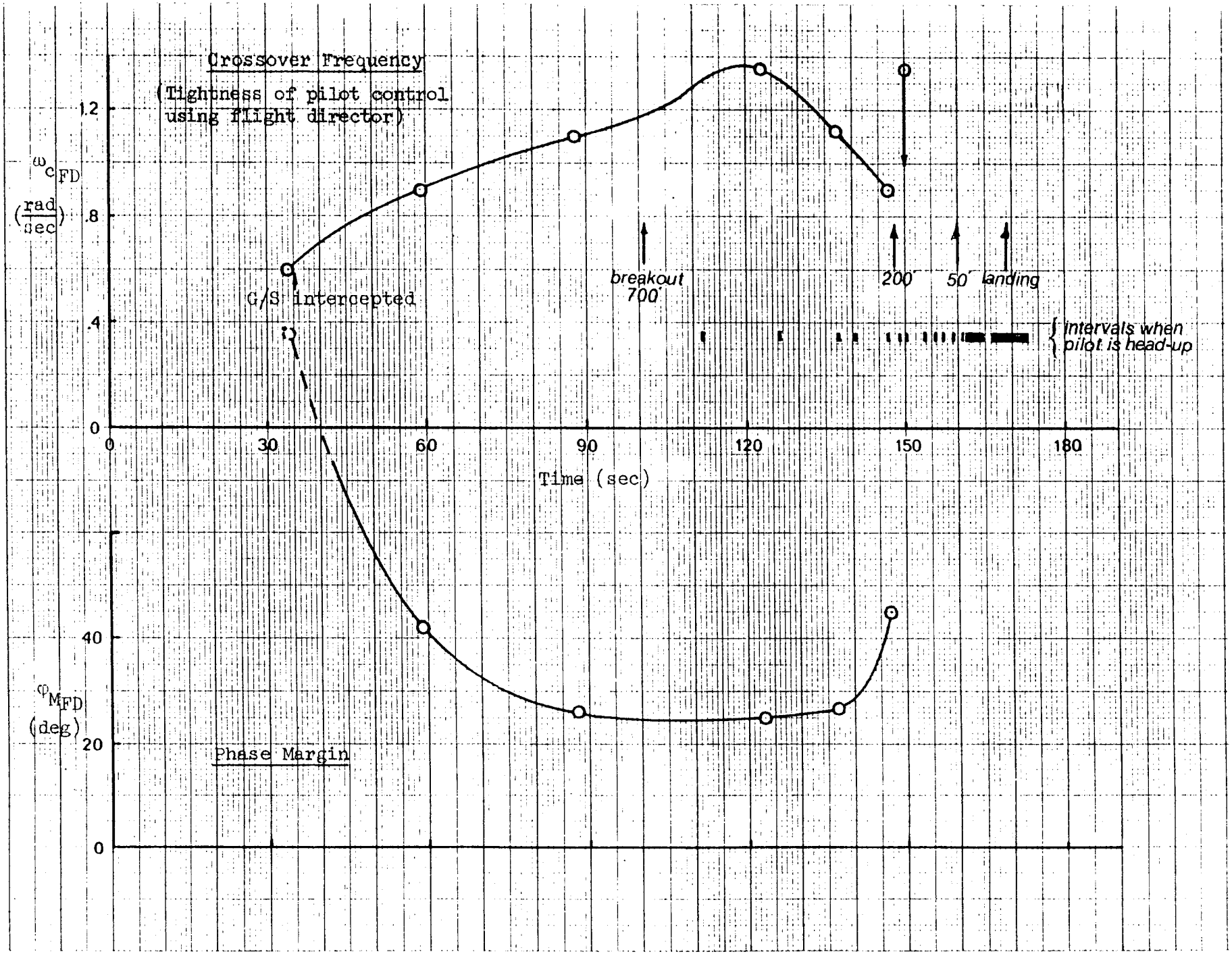

Figure 14. Time Variation of Pilot-Vehicle Performance During Approach

Clues to a sampling strategy appear as repetitive discrete maneuvers in the time domain or in the phase plane. This characteristic is likely to be more prominent in some outer control loops. One example given in the next section involves flight path control. The vertical velocity command is shown to be a series of steps with approximately 15 sec intervals. The strategy thus implied is that an outer loop on visual glide slope error is present. Further, the visual glide slope cue is being sampled with an approximately 15 sec period resulting in a succession of discrete vertical velocity commands.

F. SUCCESSIVE ORGANIZATION OF PERCEPTION (SOP) STAGE

It is possible to assume pilot control strategy forms for any of the three stages of SOP: compensatory, pursuit, or precognitive. These forms are summarized in Fig. 15.

The basic compensatory level is most frequently applied, but the higher stages should be considered where substantial skill and control coordination are involved.

G. CLOSED-LOOP PILOT-VEHICLE RESPONSE

If the predominant closed-loop pilot-vehicle response is of second order (a common occurrence), the closed-loop damping ratio, ζ, and undamped natural frequency, ω_n, can be found using the least-squares parameter identification procedure incorporated in NIPIP. The usefulness of these closed-loop parameters for interpreting pilot control strategy has been illustrated previously in the example of the landing flare maneuver at the end of Section I. Other applications are presented in Refs. 12 and 13.

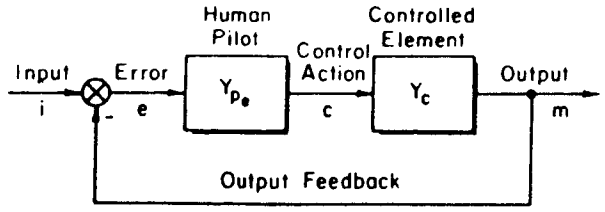

a) Initial Phase : COMPENSATORY (Single Loop)

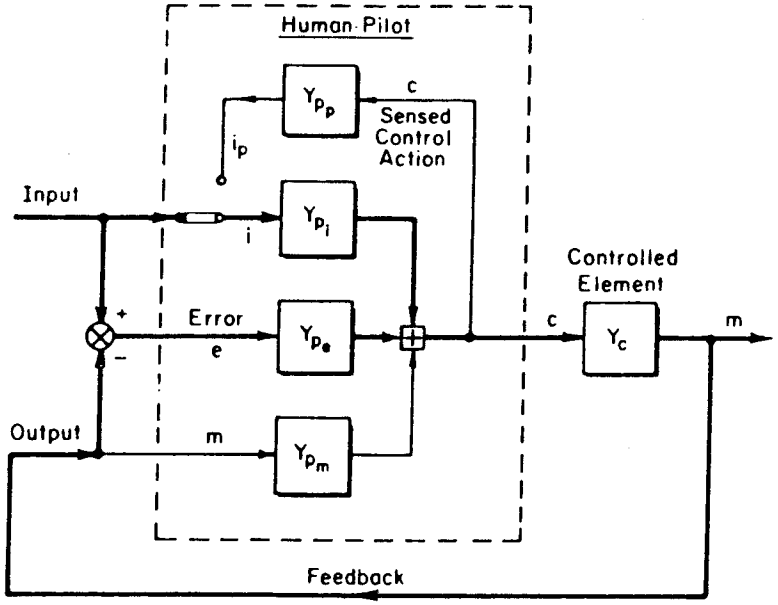

b) Second Phase: PURSUIT (Multiloop)

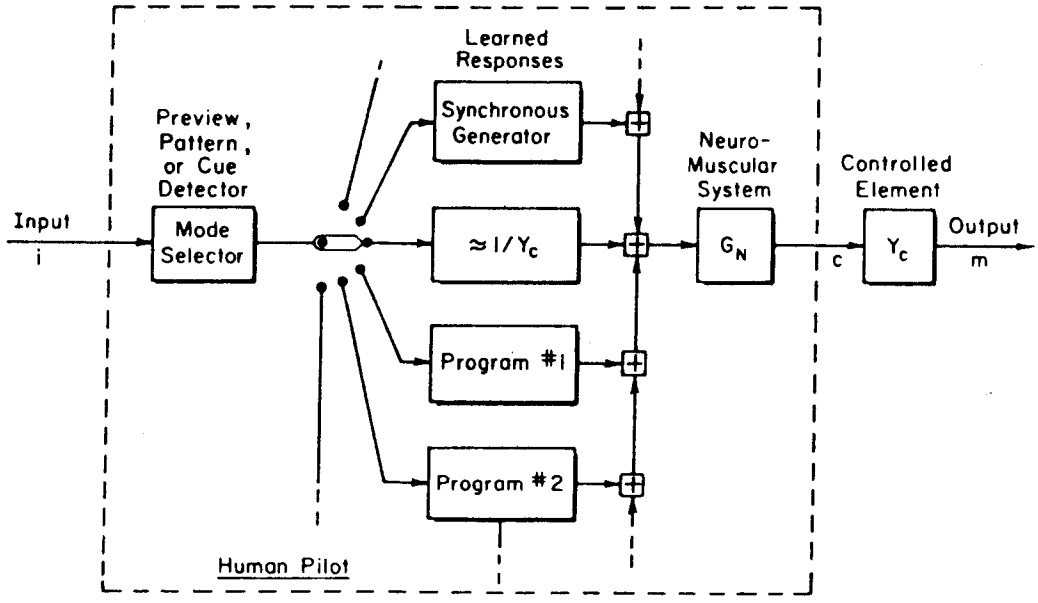

c) Final Phase : PRECOGNITIVE (Open-Loop)

Figure 15. The Three Main Phases in the Successive Organization of Perception (SOP)

This concludes our discussion of the quantifiable features of piloting technique which can be addressed by application of the NIPIP. In the next section we shall present the results from analyses of several sets of flight test data acquired at the Dryden Flight Research Facility.

SECTION IV

ANALYSIS CASES

Several sets of flight data were analyzed from the handling qualities investigation reported in Ref. 14. Each specific analysis is presented as a case study in this section. The various cases demonstrated the application of NIPIP software and presentation of some of the pitfalls associated with handling flight data.

The following cases depict several facets of pilot-vehicle analysis including:

1. Closed-loop task execution dynamics
2. Inner- and outer-loop pilot control strategy
3. Control of flight path in vertical and lateral planes
4. Identification of vehicle characteristics.

Owing to problems with the quality of flight data, a number of the results have a practical value in terms of pointing out difficulties or limitations with this or any other identification process. Where flight data appear to be adequate, a few of the results are meaningful and reveal time varying pilot gains as well as the nature of the pilot compensation.

A. NORMAL APPROACH AND LANDING

1. Case 1: Closed-Loop Longitudinal Task Dynamics—Approach

As a prelude to examining pilot control strategy, the closed-loop task execution response is first considered. The maneuver is characterized both in terms of selected time histories (Fig. 16) and a phase plane plot of the assumed command loop state variable, vertical velocity (Fig. 17). No visual approach slope indication nor other visual landing aid was employed in these approaches.

From the time histories it appears that the approach is composed of several segments each having a different sink rate command and is followed by the flare segment. This is more readily visible in the phase plane in terms of the various second-order response loops. Here the flare segment is treated as a response to a variable sink rate command; in Ref. 6 and subsequently in Case 4, the flare segment is regarded as an unforced response from an initial velocity, sink rate, and height to a set of desired conditions at touchdown. Touchdown is inferred from the abrupt increase in the amplitude of estimated vertical acceleration. The quantization of height (30 ft) was too coarse to define touchdown, and sink rate was not recorded.

What is not discernible in the data is the factor responsible for the sink rate commands, i.e., the outer-loop flight path cue. Since the pilot is flying a visual approach, there is no direct record of a flight path error signal. Thus it is possible to log only the discrete steps.

NIPIP can be used to identify the sink rate commands as well as the response parameters connected with following those commands. Thus if the closed-loop response were considered to be second order (e.g., based on Fig. 17), that is,

$$\dddot{h} = -2\zeta_a \omega_a \ddot{h} - \omega_a^2 \left(\dot{h} - \dot{h}_c\right) , \qquad (9)$$

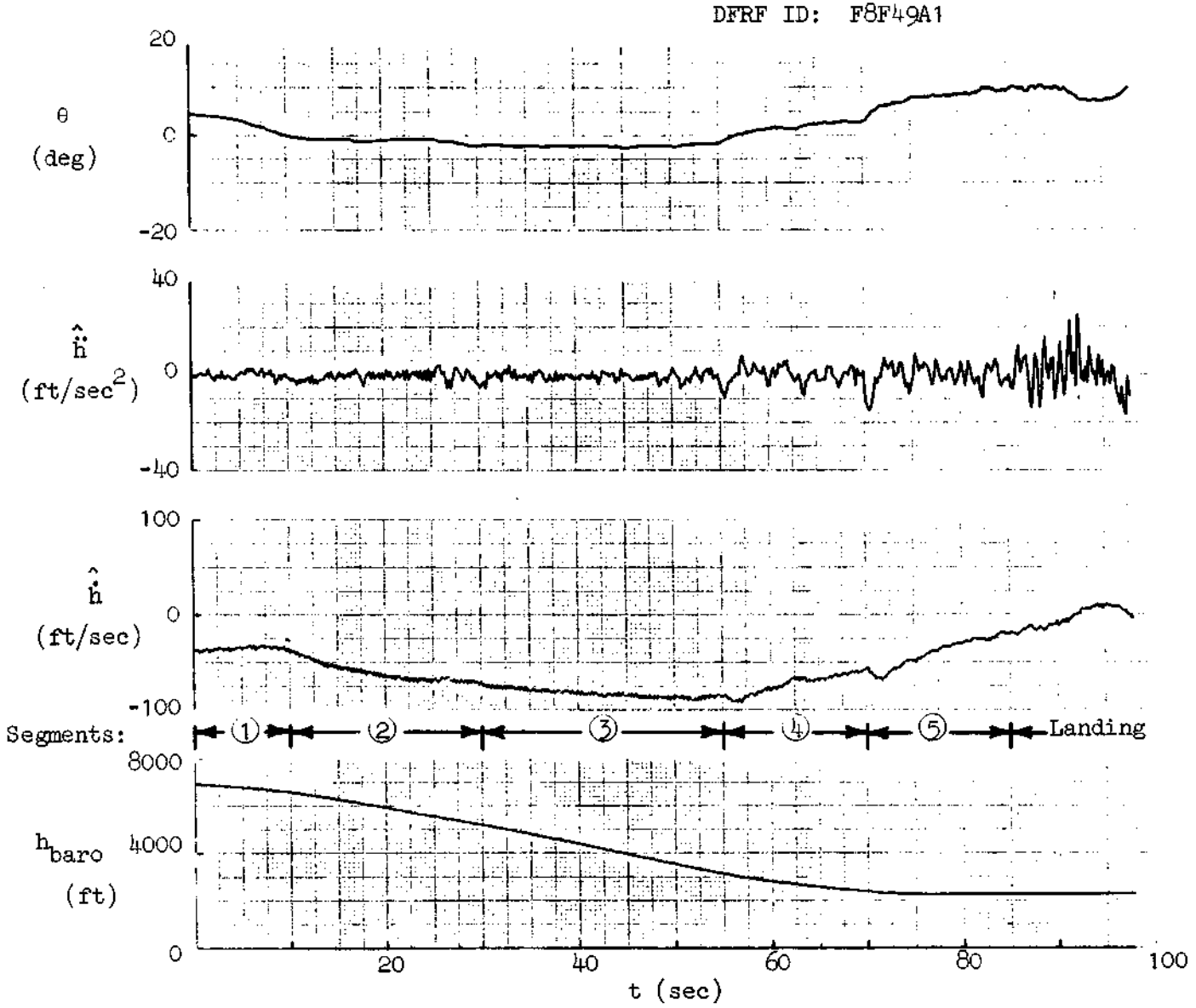

Figure 16. Case 1: Time Histories for Closed-Loop Task Analysis, Normal Approach and Landing

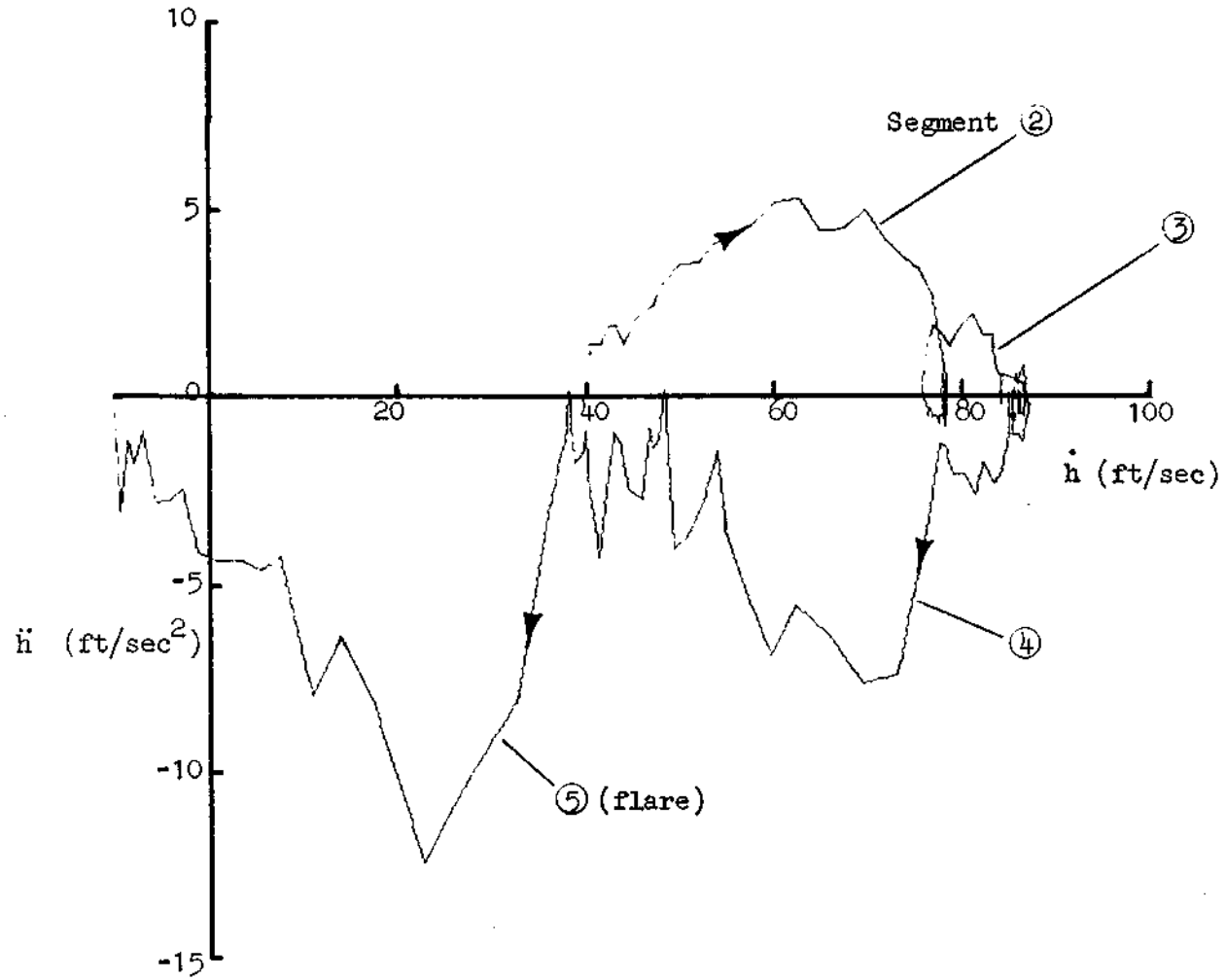

Figure 17. Case 1: Phase Plane for Closed-Loop Task Analysis, Normal Approach and Landing

then NIPIP should be able to solve for ζ_a, ω_a, and $\dot{h}_c$ provided we have suitable data for $\dddot{h}$, $\ddot{h}$, and $\dot{h}$. (A description of filtering used to obtain $\dddot{h}$, $\ddot{h}$, $\dot{h}$ is found in Appendix A.)

The above response function was analyzed using NIPIP for each of the approach segments indicated (in Figs. 16 and 17). The results are shown in Fig. 18. Three solutions are plotted for most of the segments. The solid line describes the NIPIP solution using all data which were sampled at 50 Hz; the broken line describes the NIPIP solution using every fifth data sample (sampling rate 10 Hz) from the total length of the segment; hence, the legend "decimated 1/5" is given for the broken line in Fig. 18. First the closed-loop natural frequency tends to lie in the range of 0.5 to 0.6 rad/sec--in basic agreement with other data previously analyzed (Ref. 6). This frequency can also be observed in the phase plane plot using the analysis technique presented earlier (i.e., the aspect ratio of each phase plane loop).

The damping ratio, ζ_a, obtained by NIPIP is very large; however, and we would expect values slightly less than one from Ref. 6. The damping ratio solutions between one and three, shown by the solid and dashed lines in Fig. 18, were obtained with the more exact estimate of $\ddot{h}$. The lower values were obtained using a less exact, more filtered estimation for $\dddot{h}$. There is the suggestion that state variable estimation and/or $\ddot{h}$ basic flight data quality is a factor. Since the main concern of this report is to outline the NIPIP analysis process and not to describe techniques in state variable estimation, only two simple methods of estimating $\ddot{h}$ were chosen. Without a doubt it would be possible, using more sophisticated filtering and estimation techniques, to reconstruct desired states in order to obtain more reasonable values of the second-order response parameters.

Finally the NIPIP vertical velocity command solutions appear to be reasonable but not as accurate as one would wish in Segments 1 through 4; recall that the flare, Segment 5, is treated here as a response to a variable sink rate command for which we have no independent "apparent" estimate. At the same time, improved data quality could be expected to

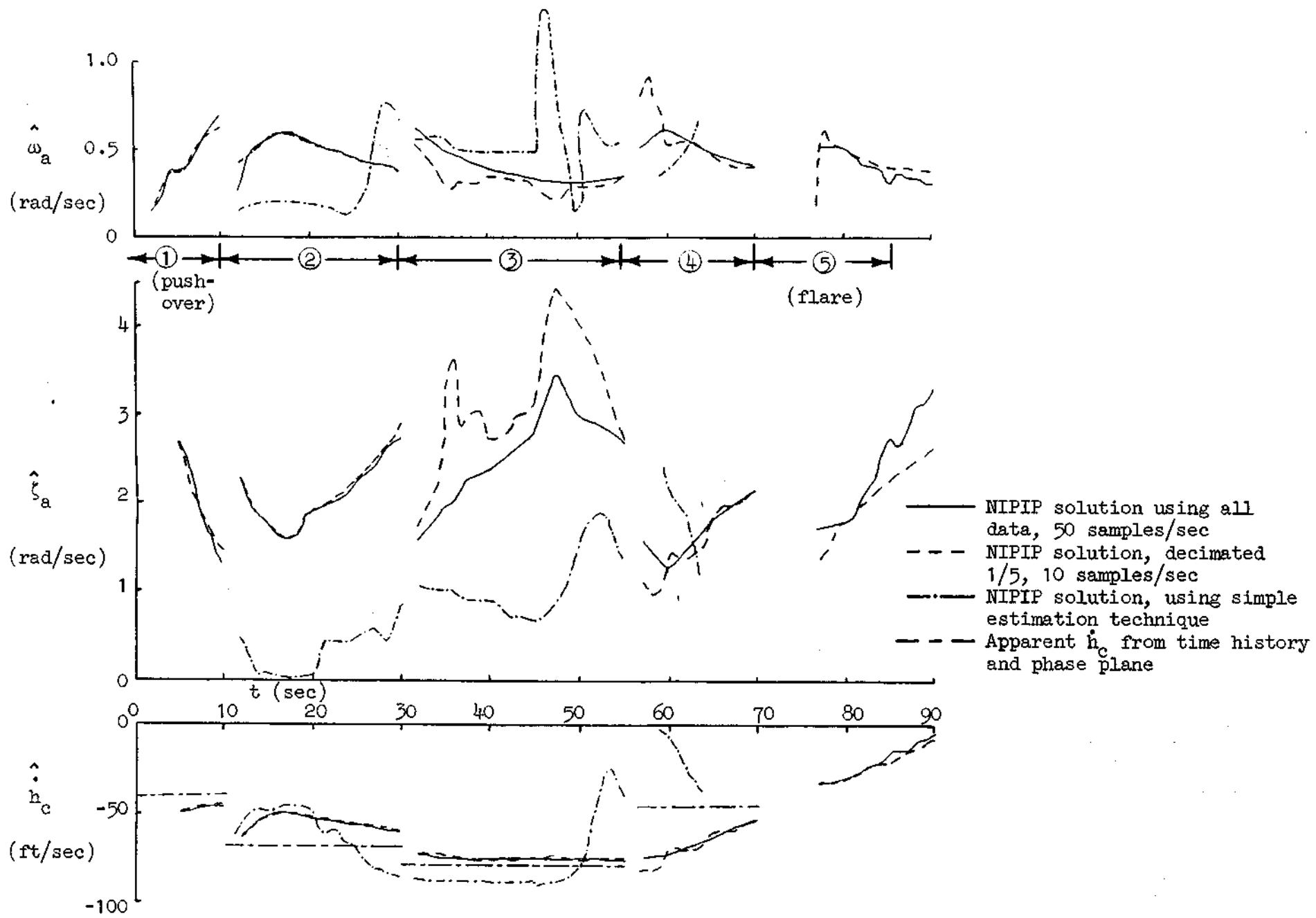

Figure 18. Case 1: Identified Parameters for Closed-Loop Task Analysis, Normal Approach and Landing

improve these estimation results as well as those for closed-loop undamped natural frequency and damping ratio.

2. Case 2: Longitudinal Pilot Control Strategy—Approach

This case in which the task segmentation was formulated is a natural progression from the first. Here the role of NIPIP is to identify pilot control strategy characteristics for the inner (pitch attitude) and outer (vertical velocity) loops. A block diagram of the hypothetical control technique was shown previously in Fig. 4(a), provided we interpret the outer loop for the explicit tracking task in terms of vertical velocity, $\dot{h}$, instead of height, h, and the command as $\dot{h}_c = \dot{h}_{ref}$.

Figure 19 shows the primary control and command loop state variables for the inner and outer loops. Also shown are the four approach segments and one flare segment. NIPIP was used to obtain estimates of Y_{p_θ} [Fig. 4(a)] and $Y_{p_{\dot{h}}}$ for each of these finite time segments.

The inner-loop solutions are shown in Fig. 20, but the results are confounded by a fundamental data quality problem. Note that for the first segment (the initial pushover onto the approach path) the identified phase angles for Y_{p_θ} quickly converge on about -180 deg, thus indicating an established negative feedback control loop. Very quickly, however, the phase shifts to nearly -90 deg and remains for the duration of the approach. Further, the amplitude of Y_{p_θ} shows a -6 dB/octave slope (the frequencies shown are separated by approximately one octave). Hence the Y_{p_θ} solution appears to be an integrator--not the form expected for the pilot in this case. A pure gain would be considered more likely.

The explanation for the above behavior is believed to be the coarseness in pitch attitude quantization in the flight data records. Consider one of the finite difference equation forms assumed for NIPIP:

$$\delta_{e_n} = a_1 \delta_{e_{n-1}} + b_1 \theta_{n-1} + b_2 \theta_{n-2} + c\dot{h}_{n-1} + \text{bias} \qquad (10)$$

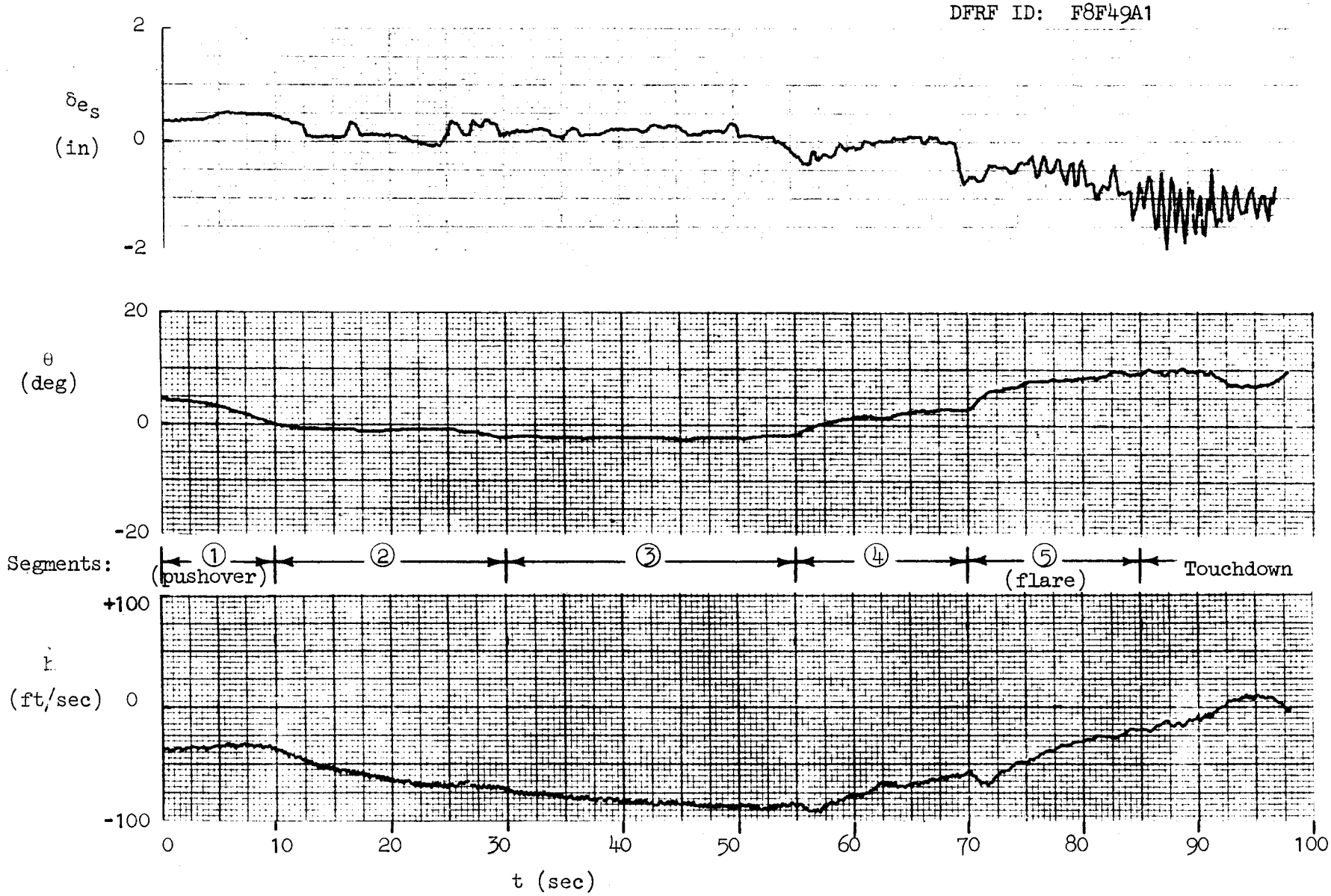

Figure 19. Case 2: Time Histories for Longitudinal Control Strategy, Normal Approach and Landing

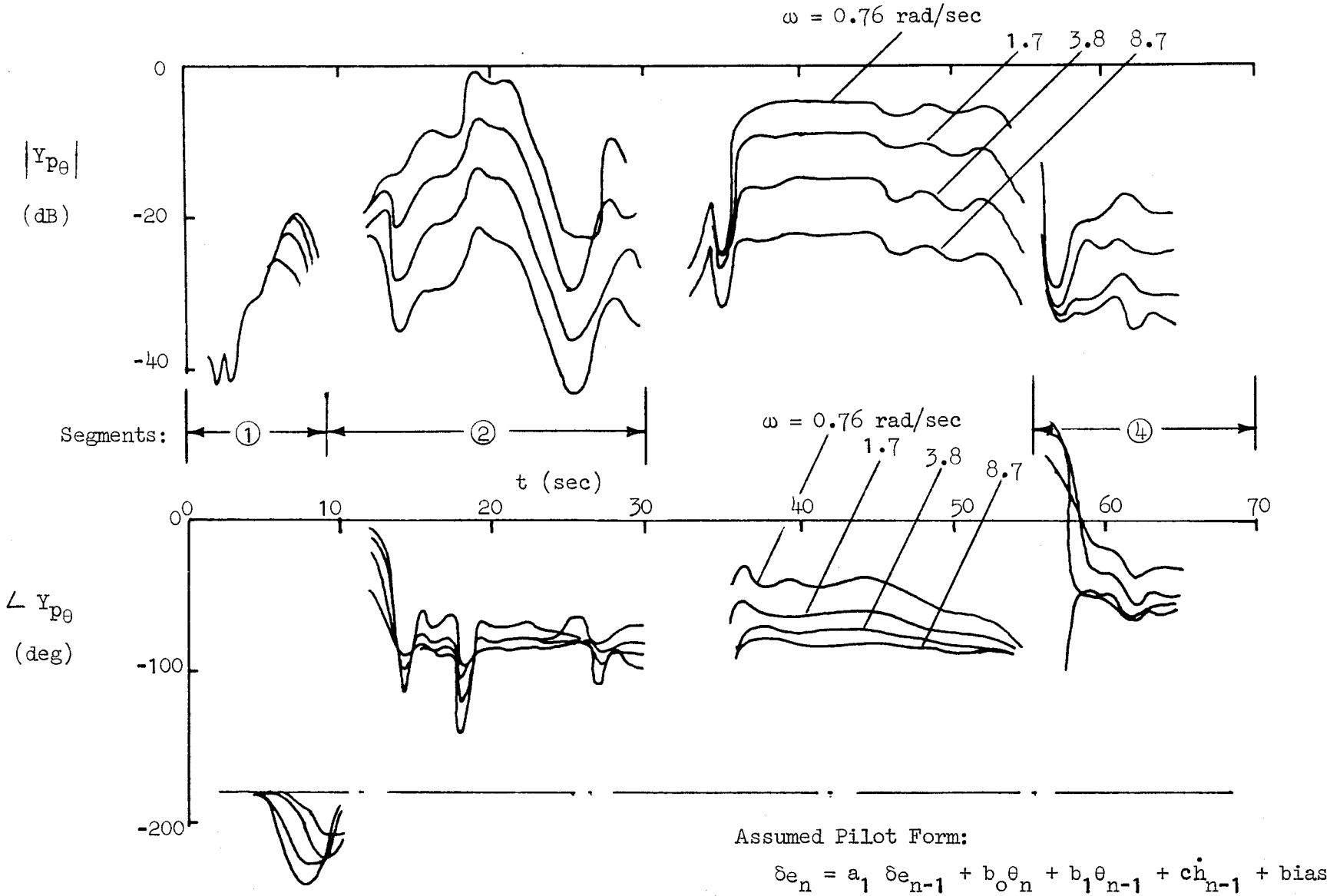

Figure 20. Case 2: Inner Loop Pilot Longitudinal Control Strategy Solution (Lower Order Model Form), Normal Approach and Landing

Note that for any interval in which the attitude and vertical velocity are varying within the quantization (round off) band, the last four terms on the right side of the equation all act as constant, say ε_θ. Thus if δ_e is continuing to vary,

$$b_1\theta_{n-1} + b_2\theta_{n-2} + c\dot{h}_{n-1} + \text{bias} = \varepsilon_\theta = \text{constant} \qquad (11)$$

and

$$\delta_{e_n} = a_1 \delta_{e_{n-1}} + \varepsilon_\theta \qquad (12)$$

Hence for moderately slow changes in δ_e compared to the sampling rate,

$$a_1 \approx 1 \qquad (13)$$

and

$$\delta_e(z)\left(1 - z^{-1}\right) \approx \varepsilon_\theta(z) \qquad (14)$$

where ε_θ is a residual non-zero quantity related to the quantization of θ

or

$$Y_{p_\theta}(z) \approx \frac{\delta_e(z)}{\varepsilon_\theta(z)} \approx \frac{1}{1 - z^{-1}} \qquad (15)$$

Thus Y_{p_θ} would appear as an integrator with -6 dB/octave rolloff in amplitude and -90 deg phase--the behavior observed during much of the approach. Therefore the NIPIP solution, except for the short periods during the pushover and later in the pre-flare, appears to yield a false pilot control strategy model, because the pitch attitude was recorded with too coarse a quantization in the flight test.

Note that in Fig. 21 where the assumed form of Y_{p_θ} is given more degrees of freedom no improvement is seen.

Similar kinds of problems carry over into the outer loop solution except for the fact that the false solution of $Y_{p_{\dot{h}}}$ takes on a different character. In this case, when the attitude begins to dwell within the quantization bands for long periods, it appears that $Y_{p_{\dot{h}}}$ simply reflects the ratio of the steady-state attitude to sink rate, i.e.,

$$Y_{p_{\dot{h}}} \approx \frac{-\theta}{\dot{h}} \tag{16}$$

e.g., for $\theta = -2$ deg $= -0.0349$ rad

$$\dot{h} = -75 \text{ ft/sec} \tag{17}$$

and the steady-state solutions are

$$\left|Y_{p_{\dot{h}}}\right| = 20 \log \frac{2}{75} = -31 \text{ dB} \tag{18}$$

and

$$\sphericalangle Y_{p_{\dot{h}}} = -180 \text{ deg} \tag{19}$$

both of which are displayed quite consistently in Segments 2 and 3 of Fig. 22 and somewhat erratically in Segments 1 and 4.

An increased order form for $Y_{p_{\dot{h}}}$ (Fig. 23) does little to help except in Segment 4 where θ is changing significantly, and even there only the phase angle appears to converge to a valid solution.

Appendix B presents the results of a more detailed investigation of the effects of quantization in pitch attitude on the identification of pitch attitude and sink rate control strategy.

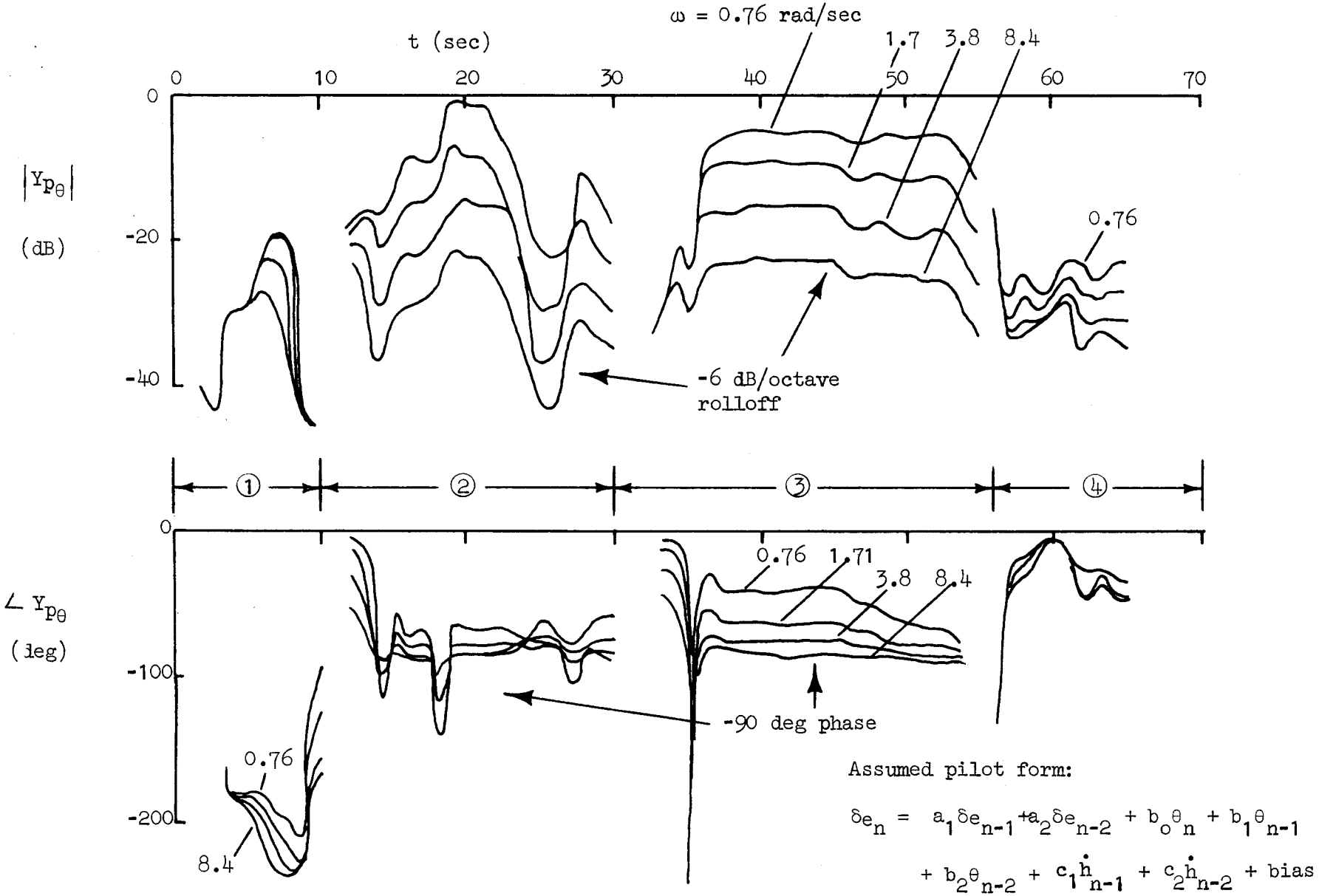

Figure 21. Case 2: Inner Loop Pilot Longitudinal Control Strategy Solution (Higher Order Form), Normal Approach and Landing

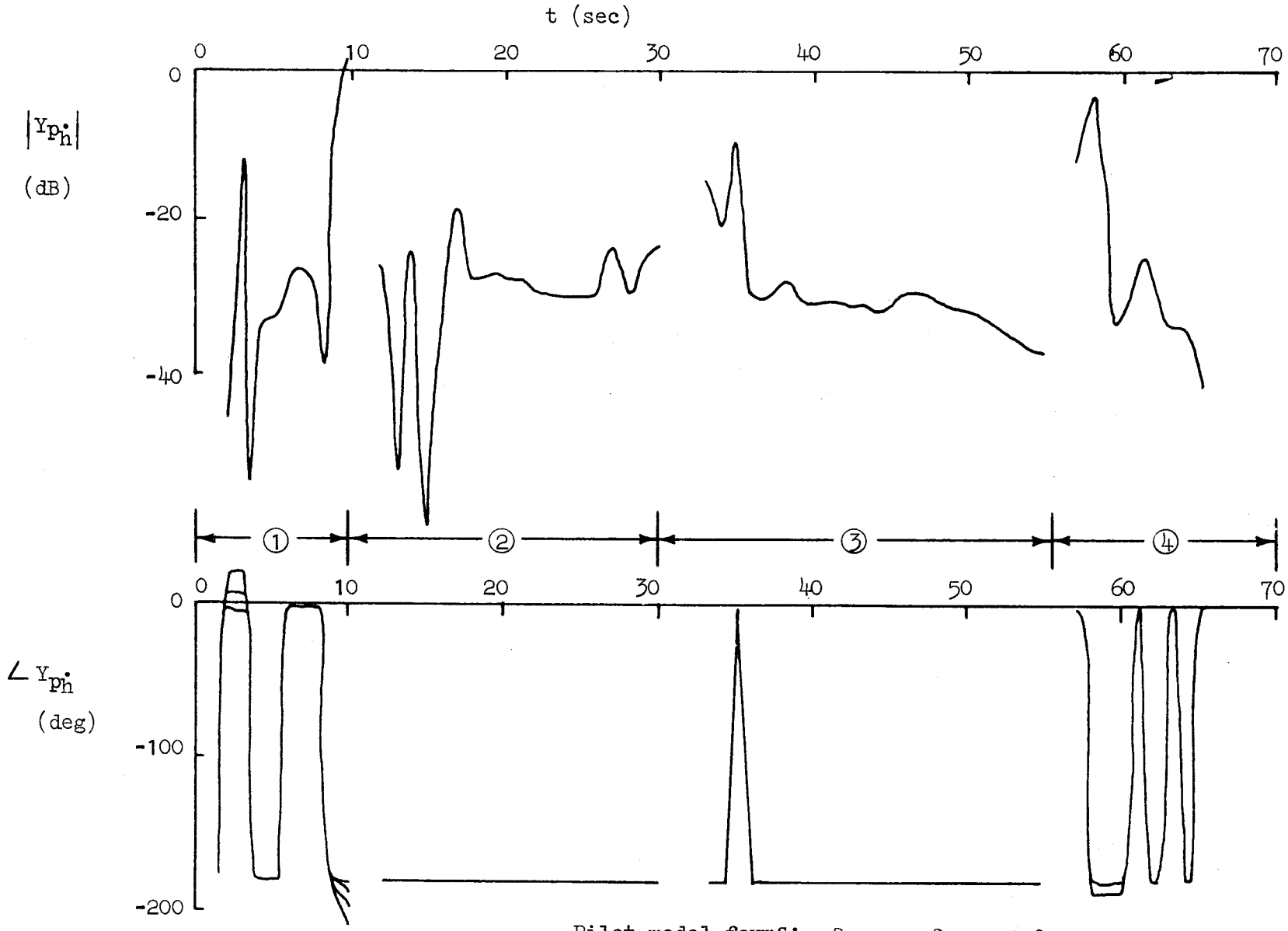

Figure 22. Case 2: Outer Loop Pilot Longitudinal Control Strategy Solution (Lower Order Model Form), Normal Approach and Landing

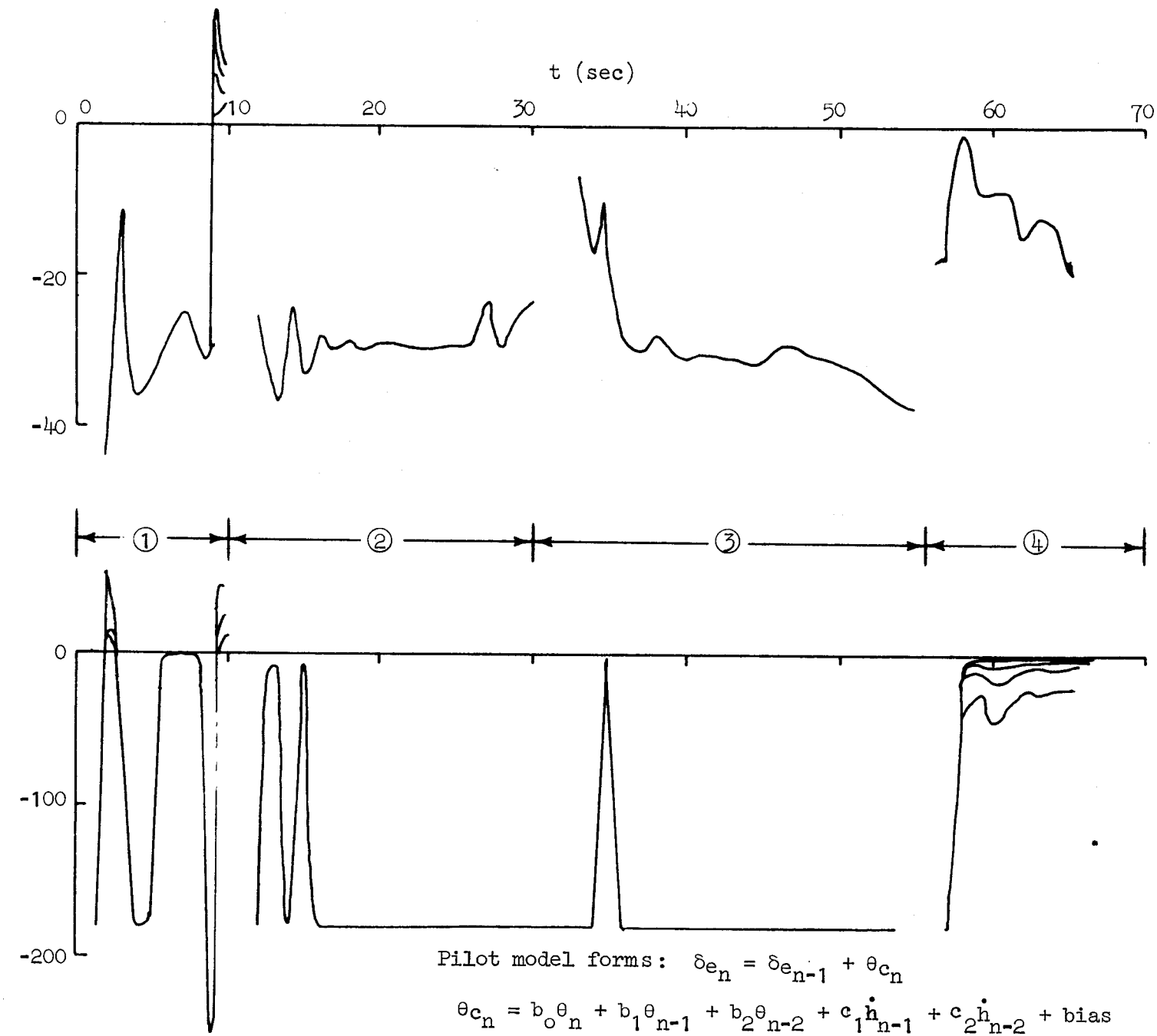

Figure 23. Case 2: Outer Loop Pilot Longitudinal Control Strategy Solution (Higher Order Model Form), Normal Approach and Landing

3. Case 3: Lateral Pilot Control Strategy—Approach

It was hoped that a heading control strategy via bank angle control, like that shown previously in Fig. 4(c), might permit the identification of the pilot's lateral technique during at least part of the approach. Figure 24 shows the available time histories for the lateral control and command loop state variables. As indicated in Fig. 24, a gentle turning maneuver was performed early in the approach, ostensibly to acquire the final approach course, just following the pushover shown previously in Fig. 19. The heading (ψ) record, however, shows a gradual change throughout the entire approach. This is typical of an approach in a cross-wind shear and/or an approach with a varying airspeed during the final (supposedly straight) portion of which approach the pilot is tracking the runway centerline perspective (and extension thereof) with an outer lateral displacement regulation loop. Recorded variations in altitude and true airspeed suggest that this interpretation may be valid. Neither lateral displacement nor ground speed time histories were recorded, however, from which to identify an outer lateral displacement control strategy, Y_{p_ψ}*. Therefore no attempt could be made to identify the pilot's three-loop lateral technique as depicted in Fig. 4(d) through either the acquisition or the final (supposedly straight) portion of the approach in Fig. 24.

Notwithstanding the foregoing limitation, a heading control strategy like that shown previously in Fig. 4(c) was assumed for the lateral axis, and the NIPIP was applied to the time histories for the lateral control and command loop state variables in Fig. 24.

---

*Given an initial condition, y_o, one might estimate lateral displacement, y, from ground speed, V_g, and heading, ψ, by means of the equation

$$y = y_o + \int_o^t V_g(\xi) \sin \psi(\xi)\, d\xi$$

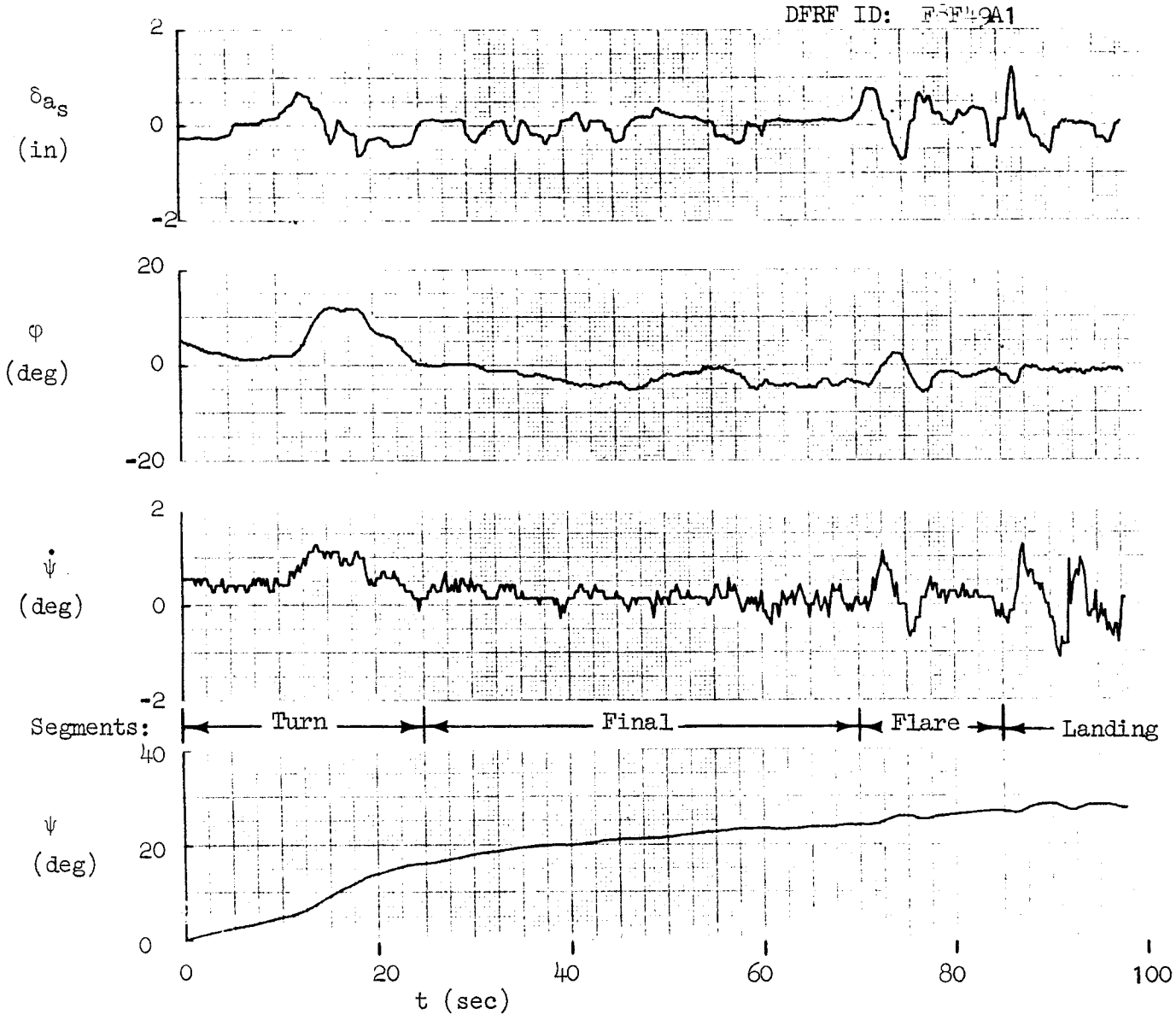

Figure 24. Case 3: Time Histories for Lateral Control Strategy, Normal Approach and Landing

Three segments were chosen: the early turn maneuver (0 to 25 sec), the final approach (25 to 70 sec), and the flare (70 to 90 sec) which includes landing at 85 sec. The inner-loop control strategy for Y_{p_ϕ} is shown in Fig. 25 at three frequencies, 0.1, 0.51, and 5.77 rad/sec. Note that in the first and second segments, the identified phase angles for Y_{p_ϕ} quickly converge toward -180 deg, thus indicating an established negative feedback control loop. Convergence of neither phase angle nor amplitude is sustained, however, until in the second segment the phase shifts to approximately -190 deg (at 0.1 rad/sec), -230 deg (at 0.51 rad/sec), and -270 deg (at 5.77 rad/sec); and the amplitude shows a -20 dB/decade slope in the frequency decade between 0.51 and 5.77 rad/sec. Similar convergence occurs in the third segment. Hence the Y_{p_ϕ} solution appears to represent a first-order lag at 0.5 rad/sec at times of 33 sec and 74 sec; but then, at 50 sec, the phase changes to that of an integration--not the form expected for the pilot in this case either. First-order lag compensation for Y_{p_ϕ} at 0.5 rad/sec seems low in frequency, but may be plausible since the pilot was dividing his attention between flare and line-up control.

The abrupt change at 50 sec to identify an integration was not anticipated here, because roll attitude quantization is 0.02 deg (one-fifth that of pitch attitude), and roll attitude exhibits some variation in Fig. 24. At 50 sec, however, Fig. 24 shows an interval of relative quiescence in the pilot's control activity and in roll attitude. In hindsight, it might have been preferable to change the past value of the lateral control stick displacement from $\delta_{a_{n-1}}$ to $\delta_{a_{n-2}}$ in the difference equation

$$\delta_{a_n} = a_1 \delta_{a_{n-1}} + b_1 \phi_{n-1} + b_2 \delta_{n-2} + c_1 \psi_{n-1} + \text{bias} \qquad (20)$$

in order to verify the tendency for a_1 to converge on a value which is approaching unity as in Case 2. Thus we offer the additional recommendation to replace $\delta_{a_{n-1}}$ by $\delta_{a_{n-2}}$ (or $\delta_{a_{n-m}}$; $m > 2$) where quantization appears sufficiently small, yet a_1 converges to unity in a

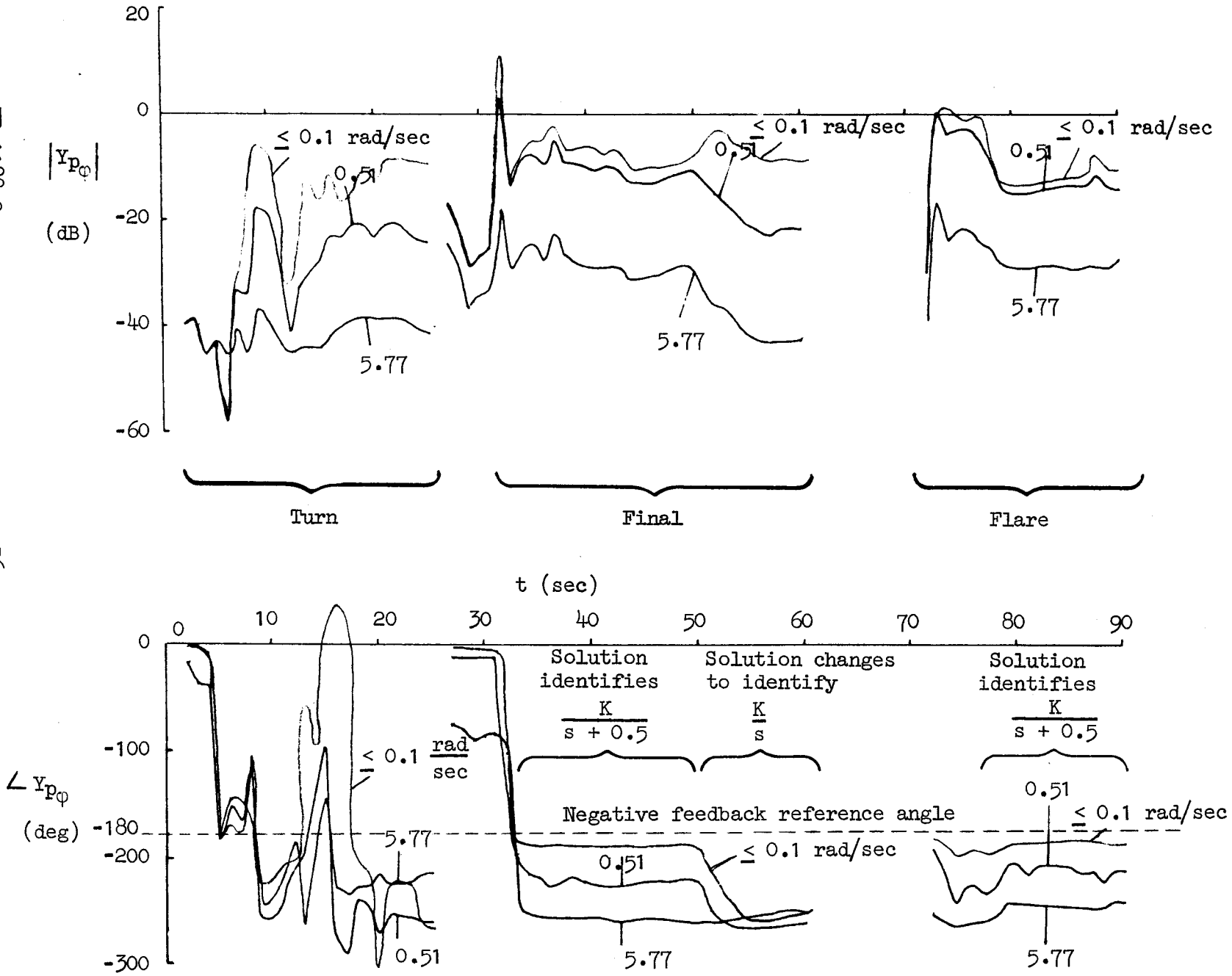

Figure 25. Case 3: Inner Loop Pilot Lateral Control Strategy Solution, Normal Approach and Landing

solution for strategy which would not otherwise be expected to identify the form of an integration. One must take this recommendation cautiously, because there may be some other cases, such as that of a pure gain controlled element, where an integration would represent the expected strategy for control in the frequency range of observation.

The outer-loop control strategy for Y_{p_ψ} is shown in Fig. 26 at three frequencies: 0.05, 0.2, and 2 rad/sec. Note that there is no semblance of convergence on a solution for Y_{p_ψ} in the turn segment. This fact is not unexpected, because the loop structure of Fig. 4(c) is inappropriate for a turn unless a ramp function representing the heading command is introduced during the identification of the pilot's strategy by NIPIP. The heading command was taken to be zero in applying NIPIP here, however.

During the segment labeled "final" in Fig. 26, the solution for Y_{p_ψ} appears to converge on a low frequency gain of 1 deg/sec with limited lead compensation above a frequency of 0.2 rad/sec. For reference a gain of 3 deg/deg is plotted in order to indicate the general agreement with the value inferred from pilot training guides in Ref. 5.

During the segment labeled "flare" in Fig. 26, the solution for Y_{p_ψ} does not appear to converge in the interval from 70 to 85 sec, at which time Fig. 24 indicates that landing occurred. Since the time histories in Fig. 24 indicate that a small lateral correction was made between 70 and 80 sec, it is likely that a three-loop lateral control strategy including an outer displacement loop should be used in future attempts to identify the pilot's lateral approach technique with Case 3.

4. Case 4: Flare Maneuver

The final segment (five) of the approach was assumed to be the flare maneuver. The time histories of all of the variables are contained in earlier figures (Figs. 16 and 19). Figure 27 shows a phase plane of $\dot{h}$ and h and indicates another serious flight data quality problem. Notably the altitude quantization band is 30 ft wide. While this did not prevent

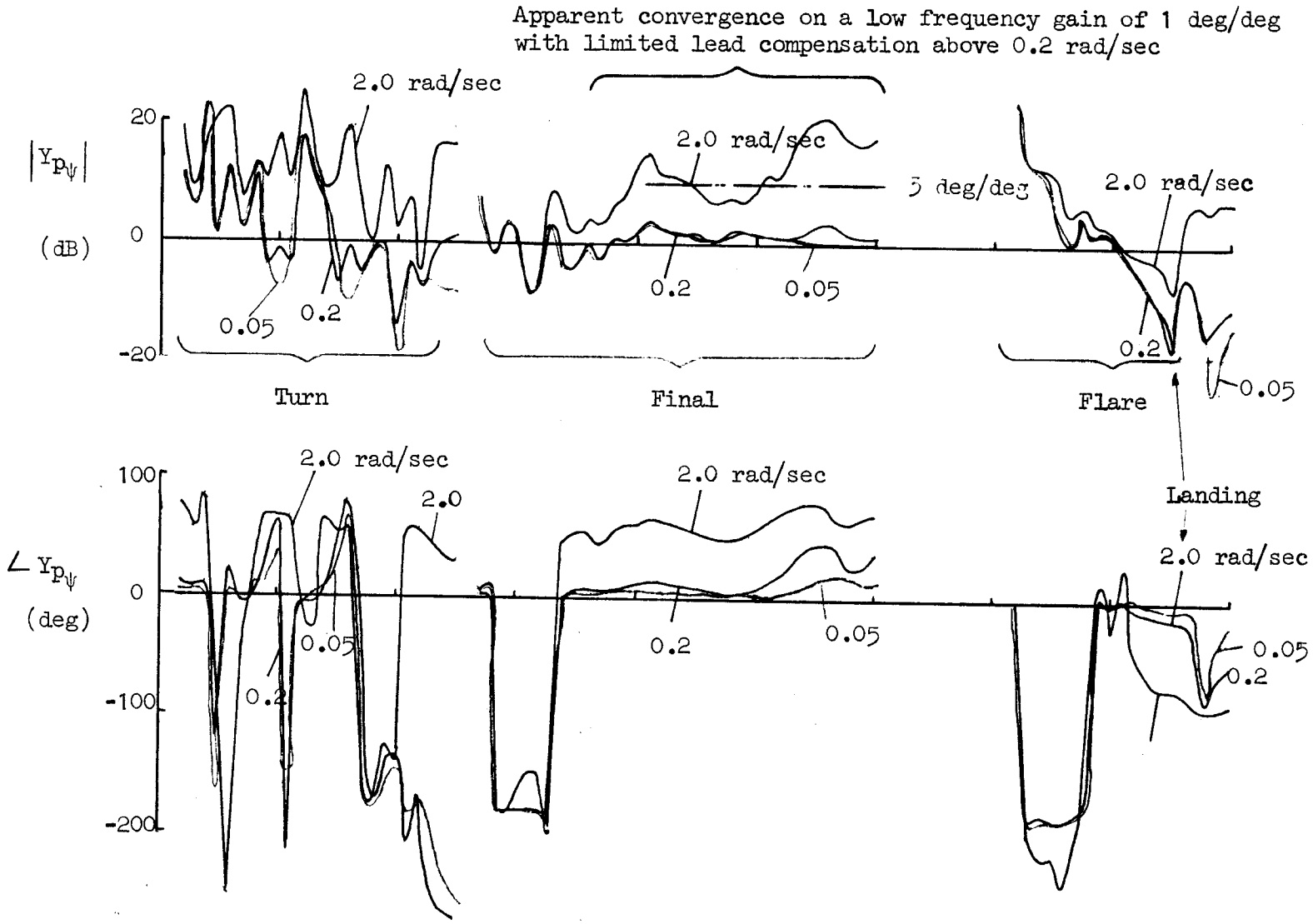

Figure 26. Case 3: Outer Loop Pilot Lateral Control Strategy Solution, Normal Approach and Landing

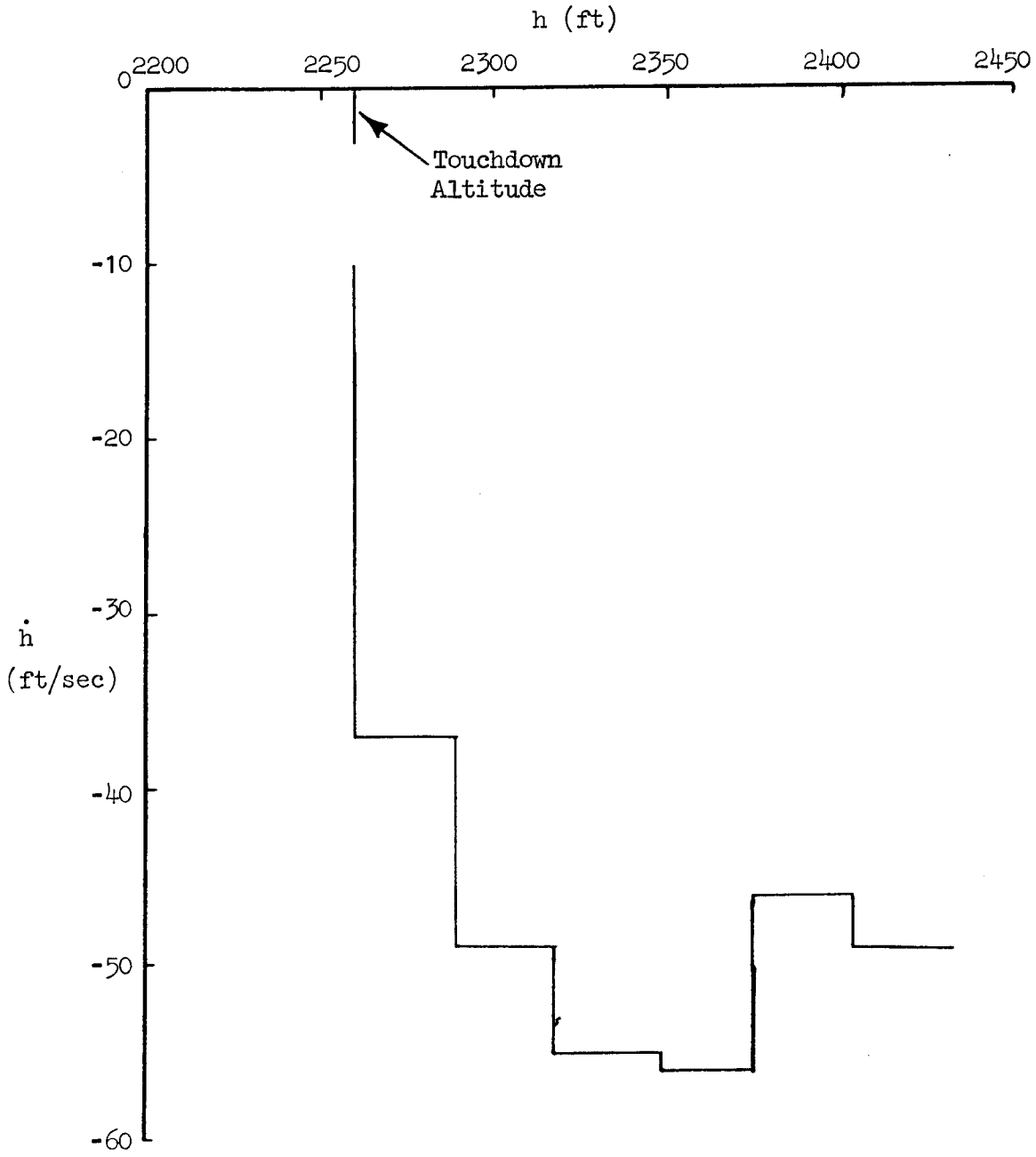

Figure 27. Case 4: Phase Plane for Landing Flare Analysis, Normal Approach and Landing

estimation of an adequate sink rate during the approach, it does present problems in the flare.

The results of closed-loop task response identification by NIPIP did not converge to valid solutions for damping ratio, ζ, and natural frequency, ω_n, because of the coarse quantization in recorded altitude (see Fig. 28).

Inner-loop pilot control strategy results are shown in Fig. 29 and outer-loop results in Fig. 30. Reasonable settling in the solution occurs during the initial half of the maneuver. The solutions are invalid after 77 sec, because the altitude remains invariant within the last quantization band whereas the estimated sink rate continues to decrease until touchdown at 85 sec. Both Y_{p_θ} and Y_{p_h} are practically pure gains. Inner-loop gain, Y_{p_θ}, is about 0.1 (-20 dB) and is comparable to those found during the approach. Outer loop gain, Y_{p_h}, is about 0.01 deg/ft (-40 dB)--lower than those values found in the DC-10 study, Ref. 6--but evident in the flight records.

B. SPOT LANDING WITH A LATERAL OFFSET

1. Case 5: Closed-Loop Longitudinal Task Dynamics—Approach

In the previous cases the pilot was flying a "normal" visual approach and landing. In the following four cases, the pilot was to fly a spot landing with a lateral offset. This consisted of an approach that was lined up with the edge of the runway, followed by an offset maneuver (initiated 100 ft above ground level) to line up with the runway centerline, and a touchdown at the 5000 ft marker.

As before, the closed-loop task execution response is first considered. The maneuver is again characterized in terms of the time history of the assumed command loop state variable, vertical velocity (Fig. 31). As seen in Fig. 31, it appears that the approach is again composed of

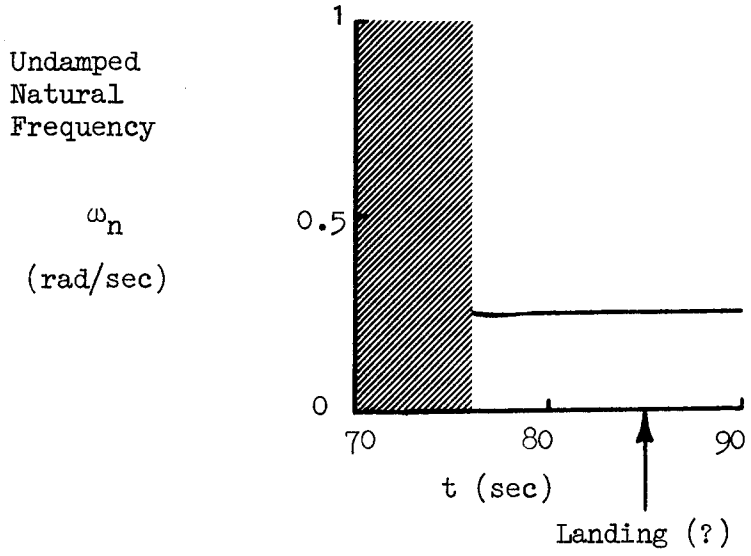

Solutions failed to converge in the shaded interval

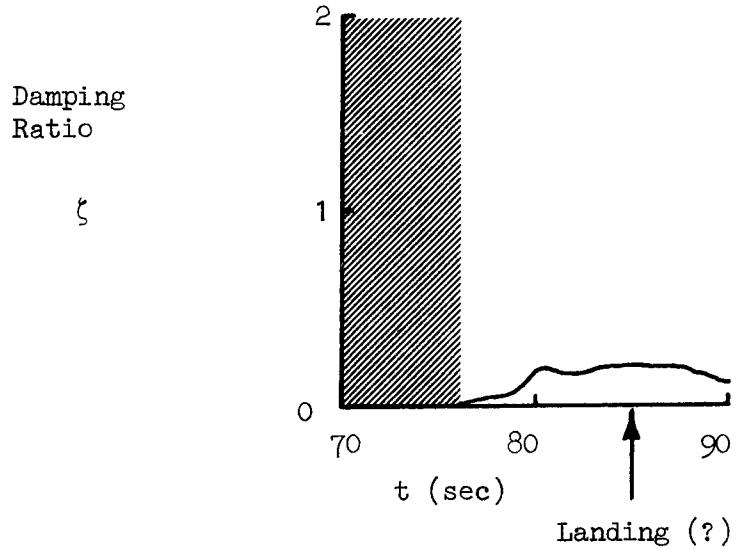

Figure 28. Case 4: Identified Parameters for Closed-Loop Flare Task Analysis, Normal Approach and Landing

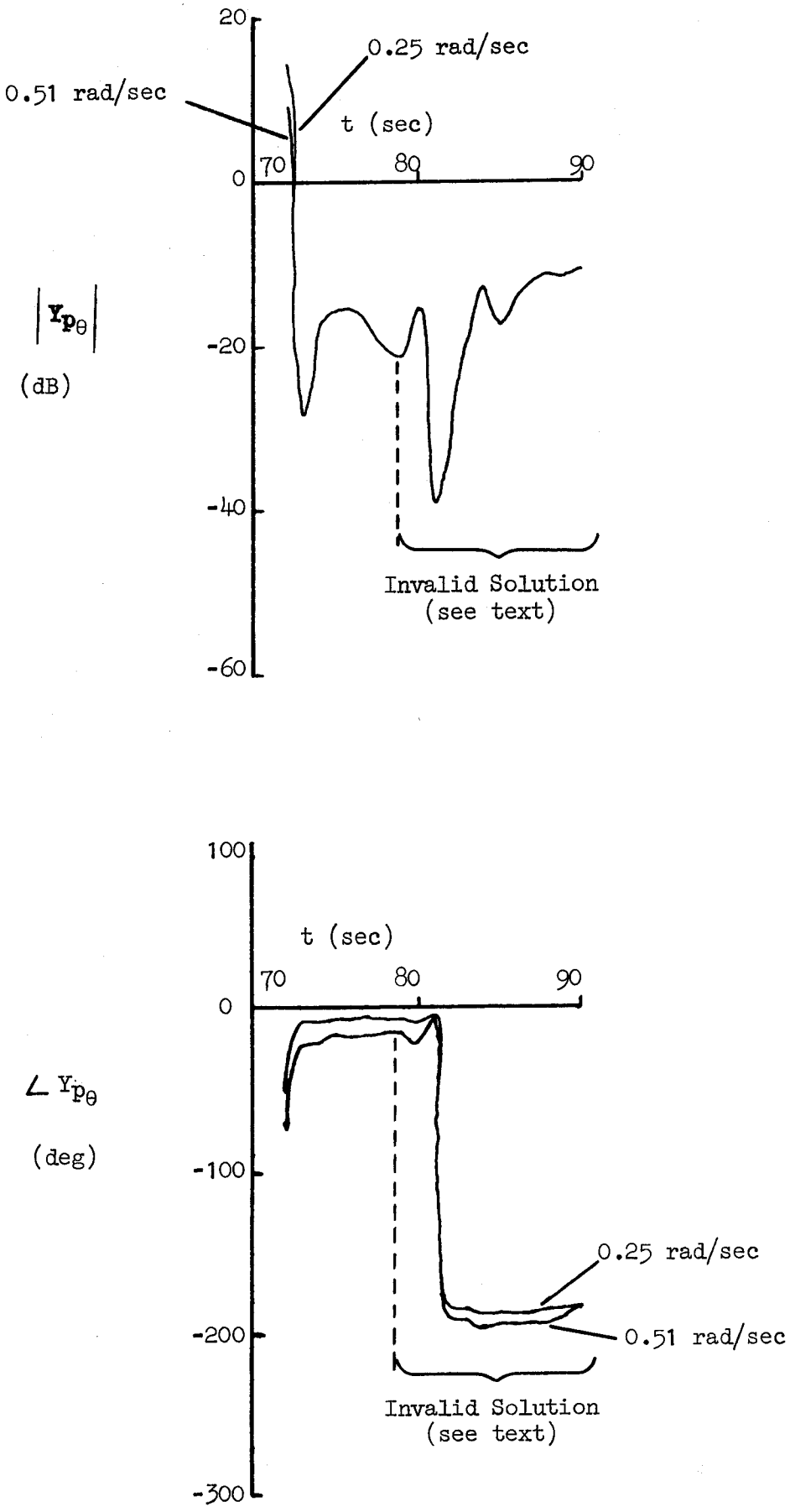

Figure 29. Case 4: Inner-Loop Pilot Longitudinal Control Strategy Solution, Normal Approach and Landing

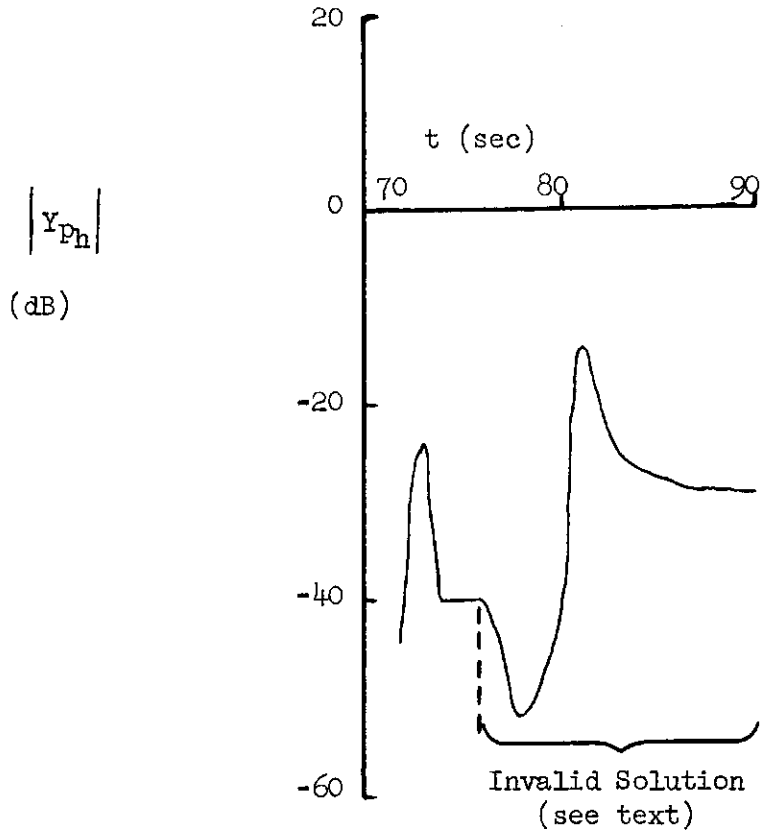

Note: All frequencies < 2 rad/sec

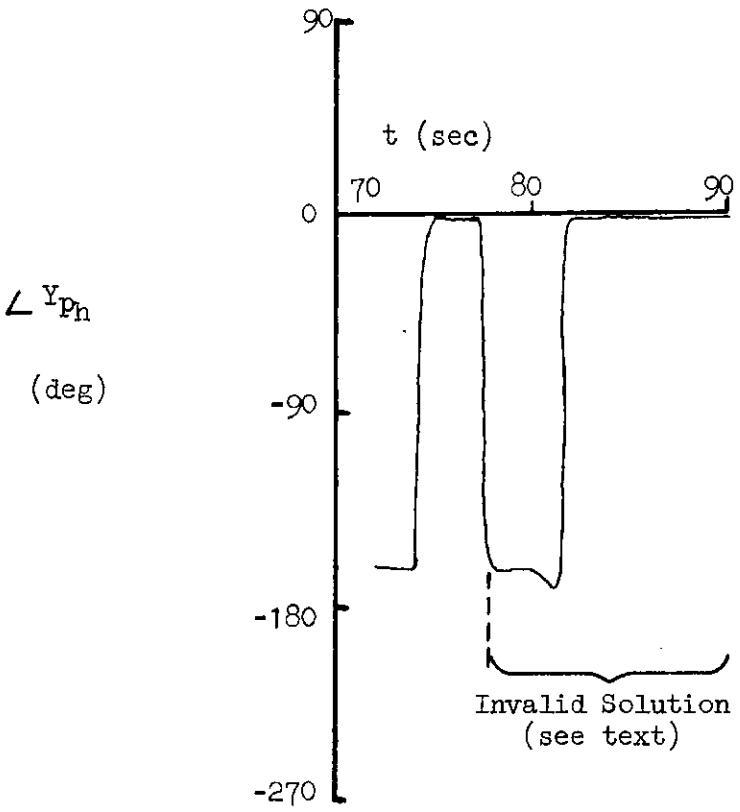

Figure 30. Case 4: Outer-Loop Pilot Longitudinal Control Strategy Solution, Normal Approach and Landing

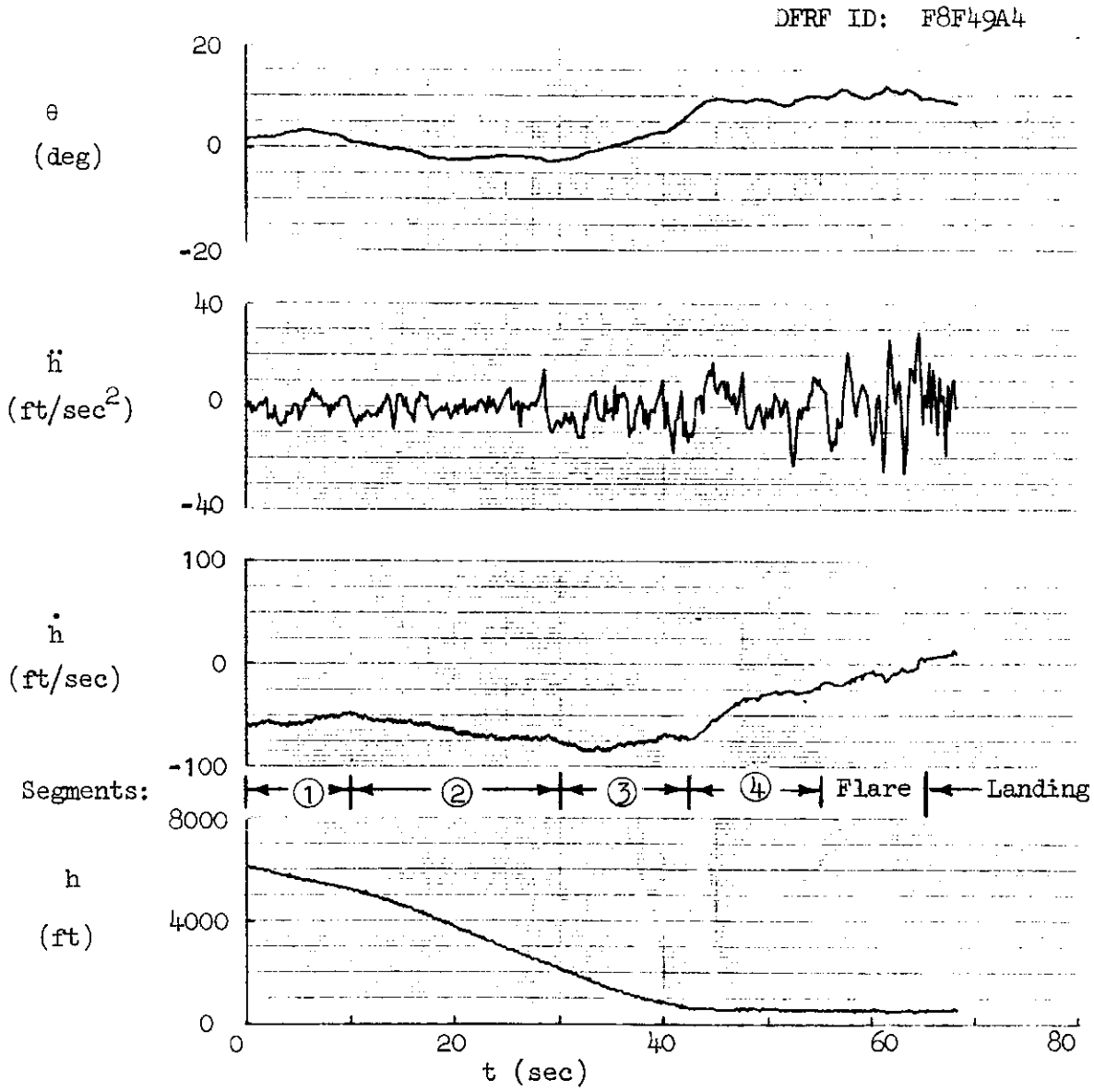

Figure 31. Case 5: Time Histories for Longitudinal Closed-Loop Analysis, Lateral Offset Approach, Spot Landing

several segments each having a given sink rate command. These segments are indicated in Fig. 31. Here it is necessary to infer touchdown from the abrupt increase in the frequency of estimated vertical acceleration, because the quantization of height (30 ft) was too coarse to define touchdown, and sink rate was not recorded.

NIPIP is again used to identify the sink rate command as well as the response parameters, ζ_a and ω_a, by considering the closed-loop response to be second order. The second-order response function of Eq. 9 was analyzed using NIPIP for each of the approach segments indicated in Fig. 31. The results are shown in Fig. 32. In the first segment the identified solution for the vertical velocity command, $\dot{h}_c$, does not predict the appropriate value; in fact, the predicted $\dot{h}_c$ value was greater than zero beyond 7 sec. (The positive $\dot{h}_c$ scale is not shown.)

In the second segment the identified undamped natural frequency, ω_a, approaches zero during the initial 10 sec of the segment, and NIPIP estimates a subsidence and divergence thereafter. This leads to the estimation of an infinite value of damping ratio, ζ_a, and zero for the vertical velocity command. Possible reasons for these anomalous results appear in the time histories of Fig. 31 between 18 and 22 sec. The pilot appears to have trimmed the aircraft in the descent so that pitch attitude is virtually constant ($-2.5 < \theta < -2$ deg), vertical acceleration is fluctuating about null ($-4 < \ddot{h} < 4$ ft/sec^2), and vertical velocity is almost constant ($-75 < \dot{h} < 65$ ft/sec). The estimate of $\dddot{h}$ from $\ddot{h}$ in this portion of the second segment is evidently also fluctuating about null so as to cause the identification of ω_a in Eq. 9 to approach zero. (For example, ω_a must vanish in Eq. 9, if $\dddot{h} = \ddot{h} = 0$.) Anomalous results such as this are typical of trimmed flight conditions where neither the pilot nor the turbulence is disturbing the recorded variables sufficiently to permit reliable estimation of the variations in the states. This further indicates that there are basic underlying limitations in using the flight data. Again, since the main concern of this report is to outline the NIPIP analysis process and not to describe techniques in state variable estimation, only a single simple method of estimating $\dddot{h}$ was chosen. (Vide Appendix B.) Provided that the trimmed flight condition is

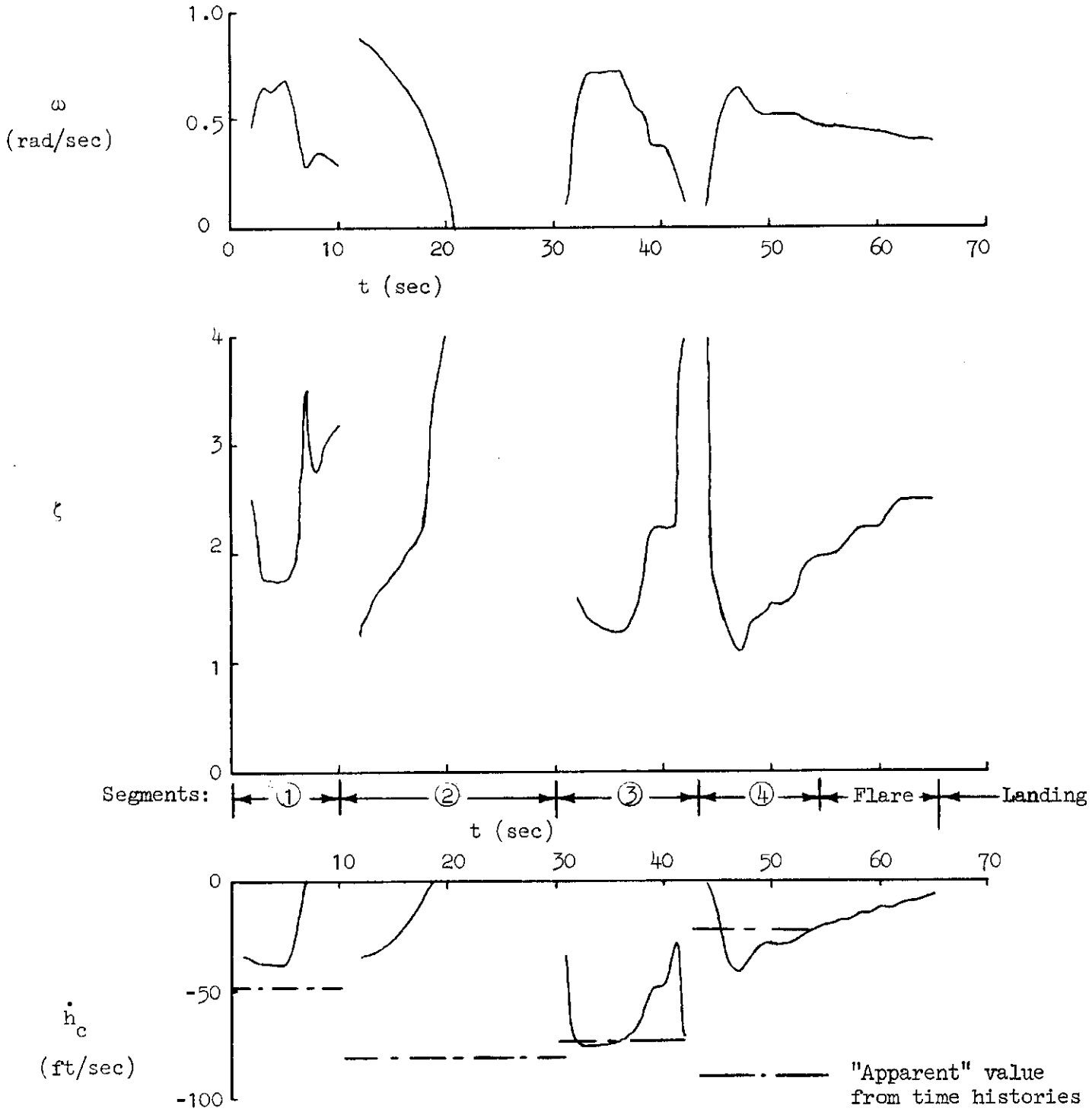

Figure 32. Case 5: Identified Parameters for the Longitudinal Closed-Loop Task Analysis, Lateral Offset Approach, Spot Landing

disturbed sufficiently, it would be possible, using more sophisticated filtering and estimation techniques, to reconstruct desired states in order to obtain more reasonable values of the second-order response parameters.

Finally in Segments 3 and 4 of Fig. 32, the overall trends in the identified solution are similar to those observed in Case 1. The identified closed-loop undamped natural frequency, ω_a, is in the range of 0.4 to 0.6 and the damping ratio, ζ_a, is greater than one. The vertical velocity command solutions appear to be reasonable for these segments.

2. Case 6: Longitudinal Pilot Control Strategy—Approach

Figure 33 shows the primary control and command loop state variables for the inner and outer loops. Also shown are the four approach segments. The flare segment will be discussed in Case 8. NIPIP was used to obtain estimates of Y_{p_θ} and $Y_{p_{\dot{h}}}$ for each of these finite time segments. The inner loop solutions are shown in Fig. 34. As before, the results are confounded by the fundamental flight data quality problem experienced in Case 2, and the identified solution in each case appears to be an integration.

This result is explained using the reasoning presented in Case 2. It is believed to be caused by the coarse quantization in pitch attitude in the flight data records. Thus, as before, the NIPIP solution yields a false pilot control strategy model.

For this case, additional degrees of freedom in the assumed form of Y_{p_θ} were tried and, as before, did not improve the identified solution.

The identification of the outer-loop pilot control strategy in Fig. 35 also suffered from similar problems experienced earlier in Case 2. It appears that $Y_{p_{\dot{h}}}$ simply reflects the ratio of the steady-state attitude to sink rate. Increased order for $Y_{p_{\dot{h}}}$ did little to help in identifying the pilot's control strategy.

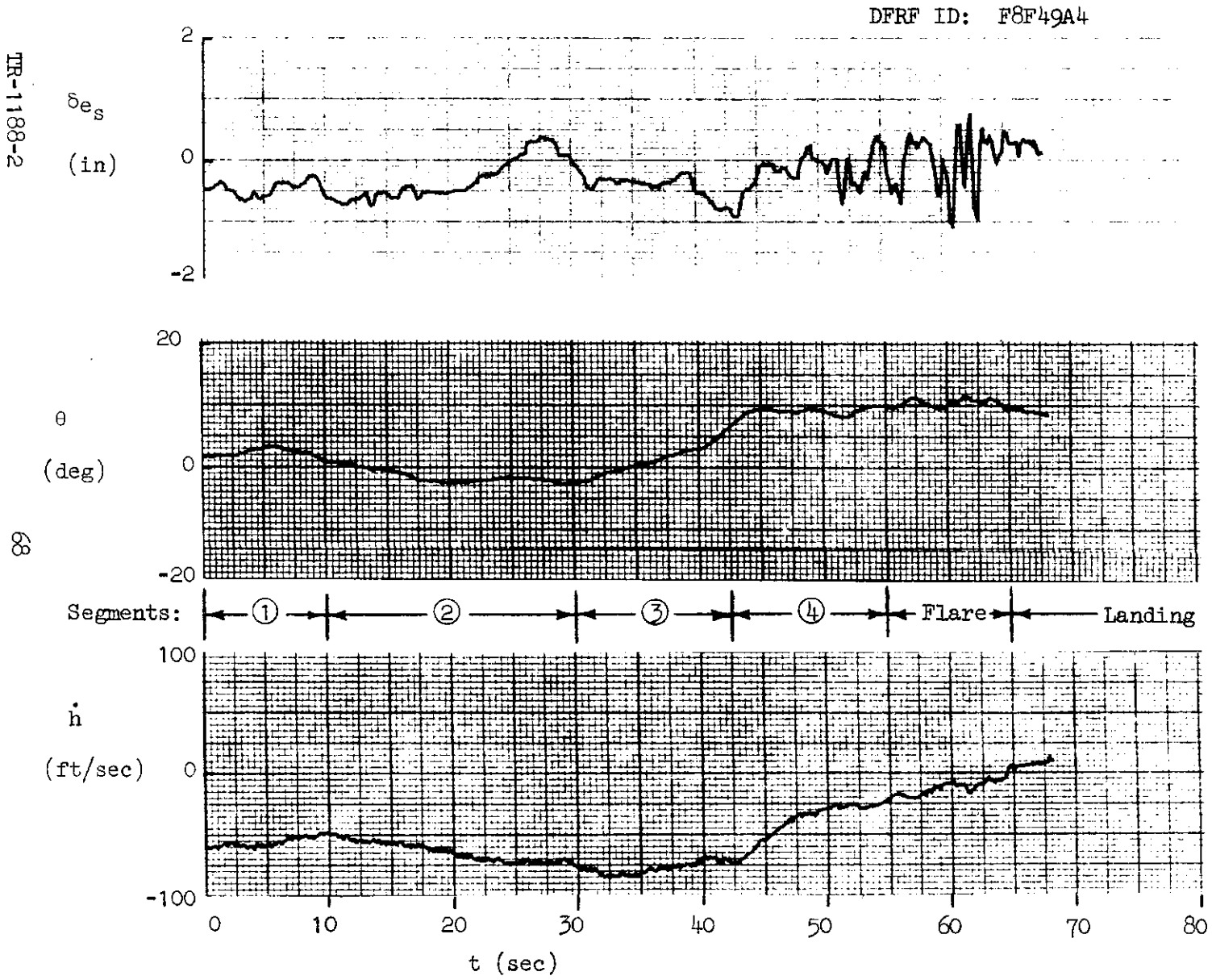

Figure 33. Case 6: Time Histories for Longitudinal Control Strategy, Lateral Offset Approach, Spot Landing

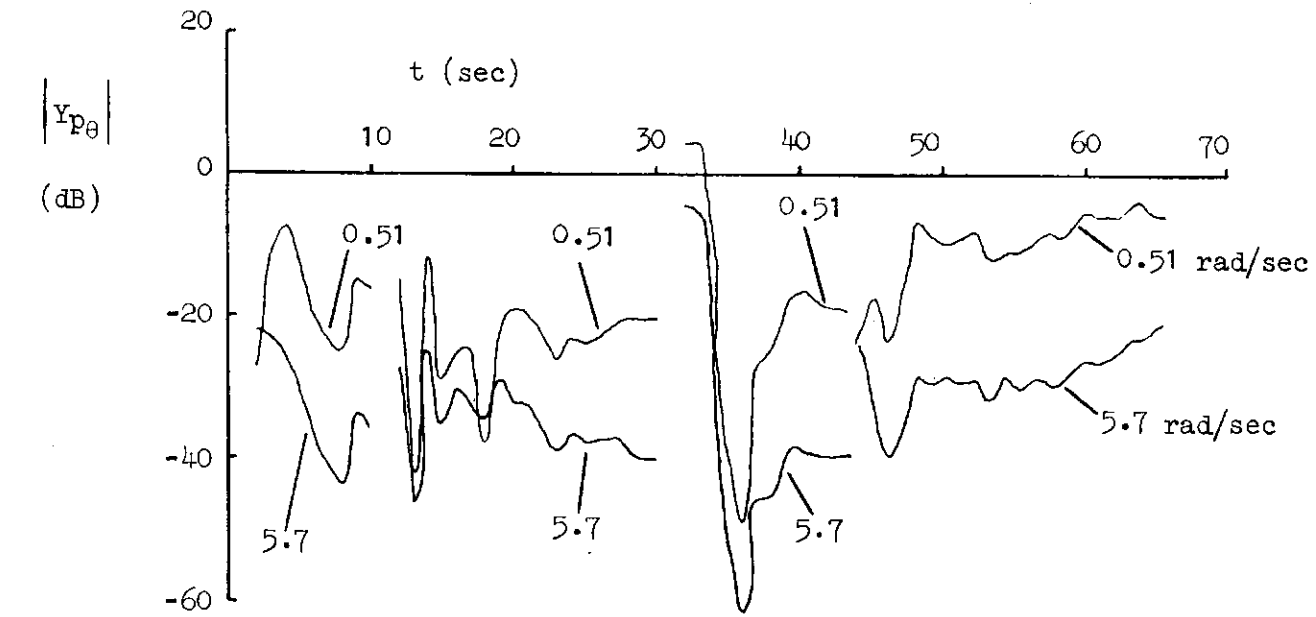

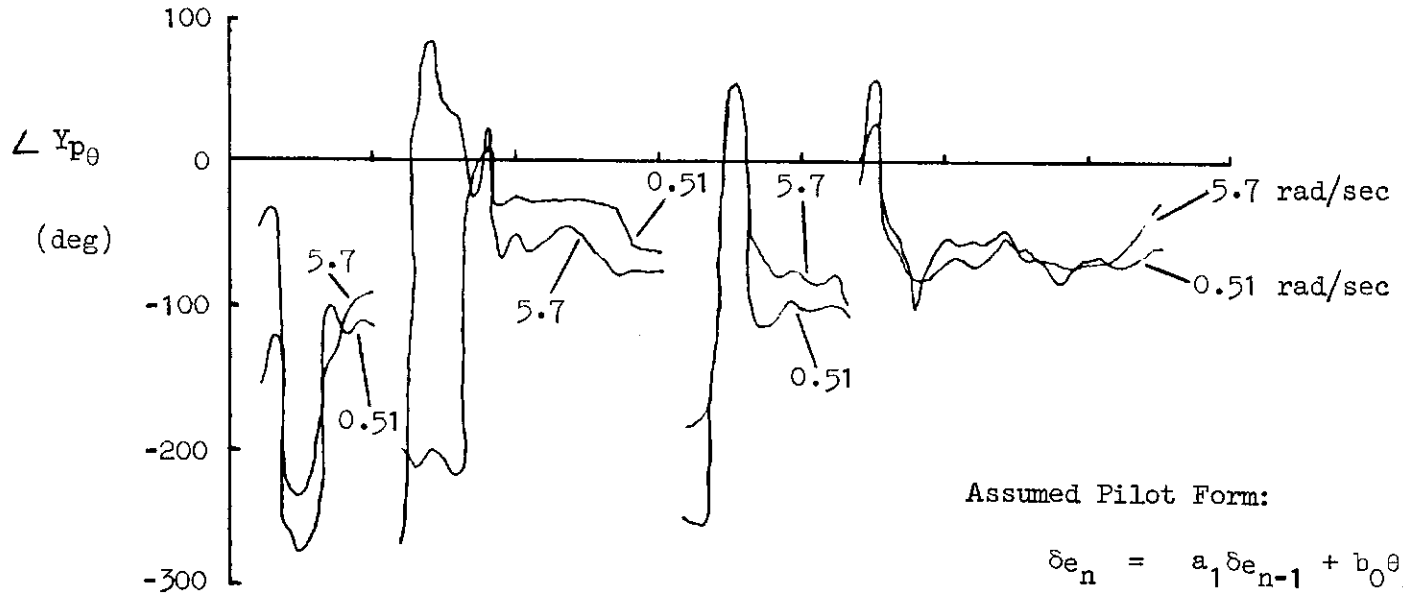

Assumed Pilot Form:

$$\delta e_n = a_1 \delta e_{n-1} + b_0 \theta_n + b_1 \theta_{n-1} + \text{bias}$$

Figure 34. Case 6: Inner Loop Pilot Longitudinal Control Strategy Solution, Lateral Offset Approach, Spot Landing

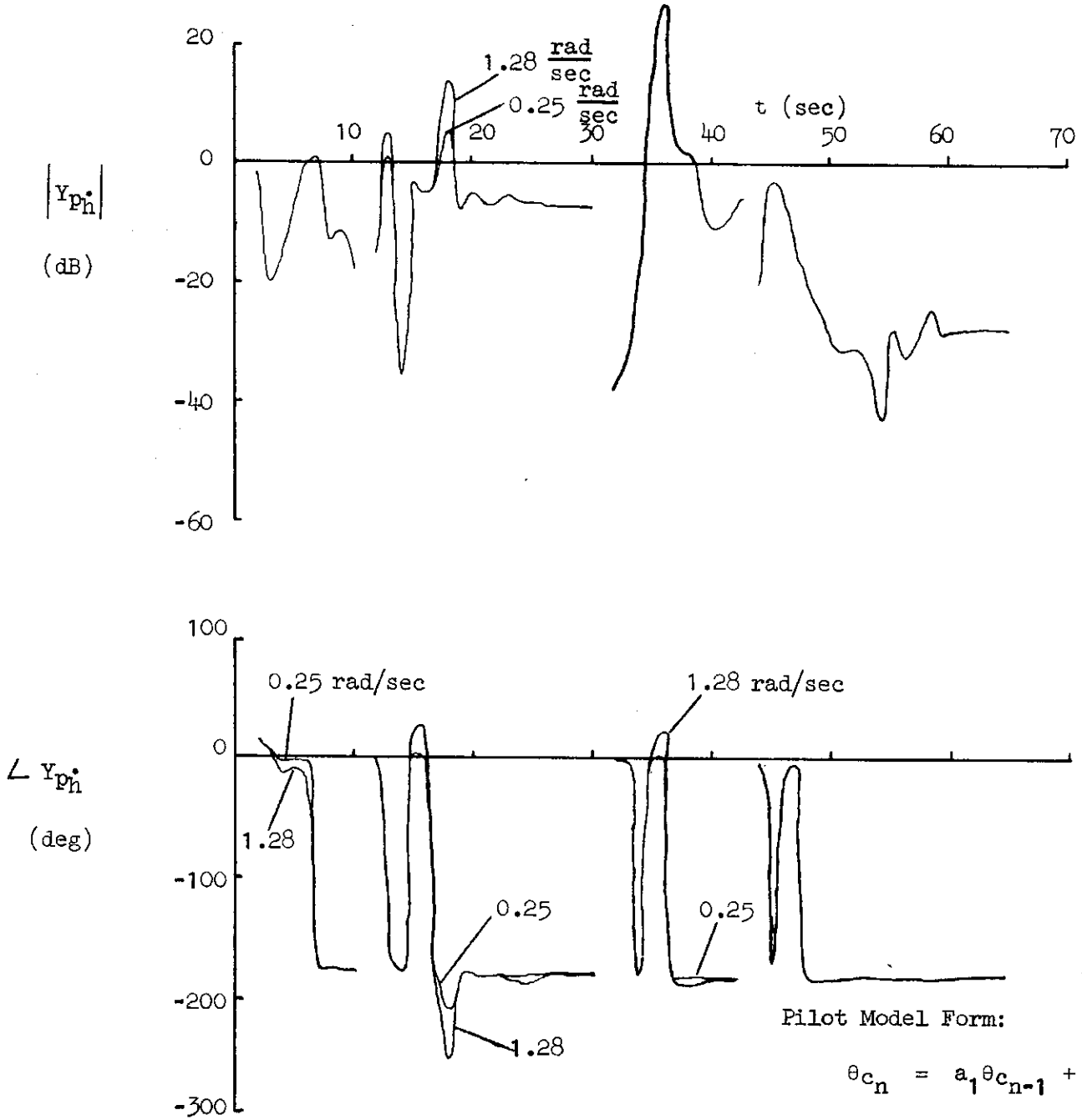

Figure 35. Case 6: Outer Loop Pilot Longitudinal Control Strategy Solution, Lateral Offset Approach, Spot Landing

3. Case 7: Lateral Pilot Control Strategy—Approach

As previously mentioned in Case 5, the lateral task during this approach differed from the first by the offset maneuver. In terms of the NIPIP solution for lateral control strategy, only two segments were used--course acquisition and offset maneuver. Figure 36 reveals the recorded variables as functions of time and identifies the two segments in which NIPIP was applied. A 2 to 3 deg/sec turn was in progress during the first half of the course acquisition segment. The second half of the course acquisition segment is labeled "final" where tracking of the final approach course commences and continues. One would hope that the heading control strategy via bank angle in Fig. 4(c) would yield valid solutions during at least the "final" half of the course acquisition.

Lateral inner-loop control strategy solutions for Y_{p_ϕ} in Fig. 37 during the initial turn start to converge on a first-order lag at 0.5 rad/sec and then shift to represent an integrator at about 15 sec. (Recall that -180 deg is the negative feedback reference for judging phase angle solutions for Y_{p_ϕ}.) This unexpected result was also observed in the former Lateral Case 3 in Fig. 25, although formerly during the straight final approach and not during the initial turn. Then in Fig. 37 when the final course has been acquired at 20 sec, the solution for the phase angle of Y_{p_ϕ} changes abruptly to represent the expected lead-lag compensation. Again at 30 sec there is a hint of another change in the amplitude of Y_{p_ϕ}.

The solutions for Y_{p_ϕ} in the "final" half of the course acquisition (i.e., the on-course portion) were recalculated using a segment between 20 and 45 sec. The results are shown in Fig. 38. Convergence appears to occur at 32 sec. The amplitude of Y_{p_ϕ} is about -30 dB at low frequencies and decays at -10 dB/decade in the frequency decade from 0.51 to 5.77 rad/sec. The phase angle of Y_{p_ϕ}, which is -187 deg at 0.1 rad/sec, changes to -200 deg at 0.51 rad/sec and to -215 deg at 5.77 rad/sec. (Recall that the negative feedback reference angle for Y_{p_ϕ} is -180 deg.) Clearly this is lag compensation, albeit slight, and not lead-lag compensation as Fig. 37 appeared to suggest. This unexpected low frequency lag

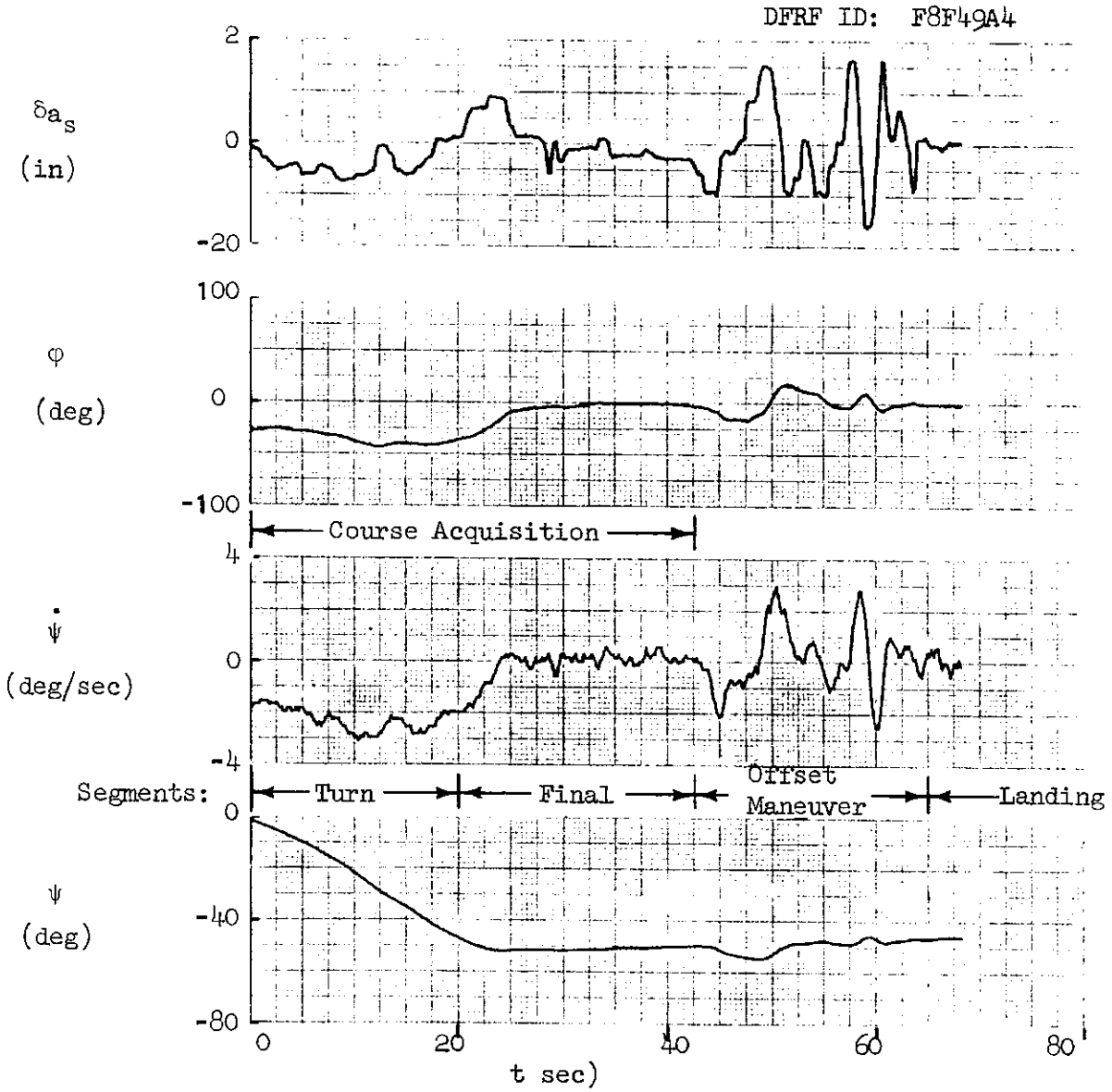

Figure 36. Case 7: Time Histories for Lateral Control Strategy, Lateral Offset Approach, Spot Landing

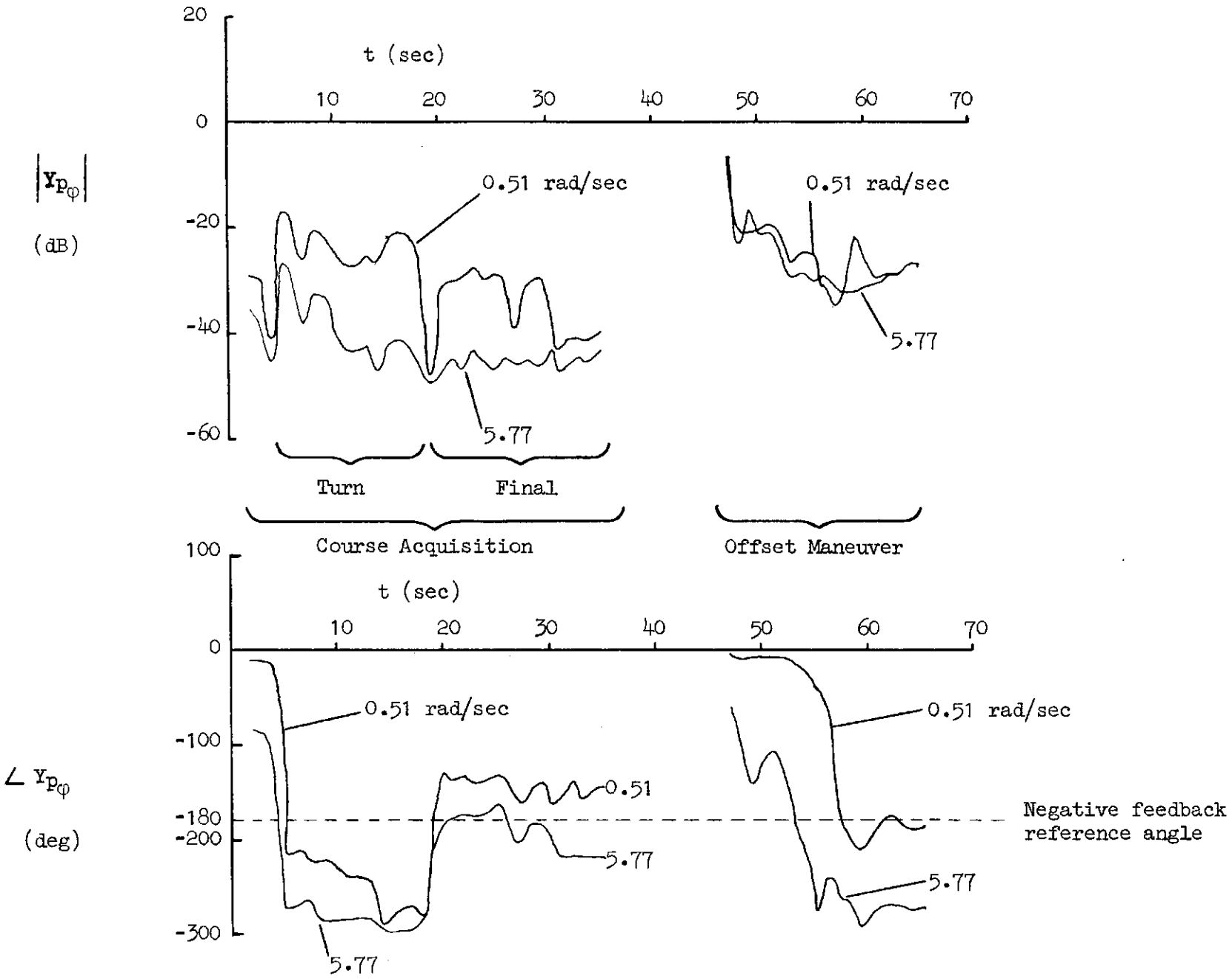

Figure 37. Case 7: Inner Loop Pilot Lateral Control Strategy, Lateral Offset Approach, Spot Landing

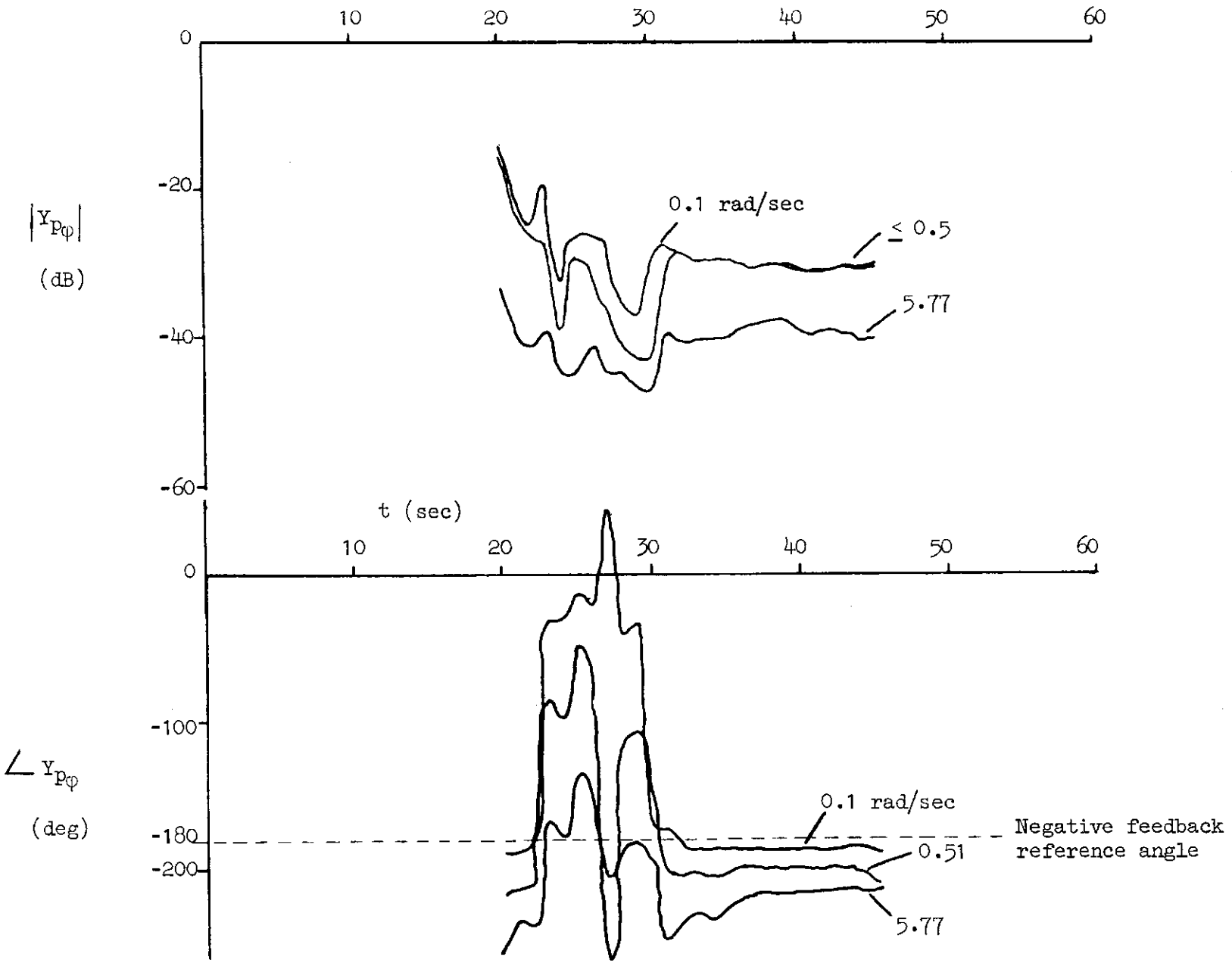

Figure 38. Case 7: Inner-Loop Pilot Lateral Control Strategy for On-Course Segment

(circa 0.5 rad/sec) in the estimated roll control strategy may have resulted from the division of attention between flare control and line-up control coupled with the apparent absence of disturbing variability in crosswind affecting lateral displacement, heading, and roll attitude. Consequently less frequent roll attitude corrections were needed during this particular on-course segment. The solutions for Y_{p_ϕ} during the "offset maneuver" in Fig. 37 appear to converge only after 60 sec to represent a pure gain of -30 dB and a time delay of about one-quarter second, both of which are at least plausible.

Heading control strategy solutions for Y_{p_ψ} in Fig. 39 during the initial turn appear to be incorrect, because the large turn rate command was not incorporated as a dependent variable. Even after course acquisition occurs at 20 sec, the solutions for Y_{p_ψ}, although changed, still appear to be incorrect. We would expect a pure gain on the order of 10 dB (3 deg/deg) for Y_{p_ψ} between 20 and 45 sec. The solutions for Y_{p_ψ} during the "offset maneuver" in Fig. 38 do not appear to converge at all.

The solutions for Y_{p_ψ} in the "final" half of the course acquisition (i.e., the on-course portion) were recalculated using a segment between 20 and 45 sec. The results are shown in Fig. 40, which is the counterpart of Fig. 38 for Y_{p_ϕ}. Convergence appears to occur at 32 sec. The amplitude of Y_{p_ψ} is about +10 dB (3 deg/deg) at low frequencies (0.05 and 0.2 rad/sec) and rises only about 2 to 4 dB in the frequency decade from 0.2 to 2 rad/sec; the phase angle is about zero at low frequencies and rises only about 10 to 20 deg on the same frequency decade (0.2 to 2 rad/sec). Thus Y_{p_ψ} is nearly the pure gain expected with a very slight tendency for lead compensation, and it exhibits a slightly increasing gain with time to over +12 dB (4 deg/deg). These results appear to be plausible and compatible with the value of 3 deg/deg inferred from pilot training guides in Ref. 5.

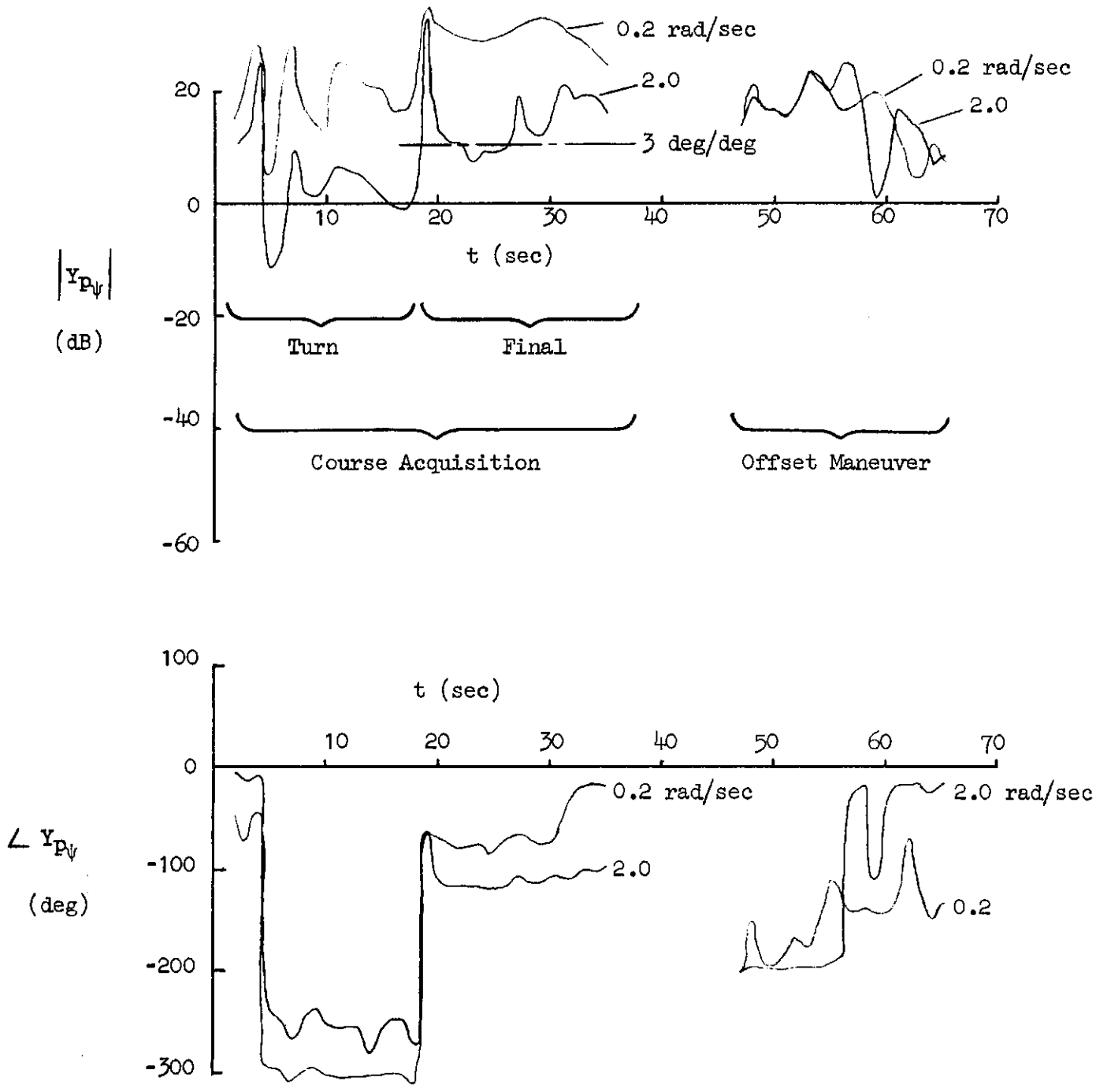

Figure 39. Case 7: Outer Loop Pilot Lateral Control Strategy, Lateral Offset Approach, Spot Landing

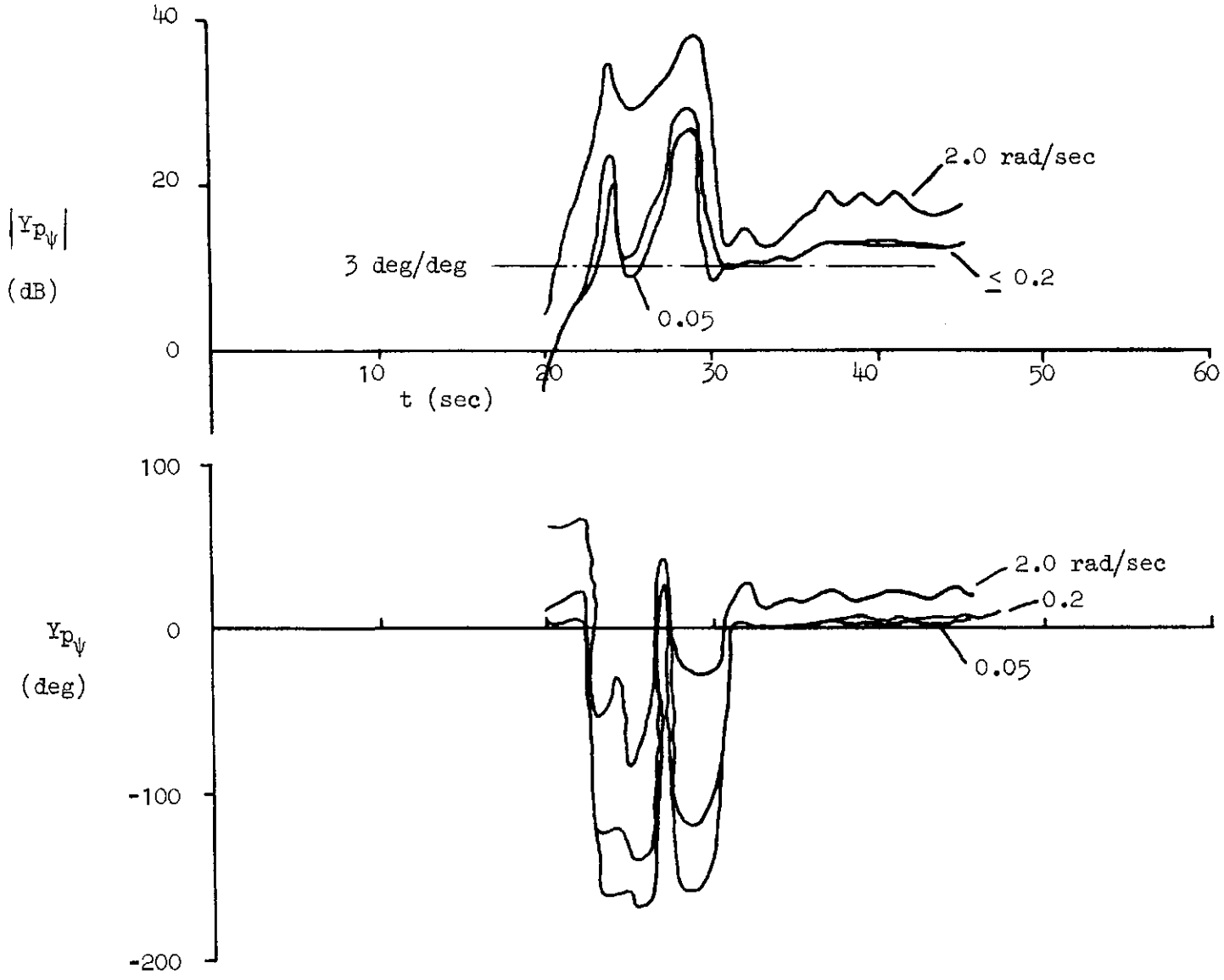

Figure 40. Case 7: Outer Loop Pilot Lateral Control Strategy for On-Course Seqment

4. Case 8: Flare Maneuver

As shown in Figs 41 through 44, the results are similar to those obtained in the former (Case 4) Figs. 24 through 27. The large (30 ft) height quantization band evident in the phase plane of Fig. 41 precludes reliable estimates of the undamped natural frequency and damping ratio of the closed-loop flare in Fig. 42. The solutions failed to converge in the cross hatched interval in Fig. 42. The undamped natural frequency ultimately converged on a value of approximately 0.25 rad/sec, which is comparable to other flight results in Ref. 6; but, as in Case 4, the damping ratio converged in the neighborhood of 0.2, an unexpectedly low value for such a protracted floating flare.

The inner- and outer-loop pilot control strategy solutions are shown in Figs. 43 and 44, respectively, and are practically pure gains. Attitude gain, Y_{p_θ}, is about 0.3 (-10 dB), which is triple that value found previously for the flare in Fig. 26 (Case 4), perhaps because the pilot was to fly a spot landing in the present case. Yet the outer loop gain, Y_{p_h}, is again identified in Fig. 43 as 0.01 deg/ft (-40 dB) (cf. Fig. 27, Case 4) before the solution becomes invalid, because the altitude remains invariant within the last quantization band, whereas the vertical velocity remains negative until touchdown.

C. VEHICLE IDENTIFICATION—CASES 9 AND 10

This topic describes and demonstrates two possible techniques for identifying the transfer functions between the perturbed body-axis normal acceleration, a_z, and the body-axis pitch acceleration, $\dot{q}$, due to the elevator, δ. The first technique employs specific forms for transfer functions between the vehicle accelerations and controls with undetermined parameters. NIPIP can then be used to determine the unknown parameters. This technique is similar to the pilot identification method demonstrated above and in Ref. 7. Using the "short-period approximation," Ref. 15, the required transfer functions are given below:

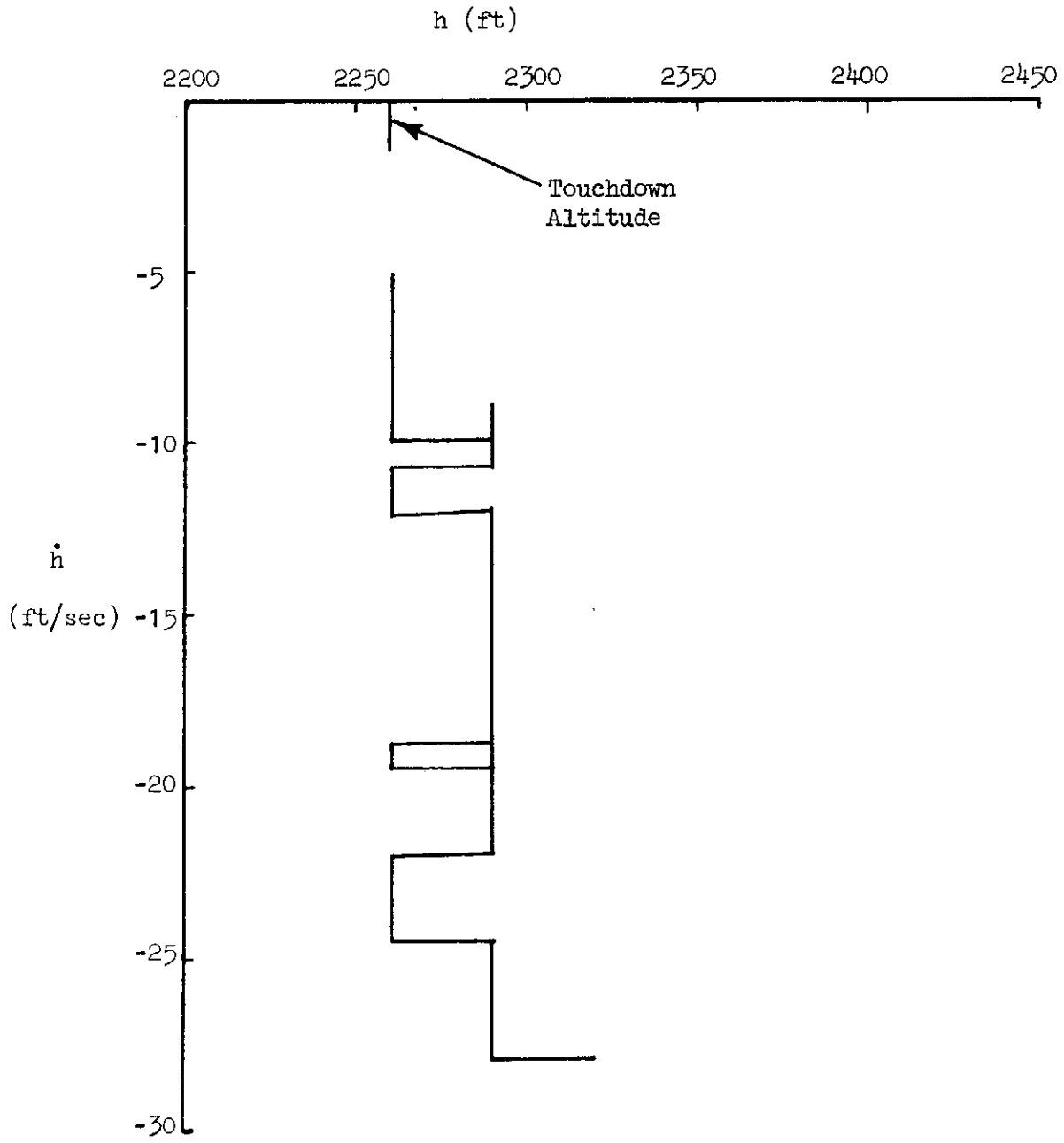

Figure 41. Case 8: Phase Plane for Landing Flare Analysis, Lateral Offset Approach, Spot Landing

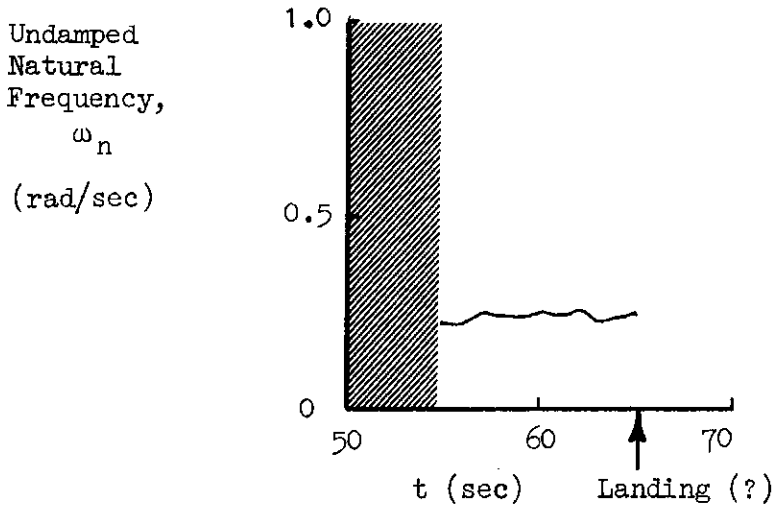

Solutions failed to converge in the shaded interval

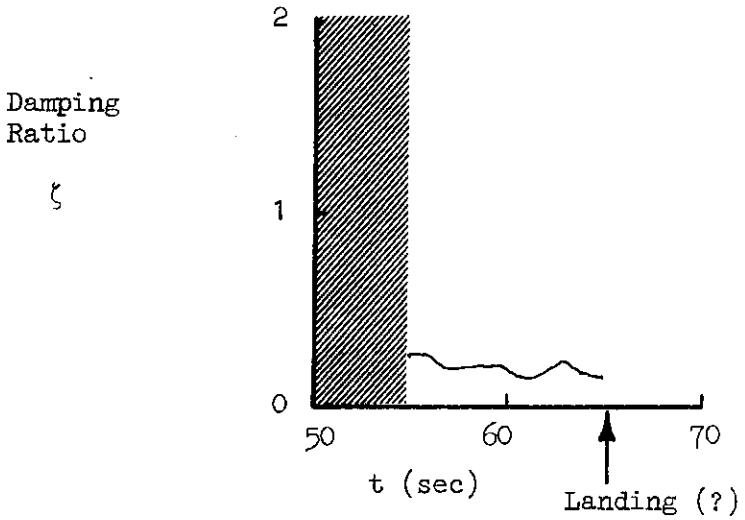

Figure 42. Case 8: Identified Parameters for Closed-Loop Flare Task Analysis, Lateral Offset Approach, Spot Landing

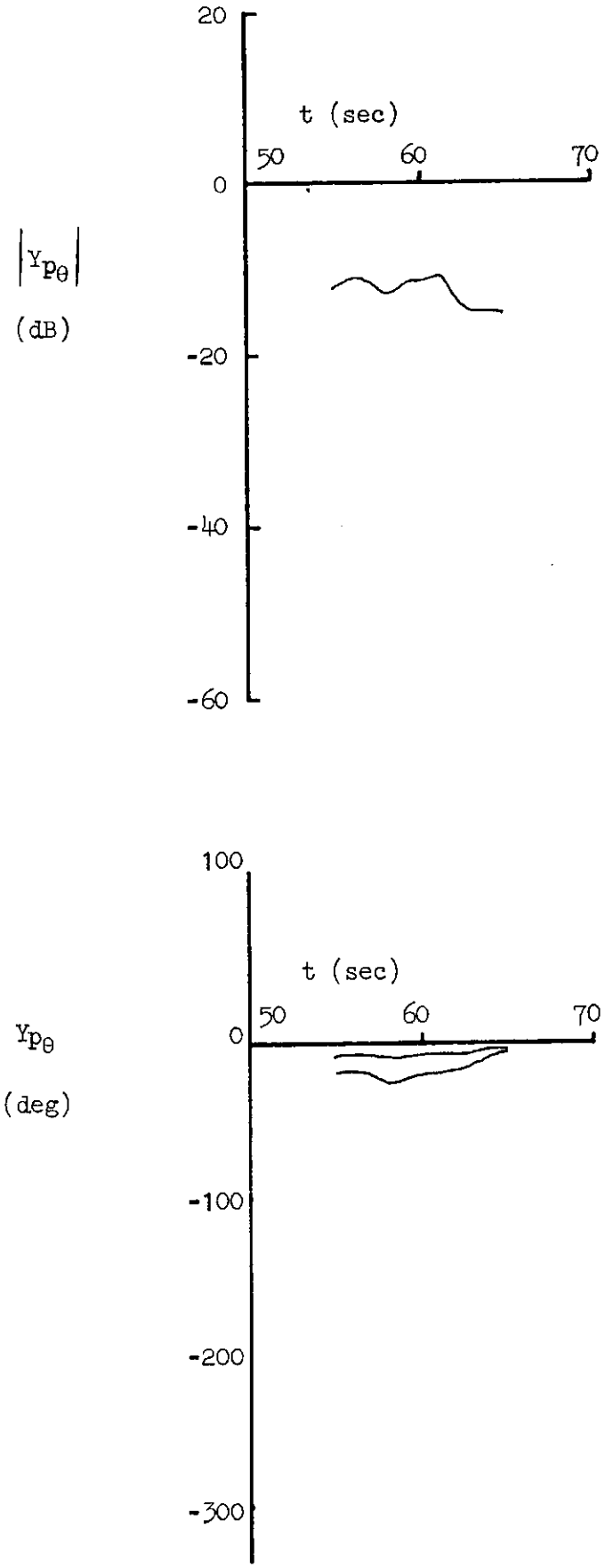

Figure 43. Case 8: Inner Loop Pilot Longitudinal Control Strategy Solution, Lateral Offset Approach, Spot Landing

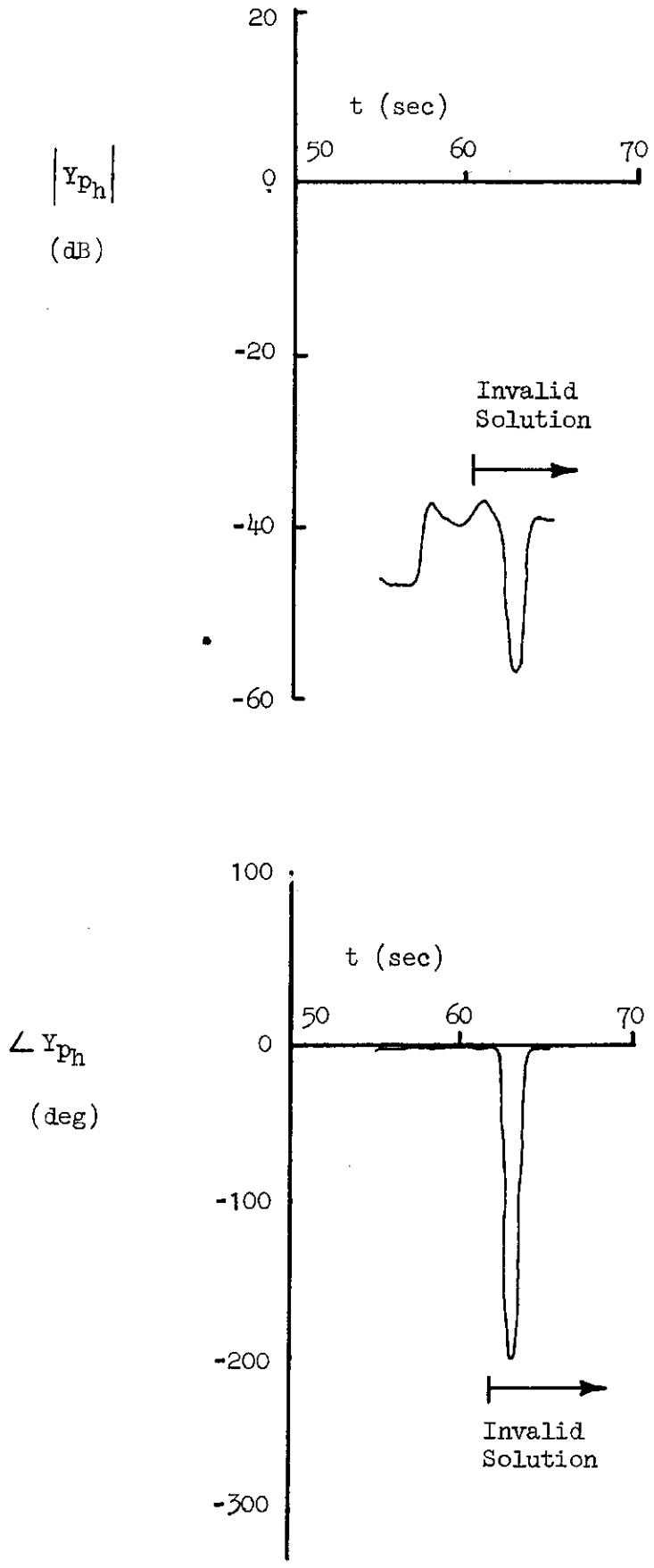

Figure 44. Case 8: Outer-Loop Pilot Longitudinal Control Strategy Solution, Lateral Offset Approach, Spot Landing

$$\frac{a_z}{\delta}(s) \doteq A_{a_z} \frac{s^2 + 2\zeta_{a_z}\omega_{a_z}s + (\omega_{a_z})^2}{s^2 + 2\zeta_{sp}\omega_{sp}s + (\omega_{sp})^2} \tag{21}$$

$$\frac{\dot{q}}{\delta}(s) \doteq A_q \frac{s(s + 1/T_{\theta_2})}{s^2 + 2\zeta_{sp}\omega_{sp}s + (\omega_{sp})^2} \tag{22}$$

The z-transform equivalents of Eqs. 21 and 22 are used as inputs to NIPIP; the outputs of NIPIP are frequency responses of $\hat{a}_z/\delta$ and $\hat{q}/\delta$.

The problem with this first technique, however, is the tacit assumption that all changes in the vehicle accelerations are due to the specified control deflections. If the vehicle is being disturbed by gusts or by another control the results will be erroneous. This was proven to be true when this technique was applied to flight test data for the F-8 aircraft described in Ref. 7. The transfer function technique could not identify a_z/δ or q/δ when the simulated pilot-vehicle system was evidently disturbed by random turbulence. Because this technique was unsuccessful, no presentation of the results is made here. The second technique, described below, was successful in identifying coefficients of equations describing the F-8 aircraft from the same flight test data; therefore we will present results only for the second technique.

The second technique is to specify forms for the equations of motion of the vehicle and then to use NIPIP to determine the unknown parameters. The following relations between <u>total</u> body-axis normal acceleration, A_z, body-axis pitch acceleration, $\dot{Q}$, and the aircraft states are used as inputs to NIPIP,

$$\frac{A_z}{U^2} = Z_{UW}\alpha + Z_{WW}\alpha^2 + Z_{U\delta}\delta + Z_{UU} \tag{23}$$

$$\frac{\dot{Q}}{U^2} = M_{UW}\alpha + M_{UQ}\frac{Q}{U} + M_{\dot{W}}^{\bullet}\frac{\dot{W}}{U^2} + M_{U\delta}\delta + M_{UU} \tag{24}$$

In Eqs. 23 and 24, U is the airspeed, α is the angle of attack, δ is the elevator, and the coefficients are called "total" derivatives (Ref. 16). The total derivatives are related to the small perturbation stability and control partial derivatives* as follows:

$$Z_u = 2U_o\left[Z_{UU} + Z_{U\delta}\delta_o\right] + Z_{UW}W_o \tag{25}$$

$$Z_w = Z_{UW}U_o + 2Z_{WW}W_o \tag{26}$$

$$Z_\delta = Z_{U\delta}U_o^2 \tag{27}$$

$$M_u = 2U_o\left[M_{UU} + M_{U\delta}\delta_o\right] + M_{UW}W_o + M_{UQ}Q_o \tag{28}$$

$$M_w = M_{UW}U_o \tag{29}$$

$$M_q = M_{UQ}U_o \tag{30}$$

$$M_{\dot{w}} = M_{\dot{W}}^{\bullet} \tag{31}$$

$$M_\delta = M_{U\delta}U_o^2 \tag{32}$$

$$U_o = V_{T_o}\cos\alpha_o \tag{33}$$

$$W_o = V_{T_o}\sin\alpha_o \tag{34}$$

*The partial derivatives are defined in Ref. 15.

The outputs of NIPIP (i.e., the "total" derivatives in Eqs. 23 and 24) are used as inputs to Eqs. 25 through 34. Frequency responses of $\hat{a}_z/\delta$ and $\hat{q}/\delta$ can then be obtained by using approximate factors (Ref. 15) to calculate the gains, damping ratios, and undamped natural frequencies of Eqs. 21 and 22.

The time histories of aircraft states shown in Fig. 45 were used to demonstrate the vehicle identification technique described above. The data are from a formation flight task using the NASA DFRF F-8 aircraft. The pilot's task was to acquire and then maintain a constant distance between his own and another aircraft.

The climb and acquisition of altitude during the first 50 sec of the time history was not part of this task and was therefore ignored. NIPIP was then set up to provide estimates using a fixed window every 10 sec between 60 and 80 sec. Table 4 summarizes the small perturbation stability and control partial derivatives at 60, 70, and 80 sec. As stated previously, these partial derivatives were then used to compute transfer functions via approximate factors, which in turn were used to compute the frequency responses for $\hat{a}_z/\delta$ and $\hat{q}/\delta$ shown in Figs. 46 and 47, respectively. The figures show a well-damped short period ($\zeta_{SP} \doteq 0.5$) with a natural frequency of about 1.5 rad/sec. The pitch numerator zero, $1/T_{\theta_2}$, is about 0.5 rad/sec.

Figures 46 and 47 also show estimates of DFRF F-8 aircraft frequency responses based on wind tunnel data with the SAS on. Note that the two sets of frequency responses are not in very good agreement. A detailed investigation into the reason for these differences was considered beyond the scope of this report. However we did compare the two different estimates of transient responses to the actual F-8 aircraft responses in the time domain. The comparison is summarized in Fig. 48. Note that the NIPIP estimate of q and a_n due to δ is much closer to the actual F-8 response than the wind tunnel estimate.

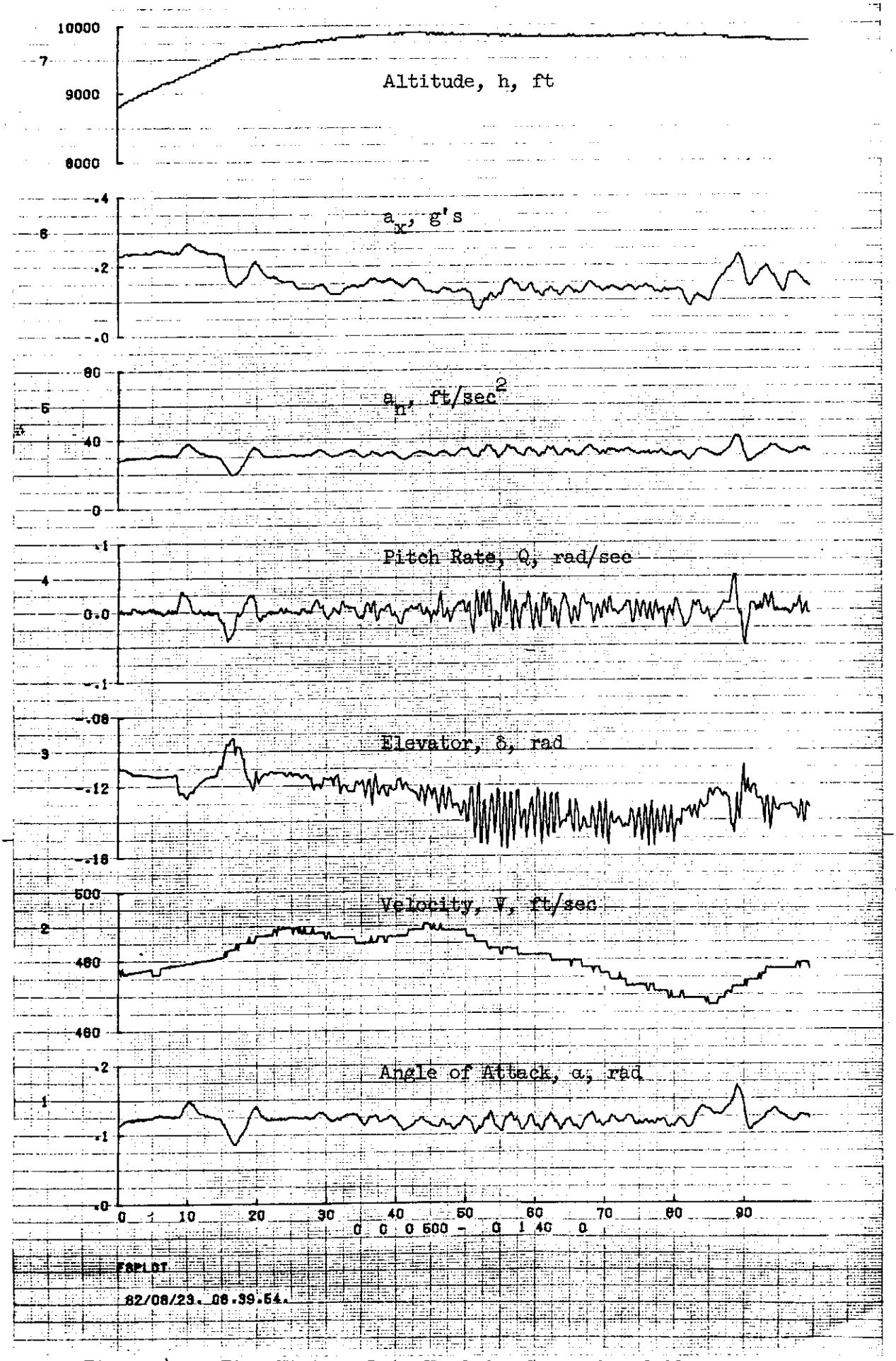

Figure 45. Time History Data Used for Cases 9 and 10
(DFRF Flight 49, Form 1)

TABLE 4

ESTIMATED STABILITY AND CONTROL DERIVATIVES FOR THE DFRF F-8 AIRCRAFT
(Flight 49, Form 1)

t (sec)	N	$R^2_{a_z}$	$R^2_{\dot{q}}$	Z_u (1/sec)	Z_w (1/sec)	Z_δ (ft/sec^2/rad)	M_u (1/sec-ft)	M_w (1/sec-ft)	M_q (1/sec)	M_δ (1/sec^2-rad)	$M_{\dot{w}}$ (1/ft)
60	100	0.996	0.930	-.0021	-.422	102.2	-.0045	-.0057	-1.35	-7.1	0.0003
70	200	0.996	0.909	-.0433	-.376	103.4	-.0044	-.00593	-1.29	-6.84	0.0002
80	300	0.996	0.868	-.0580	-.356	103.4	-.0042	-.00597	-1.10	-6.40	.000015

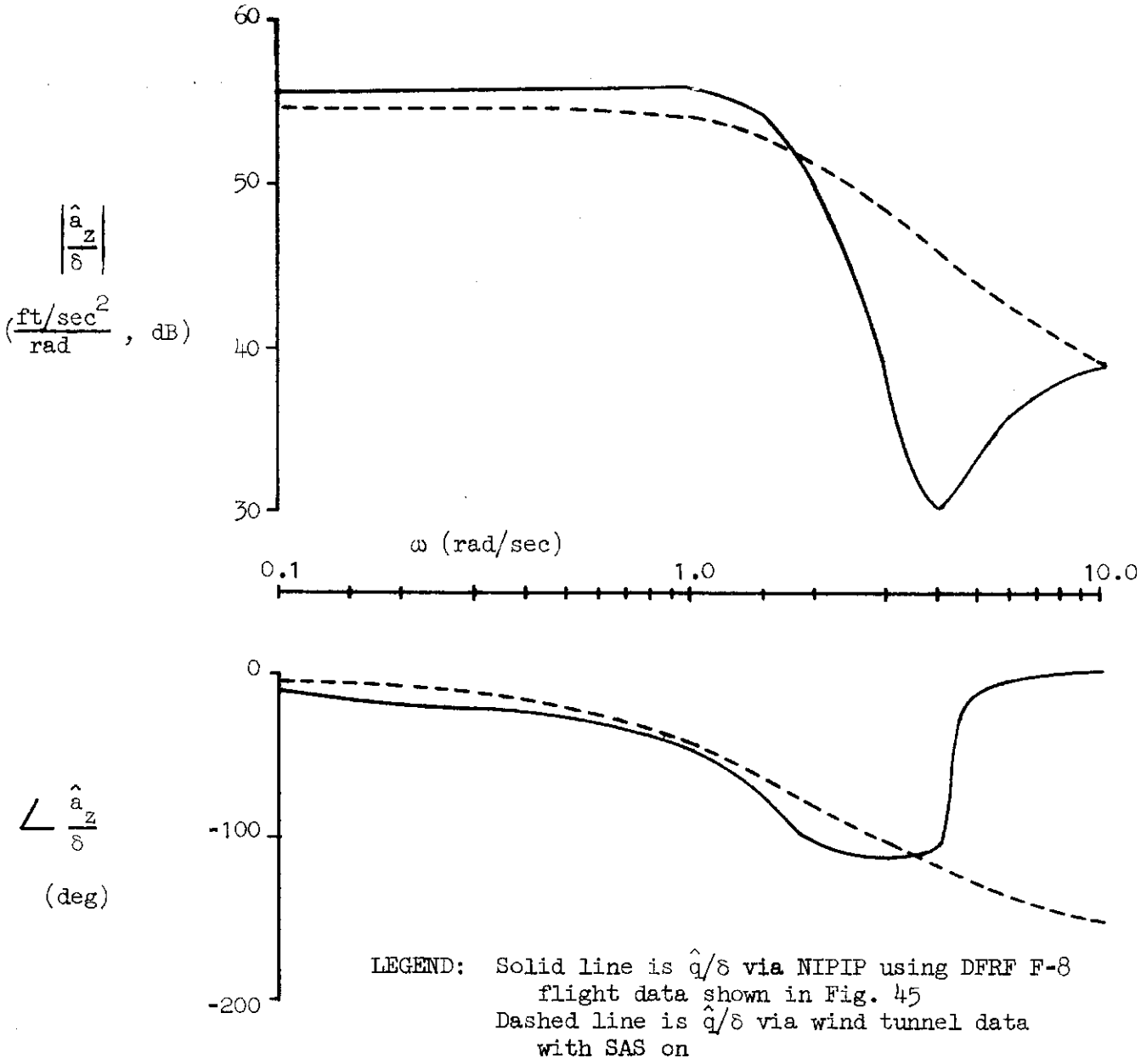

Figure 46. Estimated a_z/δ Frequency Response for the DFRF F-8 Aircraft

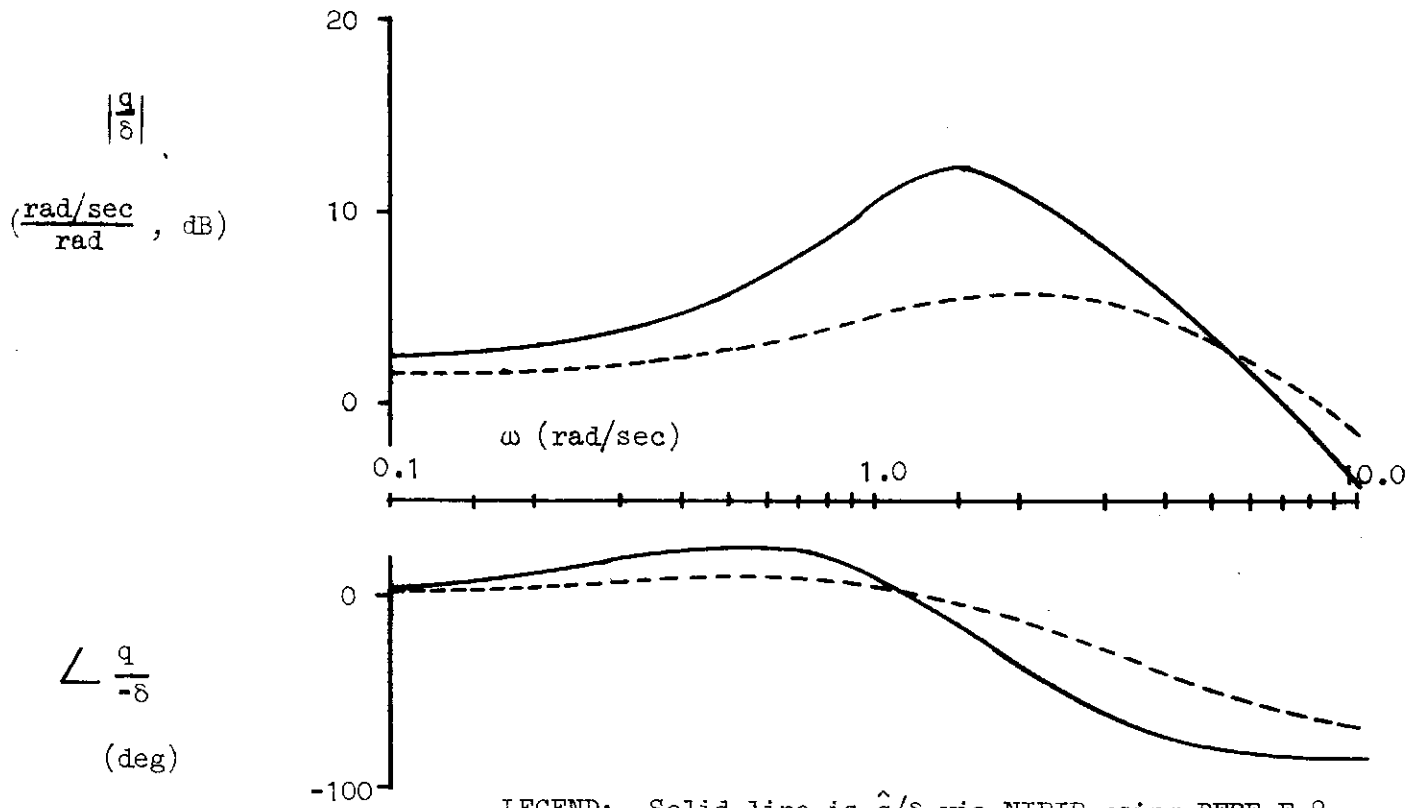

Figure 47. Estimated q/δ Frequency Response for the DFRF F-8 Aircraft

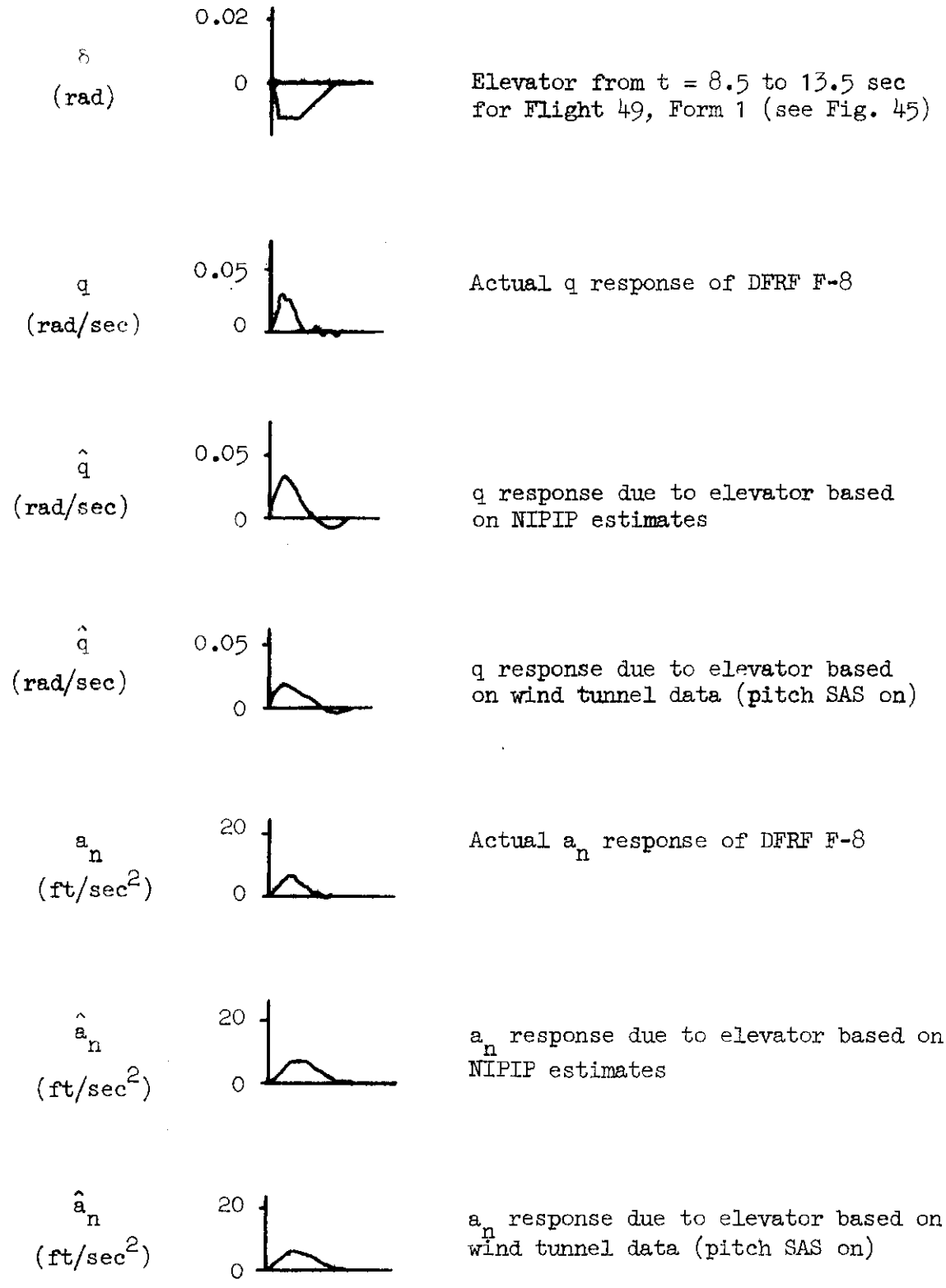

Figure 48. Comparison of Estimated and Actual Pitch Rate and Specific Force Responses Due to Elevator

SECTION V

RECOMMENDATIONS FOR APPLYING NIPIP

This project was centered around the development of a user-oriented software package and the exercising of that software using actual flight data. At this point we shall present recommendations for applying NIPIP to other programs along with suggestions for enhancing the present software package.

A. GENERAL RECOMMENDATIONS

Regardless of the specific application, the pilot-vehicle tasks, commands, and external disturbances must be sufficient to excite the relevant states of the vehicle and to require pilot control activity. In applying NIPIP the analyst should remember that a trimmed aircraft usually reveals little or nothing about the pilot's control strategy, because the pilot is, by definition, not actively involved in the control process after the aircraft has been trimmed.

The analyst of pilot control strategy should always start with suitable mathematical models of the task(s) and the controlled element before attempting to interpret the results of the NIPIP. This preparation not only increases the likelihood that the relevant candidates for the control loop structure will be exposed but also prepares the analyst with rational estimates for ranges of frequency bandwidth and likely forms of pilot compensation.

Flight data instrumentation requirements are a direct function of what piloting tasks are to be considered. For each identifiable task or "outer" control loop the following data are necessary--either from direct measurement or by suitable estimation:

- The command loop state variable for the task
- Its first and, if possible, second derivatives with respect to time
- The primary "control"
- Any states which may be associated with intermediary or "inner" control loops needed for performing the task. There may even be alternative competing candidates for inner loops.

Simulator-generated data are more likely to be complete, accurate, and noise-free, but flight data will usually suffer omissions and distortions.

The sampling rate requirements for NIPIP depend upon the bandwidth of the loop being examined. Solutions for outer- (task) loop pilot control strategy or task execution dynamics should normally require less frequent sampling than for inner-loop characteristics. Where inner- and outer-loop characteristics are estimated simultaneously (as in the previous approach cases) then the inner-loop bandwidth should dictate sampling rate. The rate of 50 samples/sec was found adequate for successful analysis of helicopter maneuvering

Nonlinearities related to quantization or roundoff of recorded data should be viewed with concern. Double precision (e.g., coarse channel plus fine channel) may be necessary for any states crucial to a given piloting task. The quantization bands of θ and ϕ for the DFBW F-8 (0.1 deg and 0.02 deg) might be used as guides for unacceptable and acceptable coarseness of attitude angles, respectively. The 30 ft quantization of height was unacceptable for identification in the flare task and precluded analysis of the formation flight task.

It is also recommended that careful consideration be given beforehand to data reconstruction and estimation schemes for any important state variables which cannot be directly measured and/or recorded, because such advance consideration may well exert an influence on the repertory of variables that can be measured and recorded.

B. AFTI/F-16 APPLICATIONS

Simulation of the overall task, pilot, and vehicle is an excellent way to verify the NIPIP outputs. That is, use the NIPIP outputs to simulate the pilot's control strategy and then compare the simulated outputs of the task, pilot, and vehicle to the actual outputs.

One particularly attractive target for NIPIP application is the Advanced Fighter Technology Integration (AFT)I/F-16 flight program. Its concern with how to use the many varied mission-oriented flight control modes makes direct measurement of pilot control strategy and task execution an appealing option.

The following excerpt, taken from Ref. 17, provides a short background description of the AFTI/F-16 and its program objectives.

> "The Advanced Fighter Technology (AFTI)/F-16 program is in response to today's European scenario, characterized by increased numbers of enemy targets both on the ground and in the air and an increasingly hostile air space surrounding these targets. This changing environment required timely improvements in present USAF fighter lethality and survivability. The primary and continuing objective of the AFTI program, co-sponsored by the Air Force, NASA, and Navy is to provide for the development, integration, flight evaluation, and demonstration of emerging fighter technologies, and transition of the integrated technologies to future system applications. The AFTI Fighter Attack Technology (AFTI/F-16) program will develop, integrate, and flight test a set of technologies to improve the survivability and weapon delivery accuracy of tactical fighters in air-to-air and air-to-ground attacks, through integration of advanced technologies into a single seat demonstrator vehicle which permits a realistic evaluation of technology benefits, penalties, and overall mission effectiveness.
>
> "The AFTI/F-16 vehicle has particular importance as a long life demonstrator aircraft with the flexibility, versatility, and capability in terms of performance and systems to serve as a future technology development testbed. A full-scale development F-16 aircraft is the test vehicle. Extensive modifications were made for installation of a sophisticated data instrumentation

system, modified inlet with canards, new flight control system, and a dorsal fairing to accommodate the instrumentation equipment. Additional information on the AFTI/F-16 can be found in Ref. [18].

"The overall objective of the AFTI/F-16 Advanced Development Program is to demonstrate separately, and in combination, advanced fighter technologies to improve air-to-air (AA) and air-to-surface (AS) weapon delivery accuracy and survivability. These technologies include a Digital Flight Control System (DFCS), Automated Maneuvering Attack System (AMAS), pilot/vehicle interface (PVI) advancements, and advanced task-tailored control modes utilizing direct force control and weapon line pointing. Development, integration, and flight validation of these fighter attack technologies have been separated into DFCS and AMAS program phases.

"The DFCS is a full-authority, triplex, digital fly-by-wire flight control system. The DFCS is mechanized to implement task-tailored manual control modes, including decoupled (six independent degrees of freedom of control-configured vehicle) flight control. Figure [49] shows that the pilot need only push a button to change the functions of cockpit controllers and displays. For the AMAS phase, the effective utilization of the advanced technologies requires the integration (coupling) of the fire and flight control functions. The integrated system will tie together a director fire control system, an advanced sensor-tracker, and the flight control system to provide precise automated weapon line control and weapons delivery. With the coupled system the azimuth and elevation fuselage pointing capability of the aircraft provides an expanded envelope of fire control solutions; i.e., an enlarged pipper. The pilot need only capture the target within the expanded pipper envelope, and the fire control system will automatically command the flight control system to null aiming errors to assure a hit. This concept will profoundly influence fighter effectiveness in both AA and AS missions.

"Pilot/vehicle interface advancements will be incorporated to provide crew station capabilities and environment commensurate with the increase in total vehicle capabilities provided by the other technologies in each phase. The DFCS phase will focus on core technology development. The technologies of prime interest will be manual flight path control, avionics integration, and advanced controllers and displays. In the AMAS phase the allocation of function between the pilot and vehicle will be redistributed as a result of the DFCS experience.

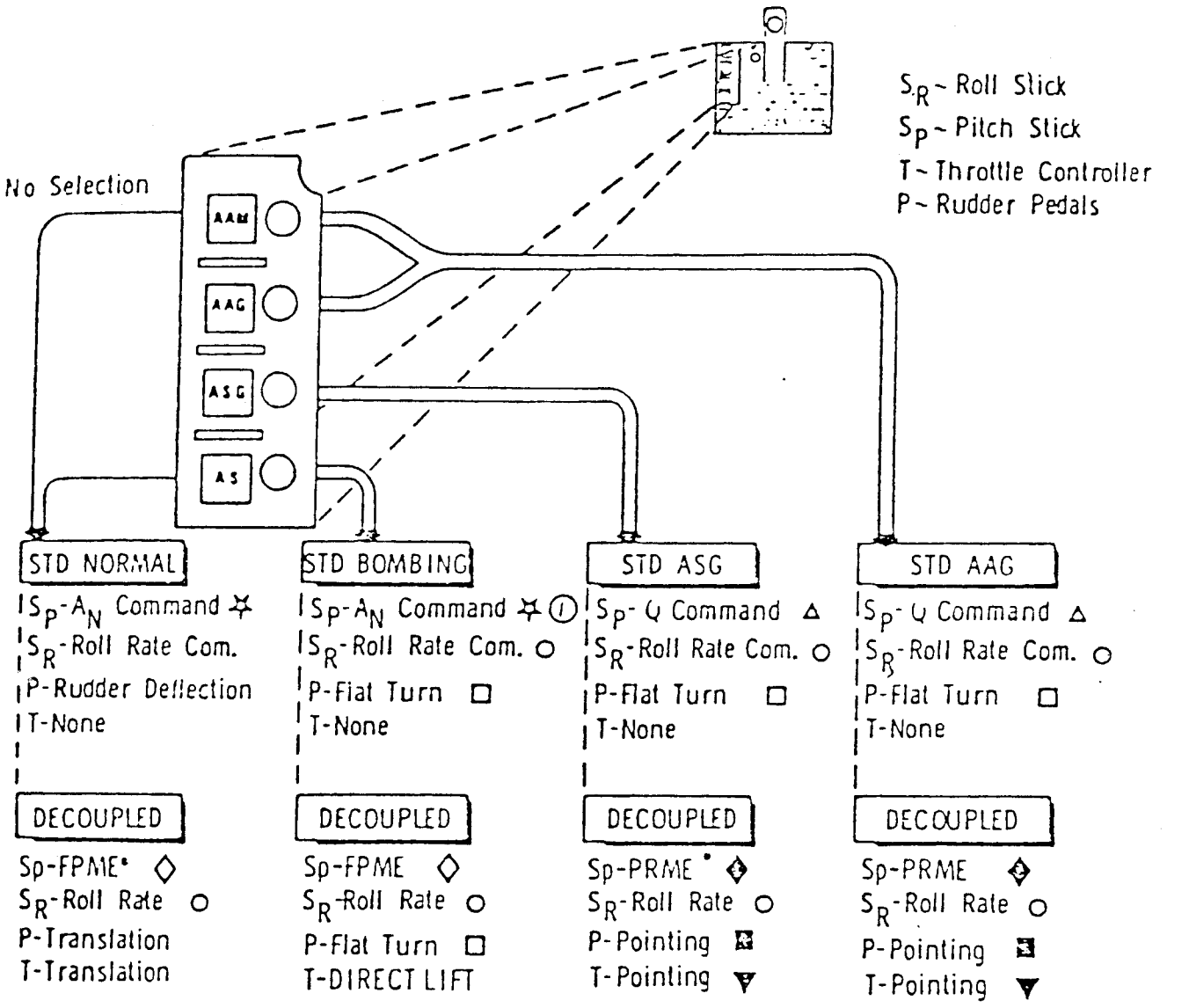

NOTE: Mode control axes with same symbols have identical control laws and gains

* FPME - FLIGHT PATH MANEUVER ENHANCEMENT
PRME - PITCH RATE MANEUVER ENHANCEMENT.

① Identical outside bombing envelope only

Figure 49. AFTI/F-16 Multimode Flight Controller Commands (From Ref. 17)

Those tasks best performed by the machine will be automated. Technological advances in sensors, fire control modes, and weapons fusing will be integrated with the DFCS capabilities.

"An example of advanced technology integration and utilization is in the AMAS precision low altitude maneuvering attack scenario. The technologies involved in this scenario include:

1. Flight path control with full authority digital flight control.

2. Task automation with integrated flight and fire control and low altitude radar autopilot.

3. Advanced sensor-tracker with low drag FLIR and laser ranger installation.

4. Integrated avionics and weapons fusing.

5. Cockpit development including multi-purpose displays, wide field of view heads up display, helmet-mounted sight and voice command.

6. Weapons interface with pilot consent and auto-release.

"These technologies together give the AFTI/F-16 the ability to more effectively attack ground targets. A low altitude radar autopilot allows survivable ingress and egress. AMAS automated air-to-surface bombing modes provide the capability for flexible target acquisition, precise tracking, automated ingress/attack steering, and automated weapon release for both low altitude, or stand-off delivery direct, or high-g turning attacks."

Because of the AFTI program's emphasis on how a pilot uses the numerous flight control modes, task and pilot control strategy measurement offers a useful kind of documentation. There is the potential for detecting subtle differences in control strategy from one mode to another which could signal display deficiencies, natural pilot-to-pilot or run-to-run

variations, relative success in task execution dynamics, and relative distribution of pilot workload among task components.

In order to succeed in pilot identification, however, the foregoing analysis cases point up the requirement for high quality flight data. This lesson should therefore play a key role in evaluating AFTI/F-16 needs.

Properly manipulated, NIPIP can be used for any of the basic tasks and maneuvers connected with the AFTI flight testing. The task and maneuver descriptions contained in Appendix A of Ref. 17 serve as a starting point for establishing command loops and primary flight controls.

An example is shown below for the "air-to-surface tracking, bomb" maneuver defined in Appendix A of Ref. 17.

Air-to-Surface Tracking, Bomb

1. Set-up inbound to the target at 3500 ft above ground level.
2. Upon reaching the point where the target is 10 deg below the horizon, pushover and track the target with the flight path marker.
3. Use only the controllers specified in the run table.
4. Recover from the dive at a safe altitude.

The corresponding configuration and flight condition run table is presented in Table 5. For Run SC-564, the decoupled bombing mode would be selected and stick and pedal controls used (direct lift control via throttle would not be available). Thus:

S_P (stick, pitch axis) for flight path maneuver enhancement

S_R (stick, roll axis) for roll rate

P (rudder pedals) for flat turn

TABLE 5

CONFIGURATIONS AND FLIGHT CONDITIONS

RUN NO.	AS/ MACH	ALT.	CONFIG.	EXT. LOAD	DFCS MODE	PRIORITY	MANEUVER
SC-560	400 kcas	3.5K	CR	A/S	SASB	1	Air-to-surface bomb tracking, stick only
SC-561					SASB		Air-to-surface bomb tracking, stick and pedals
SC-562					DASB		Air-to-surface bomb tracking, stick only
SC-563					DASB		Air-to-surface bomb tracking, stick and throttle
SC-564	400 kcas				DASB		Air-to-surface bomb tracking, stick and pedals
SC-565	500 kcas				SASB		Air-to-surface bomb tracking, stick only
SC-566					SASB		Air-to-surface bomb tracking, stick and pedals
SC-567					DASB		Air-to-surface bomb tracking, stick only
SC-568					DASB		Air-to-surface bomb tracking, stick and throttle
SC-569	500 kcas	3.5K	CR	A/S	DASB	1	Air-to-surface bomb tracking, sitck and pedals

Task segments implied are:

1. Inbound to target, level at 3500 ft above ground level
2. Pushover and track target with flight path marker (HUD symbol)
3. Recover from dive.

For each segment, the implied command loop/control combination is:

1. Inbound, level flight

$$h \rightarrow \theta_c \quad ; \quad \theta \rightarrow S_p \quad (h \triangleq \text{height})$$

$$y \rightarrow \psi_c \quad ; \quad \psi \rightarrow S_R \quad (y \triangleq \text{lateral path displacement})$$

2. Pushover, track target

$$\varepsilon_v \rightarrow S_p$$

$$\varepsilon_L \rightarrow P$$

3. Recovery

$$\theta \rightarrow S_p$$

$$\phi_c \rightarrow S_R$$

NIPIP would therefore require definition of a finite difference equation for each task or control strategy structure implied by the above combinations.

For example, for $h \rightarrow S_p$ the closed-loop task dynamics might reasonably be given by a second-order characteristic equation:

$$\ddot{h} + 2\zeta\omega\dot{h} + \omega^2 h = 0 \qquad (35)$$

Hence the finite difference equation would be:

$$\ddot{\hat{h}}(n) = -2\zeta\omega\dot{\hat{h}}(n) - \omega^2 h(n) + \text{bias} \qquad (36)$$

where $\ddot{\hat{h}}(n)$ and $\dot{\hat{h}}(n)$ can be estimated from a_z and h as described in Appendix A.

Solving for $2\zeta\omega$, ω^2, and the bias provides an estimate of closed-loop activity in holding altitude.

$\omega \rightarrow$ aggressiveness in altitude regulation

$\zeta \rightarrow$ damping, freedom from PIO

Carrying this example further, pilot control strategy in the same altitude loop could be measured by considering the correlation between the control S_p and the inner- and outer-loop states θ and h. The same differential equation form demonstrated in the previous examples (Cases 2 and 5) would be appropriate.

Note that only one of the bombing segments has an inner- and outer-loop combination. The tracking and recovery segments probably involve only inner loops. Nevertheless there are features worthy of study. For example, what does the pilot do with the lateral stick during the tracking segment? Is there stick and pedal coordination? Is such coordination subliminal or does the pilot consciously apply it?

Suggested candidates for NIPIP difference equations for the target tracking and recovery segments are:

Target Tracking, Vertical Axis:

$$S_p(n) = k_1 S_p(n-1) + k_2\varepsilon_v(n) + k_3\varepsilon_v(n-1) + k_4$$

Target Tracking, Lateral Axis:

$$P(n) = k_1P(n-1) + k_2\varepsilon_L(n) + k_3\varepsilon_L(n-1) + k_4$$

and, assuming some coordination with lateral stick,

$$S_R(n) = k_5S_R(n-1) + k_6P(n) + k_7$$

Recovery, Vertical Axis:

$$S_p(n) = k_1S_p(n-1) + k_2\theta(n) + k_3\theta(n-1) + k_4$$

Recovery, Lateral Axis:

$$S_R(n) = k_1S_R(n-1) + k_2\phi(n) + k_3\phi(n-1) + k_4$$

These forms provide for identification of pilot lead and lag (or delay) compensation along with general loop tightness. The difference equation forms can be altered to enhance the definition of any of these specific qualities where desired. For example, additional degrees of freedom involving the second (or more) previous sample(s) in the "controller" terms will better define lag characteristics.

In other instances, if anticipated loop bandwidth permits, the analyst may incorporate only the second (or mth, where m is an integer) previous

sample(s) in the "controller" terms to improve definition of lag characteristics.

Pilot questionnaires and briefing procedures should be designed to aid in the task and control strategy identification process. At the same time limitations in the pilot's ability to analyze control strategy or task execution introspectively should be appreciated.

The main factors to probe in connection with any task are the choice of controls, how tasks are segmented, and what cues are used. These questions may be aided by helping the pilot subject to construct conventional control loop block diagrams. It may also be instructive to the analyst to ask the pilot about special "tricks" in his control strategy such as coordination of two controls, anticipation, or use of unusual kinds of cues. Finally, it is important to determine any factors which might tend to make a given run atypical.

C. AUTOMATIC SELECTION OF PILOT CONTROL STRATEGIES

Provisions for automatic pilot control strategy identification were implemented in the version of NIPIP documented in Ref. 7. These consisted of multiple simultaneous pilot control strategy difference equation solutions along with conventional goodness of fit metrics. This permits online assessment of NIPIP results in either a flight or simulation environment. Comparisons can be made in terms of several parameters depending upon how the analyst chooses to specify the NIPIP difference equation options.

It must be stressed, however, that truly "automatic" pilot control strategy selection is fraught with hazards and unknown consequences at this stage. Control strategy selection must really be accomplished in a manual, interactive mode using engineering judgment and the results of past experience. With this strong caveat, we shall now expand on how the limited "automatic" selection tools might be exploited.

There are essentially two stages of pilot control strategy identification where the above NIPIP features can be effectively used. One is connected with basic control loop structure identification, the other with selection of control compensation identification or data smoothing forms, examples of which were given for the target tracking task in the previous topic. The order of these two steps is not clear--both may be done at once, in fact.

For control loop structure identification, several competing NIPIP difference equations might be chosen using different combinations of primary controls and feedback variables. For example:

"Frontside": $\delta_e = k_\theta\theta + k_{\dot{h}}\dot{h} + k_h h + b;\ \delta_T = k_u u + c$

"Backside": $\delta_e = k_\theta\theta + k_u u + k_{\int}\int u + b;\ \delta_T = k_{\dot{h}\dot{h}}\dot{h} + k_h h + c$

"Backside" with throttle coordination: $\delta_e = k_\theta\theta + k_u u + k_x\delta_T + b;\ \delta_T = k_{\dot{h}}\dot{h} + k_h h + c$

It is thus possible to distinguish the best choice of control structure by observing any of the available goodness-of-fit indicators either mentioned previously or any of those which will be suggested in the computer-graphics discussion.

D. INTERACTIVE COMPUTER GRAPHICS

Because, at this stage, pilot control strategy identification is an iterative process, it is desirable to have the means for quick, effective evaluation of NIPIP results. The version of NIPIP now operational produces a large array of tabulated calculations, but these require a separate processing in order to fully interpret their quality.

The use of an interactive computer graphics scheme directly tied to NIPIP would be helpful indeed. Some experience in this area has been gained in previous programs, and much was learned in the study reported here to serve as a basis for recommendations. The following paragraphs describe these recommendations.

In general, the dynamic response of systems can be presented in many forms, each providing its own special insights. This can include the domains of time, frequency and phase plane, continuous or discrete. None of these alone can be regarded as wholly adequate for the analyst, though. It is advisable to exploit as many separate presentations as possible for the purposes of finding an acceptable solution and for confirming it.

This report presents some of the ways of portraying NIPIP results, but it is a fairly limited sample. The recommendations of this section contain many more possibilities even though not all have been tested for their effectiveness.

Interactive computer graphics, to be effective in the NIPIP role, must be sufficiently flexible to accommodate several kinds of presentations, reasonably high resolution, fast enough to keep up with a running NIPIP solution (which could be on-line, real-time) and able to generate a hard copy if desired by the analyst. Each of these attributes will be discussed, in turn, in the following paragraphs.

First, the NIPIP user is concerned with observing (a) the data being analyzed and (b) the solution in its various alternative forms. The former provides a starting point for assuming a candidate loop structure form, the latter, the adequacy of the solution and insight for refinements. Hence a computer graphics scheme needs direct access to both the input to and the output from NIPIP.

The flexibility required in plotting relates to choice of independent and dependent variables and to scaling. There can be no hard and fast rules. For inner-loop concerns, time scales might be expanded and choice of state variable limited to inner-loop quantities--pitch attitude, roll attitude, yaw, heading, and sometimes vertical velocity or flight path

angle. Outer loops would necessitate another set of plots. While some specific plotting objectives will be given shortly, there should always be the ability to modify them.

The form of computer graphics most useful to the NIPIP user is a hard copy, scaled, two-dimensional plot. It would be convenient, however, to use a CRT display as an intermediate step in obtaining a hard copy.

Several basic plots of input data and NIPIP solutions are presented in Fig. 50. Each is discussed below:

1. Control and State Variable Time History

As a first step in the pilot identification process, it is useful to inspect simple time histories of the command loop state variable and the suspected control for that state. Other states and controls may also be of interest, however. Further it is beneficial to superimpose these time histories in order to gain insight about correlation, phasing, relative frequency content, and task segmentation.

A computer-graphics display of raw data time histories may require positive labeling of individual states. This could be difficult to accomplish via conventional line coding (solid, broken, or alphanumeric symbols). A multicolor display would be feasible, however, for both a hard copy plotter and a CRT. A variety of multicolor plotters are on the market at reasonable cost (e.g., Huston Instruments and Hewlett-Packard). Color monitors are also available and easily driven by low cost microcomputers such as Apple or TRS-80. The main difficulty in using color media lies in the cost of reproduction of large numbers for dissemination of reports. While color xerography is readily available, it is expensive.

Assumed Control Strategy:

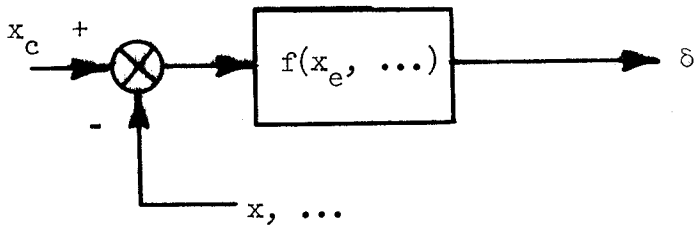

Basic Finite Difference Equation Used in NIPIP:

$$\delta_n = g(\delta_{n-i}, x_{n-i}, \ldots)$$

Graphical Forms Useful to the Analyst:

1. Time history of control, states (i.e., "raw" data), e.g.,

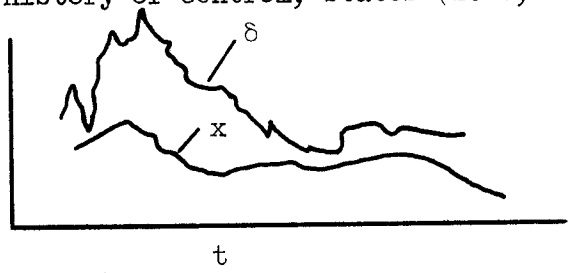

2. Phase plane of control, states (i.e., "raw" data), e.g.,

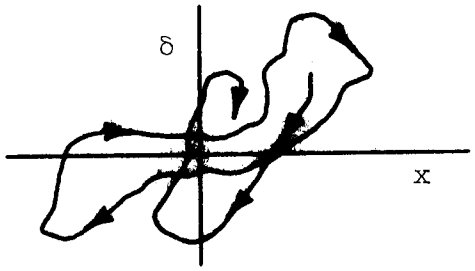

3.

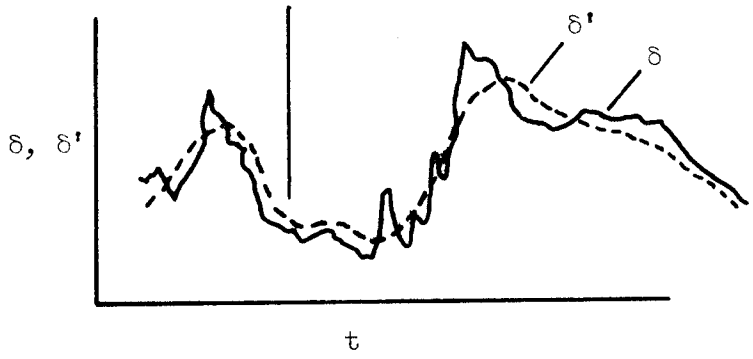

Figure 50. Recommendations for Interactive Graphics with NIPIP

4. Phase Plane Comparison

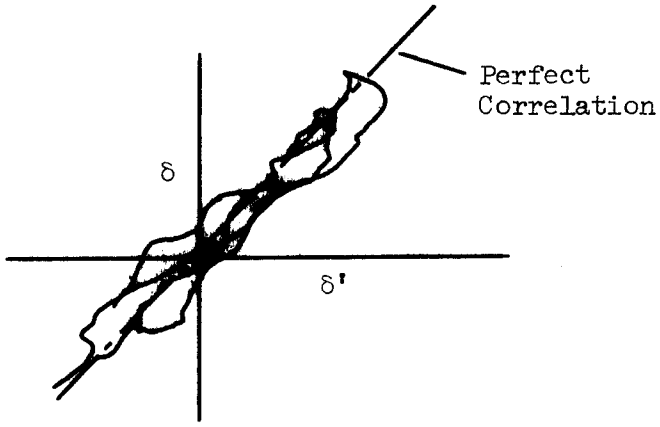

5. Time-Frequency Describing Functions

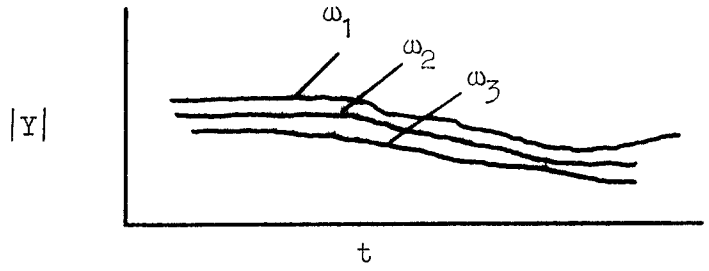

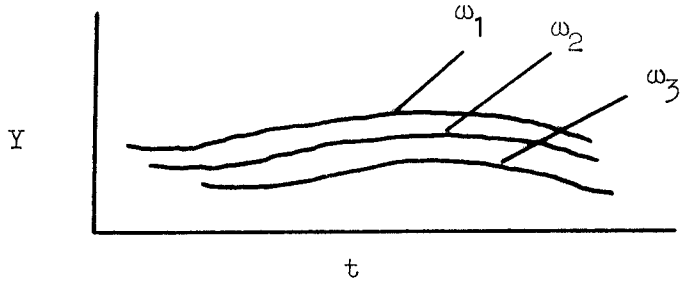

Figure 50 (Concluded)

2. Control and State Variable Phase Plane

The same data plotted as time histories can also be plotted without time as the independent variable. The value of phase planes is that correlation between pairs of variables is easily seen, and non-linearities can be detected and even identified. (Ref. 15 contains a large catalog of phase planes for nonlinear elements.)

3. Time History Comparison of Model Reconstruction with Raw Data

One rather clear way of judging goodness-of-model is to reconstruct a control or state using a set of model coefficients obtained by NIPIP. For example, if NIPIP solved for the coefficients $\hat{a}$ and $\hat{b}$ assuming the difference equation:

$$\delta_n = a\,\theta_n + b \tag{37}$$

then a modeled "$\hat{\delta}$" defined as

$$\hat{\delta}_n = \hat{a}\,\theta_n + \hat{b} \tag{38}$$

can be generated using the raw data for θ. This $\hat{\delta}$, in turn, can be compared directly with the actual δ in order to help to confirm the model.

4. Phase Plane Comparison of
Model Reconstruction with Raw Data

This is a counterpart to the previous graphic form where $\hat{\delta}$ and $\hat{\theta}$ are plotted.

5. Time-Varying Describing Functions

One interesting visualization of NIPIP results is the construction of a time history of the frequency response, i.e., gain and phase as in Section IV of this report. This concept lacks mathematical rigor, but it does help to evaluate the consistency and general character of a NIPIP solution.

APPENDIX A

SINK RATE ESTIMATION

Since the flight test data did not contain any direct measurement of approach slope or sink rate, it is necessary to provide a reasonable estimate of this parameter. Thus, as a first step in the analysis, it is necessary to use the existing flight data to estimate sink rate and to determine the sink rate command profile for the maneuver. A constraint in the choice of methods was that this report was to define the NIPIP analysis procedure, not techniques in state variable estimation.

Complimentary filtering was used in estimating sink rate to take advantage of the data available. The altitude data is appropriate for low-frequency estimation of sink rate while vertical acceleration is appropriate for high frequencies. Complimentary filtering allows the data to be combined in a way that takes advantage of these relative strengths. The complimentary filter in continuous form is:

$$\hat{\dot{h}} = \frac{as}{s + a} h + \frac{1}{s + a} \hat{\ddot{h}} \qquad (37)$$

where

s is the Laplace operator

h is the measured altitude

$\hat{\ddot{h}}$ is vertical acceleration estimated from measured normal acceleration

$\hat{\dot{h}}$ is the estimated sink rate

and a is the characteristic frequency of the filter

The complimentary filter was implemented in finite difference equation form as:

$$\hat{\dot{h}}_n = e^{-aT}\,\hat{\dot{h}}_{n-1} + ah_n - ah_{n-1} + \left(\frac{1 - e^{-aT}}{a}\right)\hat{\ddot{h}}_n \qquad (38)$$

The characteristic frequency, a, was determined empirically to accommodate the sample period as well as the quantization in the measured altitude and the noise in the vertical acceleration. A value of 0.1 was chosen for use. Larger values produced a sink rate estimate which showed the quantization of the measured altitude.

The vertical acceleration used in the complimentary filter was estimated from the flight data using two separate approaches. The first approach used all of the measured aircraft states, both lateral and longitudinal, to reconstruct the vertical acceleration. Assuming the normal acceleration to be measured at the center of gravity, one can estimate the vertical acceleration by

$$\hat{\ddot{h}} = -\left(-a_n + g\cos\theta\cos\phi - PV + QU\right)\cos\theta\cos\phi \qquad (39)$$

where a_n is the measured normal acceleration. The second approach used a simplified method which corrected measured normal acceleration only for pitch attitude effects to obtain vertical acceleration. Vertical acceleration in this case is given by

$$\hat{\ddot{h}} = \left[\left(a_n - g\cos\theta_o\right) + g\sin\theta_o\theta + QU\right]\cos\theta_o \qquad (40)$$

where $\cos\theta_o$ was taken as unity.

This latter estimation approach is appropriate when large lateral maneuvers are not present. However, as there are large lateral maneuvers in the flight data (as seen in the flight data time histories) the first method was also relied upon to estimate the vertical acceleration.

The final aircraft state to be estimated is $\dddot{h}$. This state was estimated by using pitch rate and vertical acceleration by:

$$\hat{\dddot{h}} = \frac{QU}{T_{\theta_2}} - \frac{\hat{\ddot{h}}}{T_{\theta_2}} \tag{41}$$

where T_{θ_2} was determined to be equal to 1 sec.

At this point something should also be said about the quality of the data which is to be used in the estimation technique. It goes without saying that the better the data the better the chance of success and the more reliable the outcome should be. However, there is a point at which the identification technique cannot be relied upon to provide an accurate estimate due to poor quality input data. This aspect of the quality of the input data will be addressed in the numerical results in both Section IV and Appendix B of the text.

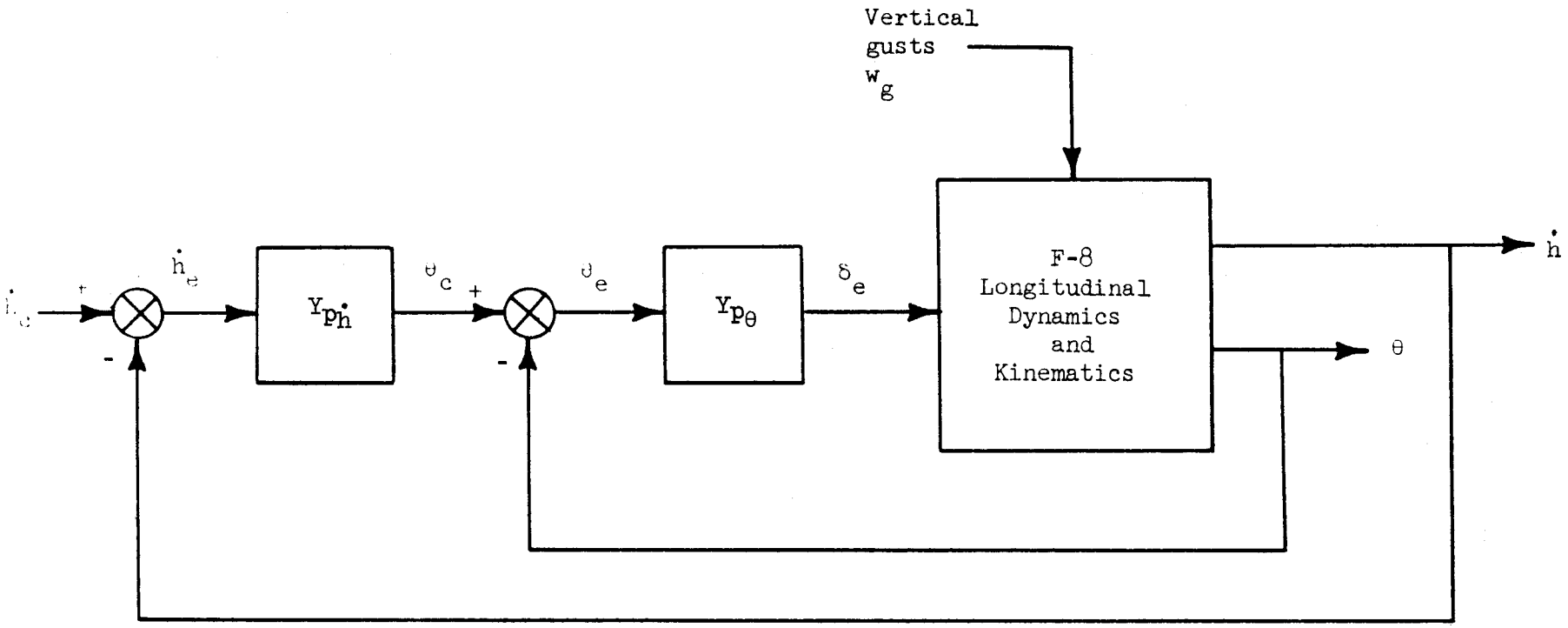

Notes: 1. Bandwidth of θ-loop is 3.0 rad/sec with $Y_{p_\theta} = 1.675$ rad/rad

2. Bandwidth of $\dot{h}$-loop is 0.2 rad/sec with $Y_{p_{\dot{h}}} = \frac{0.0005 \text{ rad/ft}}{\text{s}}$

3. $\dot{h}_c = \begin{cases} 0.0 \text{ for } 0 < t < 15 \text{ sec} \\ -87.5 \text{ fps for } t \geq 15 \text{ sec} \end{cases}$

Figure 51. Multiloop Control Task Example

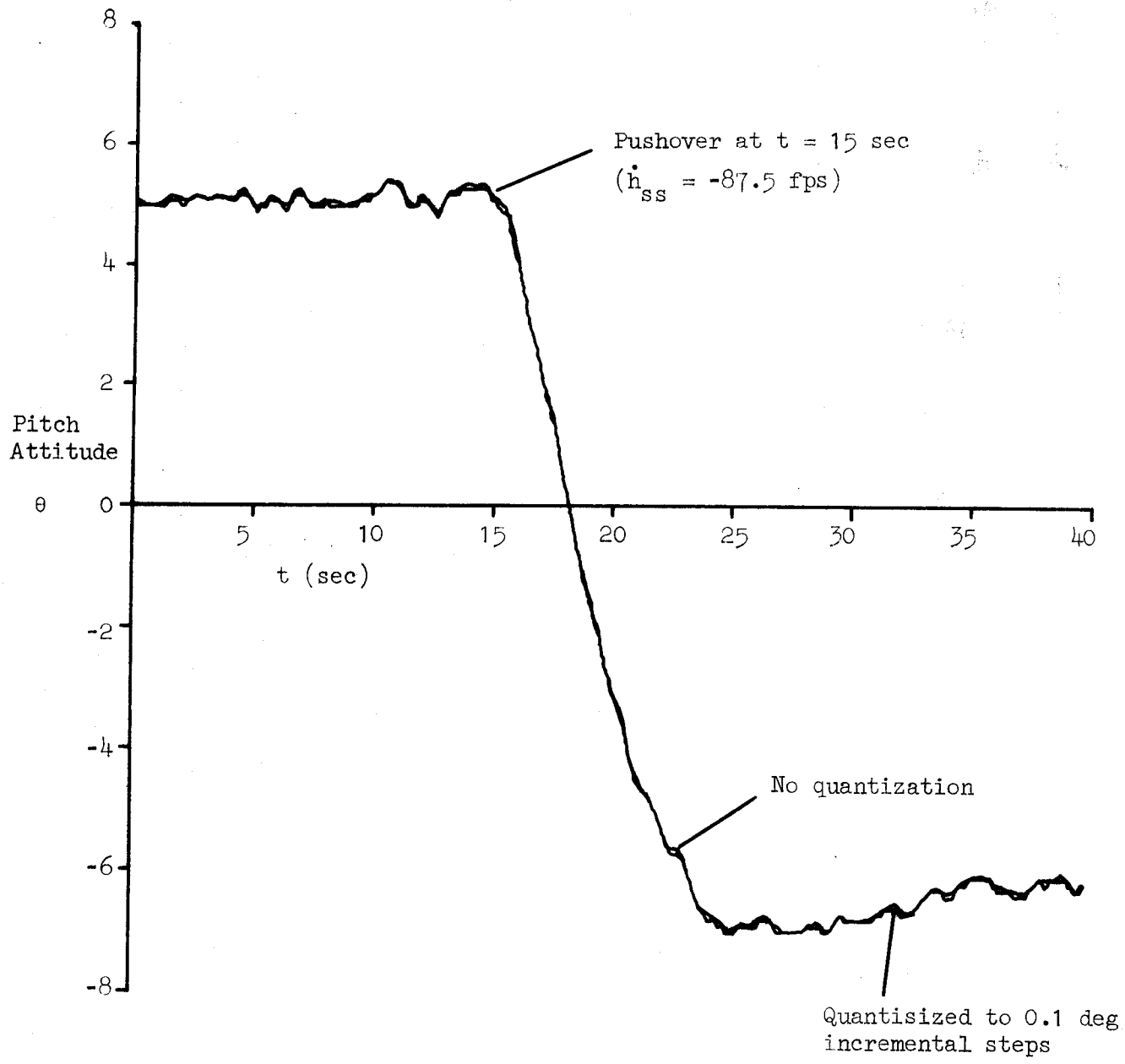

Figure 52. Pushover Time History of Pitch Attitude

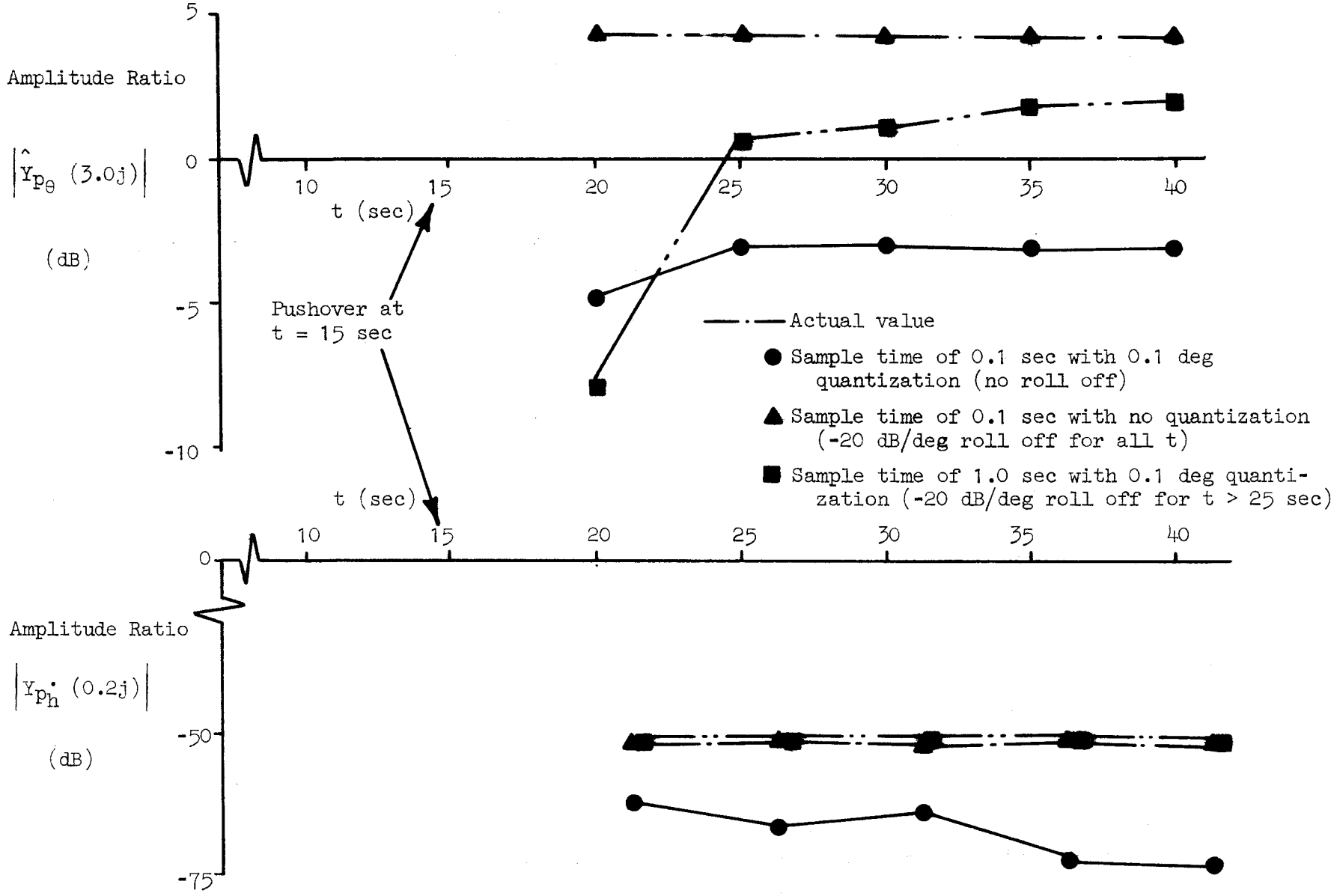

Figure 53. Effects of Quantization and Sampling Interval on the Inner-Loop Control Strategy Identification

period traces where quantization is present, merely starting the window after the push-over does not improve the ability to identify the control-loop elements. However starting after the push-over and increasing the sample period to 1 sec improves the identified solution. The outer-loop identified solution, $\hat{Y}_{p_h}$, with a 1 sec sample period and a 0.1 deg quantization in pitch attitude essentially matches the actual solution identified with a 0.1 sec sample period and no quantization. The inner-loop identified solution, $\hat{Y}_{p_\theta}$, for a sample period of 1 sec with 0.1 deg quantization does not match the actual inner-loop solution with a sample period of 0.1 sec and no quantization, because the Nyquist frequency is approximately equal to the crossover frequency of the inner loop.

Increasing the sampling period from 0.1 to 1 sec does improve the identified solution for Y_{p_h} as seen by comparing the 0.1 sec and 1 sec sampling period traces with 0.1 quantization in pitch attitude. It should be noted that usually the Nyquist frequency must be greater than the crossover frequency to obtain accurate estimates; however, in this case the effects of quantization degrade the ability of the procedure to identify the inner-loop control strategy. Thus using still longer sampling periods does not improve the ability to identify the inner-loop but does at the same time improve the ability to identify the outer-loop control strategy. Shorter sampling periods as shown by the 0.1 sec sample period degrade the ability to identify both the inner and outer control-loop elements in the presence of the specified quantization. Hence it is not possible to identify accurately the inner control-loop strategy in the presence of this particular level of quantization.

The preceeding results show the effects of quantization in an inner control-loop variable on both inner- and outer-loop strategy identification. The effects of pitch attitude quantization were shown to degrade the ability to identify the control-loop elements. However it was also shown that when the quantization is present only in the inner-loop, it was still possible to identify the outer-loop control strategy by adopting a longer sampling interval. The results of this investigation support the initial conclusion that quantization of pitch attitude does, in fact, degrade the ability of the NIPIP to correctly identify the inner-loop control strategy.

REFERENCES

1. McRuer, D. T., and E. S. Krendel, Mathematical Models of Human Pilot Behavior, AGARD-AG-188, January 1974.

2. Heffley, Robert K., Warren F. Clement, Robert F. Ringland, Wayne F. Jewell, Henry R. Jex, Duane T. McRuer, and Vernon E. Carter, Determination of Motion and Visual System Requirements for Flight Training Simulators, ARI TR 546, August 1982.

3. Truxal, John G., Automatic Feedback Control System Synthesis, McGraw-Hill Book Company, Inc., New York, 1955.

4. Graham, Dunstan, and Duane McRuer, Analysis of Nonlinear Control Systems, Dover Publications, Inc., New York, 1971.

5. Heffley, Robert K., and Ted M. Schulman, Derivation of Human Pilot Control Laws Based on Literal Interpretation of Pilot Training Literature, Systems Technology, Inc., Paper No. 295, Presented at the AIAA Guidance and Control Conference, Albuquerque, NM, August 19-21, 1981.

6. Heffley, Robert K., Ted M. Schulman, Robert J. Randle, Jr., and Warren F. Clement, An Analysis of Airline Landing Flare Data Based on Flight and Training Simulator Measurements, Systems Technology, Inc., Technical Report No. 1172-1R, July 1981, Revised August 1982.

7. Hanson, Gregory D., and Wayne F. Jewell, Non-Intrusive Parameter Identification Procedure User's Guide, NASA CR-170398, April 1983.

8. McRuer, Duane, Henry R. Jex, Warren F. Clement, and Dunstan Graham, A Systems Analysis Theory for Displays in Manual Control, Systems Technology, Inc., Technical Report No. 163-1, October 1967, Revised June 1968.

9. Anon., Instrument Flying, Air Force Manual AFM 51-37, 15 August 1979.

10. Jewell, Wayne F., and Ted M. Schulman, A Pilot Control Strategy Identification Technique for Use in Multiloop Control Tasks, Systems Technology, Inc., Technical Report No. 1153-2, August 1980.

11. Heffley, Robert K., and Wayne F. Jewell, Development of a CTOL Piloting Technique Measurement Scheme for a Real-Time Simulator Environment, NASA CR-152294, July 1979.

12. Heffley, Robert K., A Pilot-in-the-Loop Analysis of Several Kinds of Helicopter Acceleration/Deceleration Maneuvers, Systems Technology, Inc., Paper No. 318, Presented at the AHS/NASA Specialists' Meeting on Helicopter Handling Qualities, Palo Alto, California, April 1982.

13. Heffley, Robert K., Pilot Models for Discrete Maneuvers, AIAA Paper No. 82-1519CP, Presented to the AIAA Guidance and Control Conference, San Diego, California, August 9-11, 1982.

14. Berry, D. T., B. G. Powers, K. J. Szalai, and R. J. Wilson, A Summary of an In-Flight Evaluation of Control System Pure Time Delay During Landing Using the F-8 DFBW Airplane, AIAA Paper No. 80-1626, Atmospheric Flight Mechanics Meeting, Danvers, Massachusetts, August 11-13, 1980.

15. McRuer, Duane, Irving Ashkenas, and Dunstan Graham, Aircraft Dynamics and Automatic Control, Princeton University Press, Princeton, New Jersey, 1973.

16. Heffley, Robert K., and Ted M. Schulman, Mathematical Model Descriptions for a Medium Jet Transport and a Light Twin, Systems Technology, Inc., Working Paper No. 1164-2R, June 1981.

17. Crombie, Robert B., and Michael L. Frazier, The AFTI/F-16 Flight Test Program and Opportunities to Evaluate Pilot-Vehicle Interface and Mission Effectiveness, AFFTC-TR-82-5, May 1982, pp. 700-756.

18. Gill, Robert A., and Charles L. St. Sauver (Captain USAF), Advanced Fighter Technology Integration — AFTI/F-16 Test Program Overview, AIAA Paper No. 81-2352, First Flight Testing Conference, Las Vegas, Nevada, November 11-13, 1981.

1. Report No. NASA CR-170399	2. Government Accession No.	3. Recipient's Catalog No.
4. Title and Subtitle ANALYSIS OF PILOT CONTROL STRATEGY		5. Report Date April 1983 6. Performing Organization Code
7. Author(s) Robert K. Heffley, Gregory D. Hanson, Wayne F. Jewell, and Warren F. Clement		8. Performing Organization Report No. TR-1188-2 10. Work Unit No.
9. Performing Organization Name and Address Systems Technology, Inc. 2672 Bayshore Frontage Road Mountain View, California 94043		11. Contract or Grant No. NAS4-2941
12. Sponsoring Agency Name and Address National Aeronautics and Space Administration Washington, D.C. 20546		13. Type of Report and Period Covered Contractor Report — Final Feb. 1982 - Sept. 1982 14. Sponsoring Agency Code RTOP 505-31-21

15. Supplementary Notes

NASA Technical Monitor: Mary F. Shafer, Ames Research Center, Dryden Flight Research Facility, Edwards, CA 93523. Companion volume is NASA CR-170398.

16. Abstract

Methods for non-intrusive identification of pilot control strategy and task execution dynamics are presented along with examples based on flight data. The specific analysis technique is Non-Intrusive Parameter Identification Procedure (NIPIP), which is described in a companion user's guide(NASA CR-170398). Quantification of pilot control strategy and task execution dynamics is discussed in general terms followed by a more detailed description of how NIPIP can be applied. The examples are based on flight data obtained from the NASA F-8 digital fly-by-wire airplane. These examples involve various piloting tasks and control axes as well as a demonstration of how the dynamics of the aircraft itself can be identified using NIPIP. Application of NIPIP to the AFTI/F-16 flight test program is discussed. Recommendations are made for flight test applications in general and refinement of NIPIP to include interactive computer graphics.

17. Key Words (Suggested by Author(s))	18. Distribution Statement
Parameter estimation, Least-squares estimation, System identification, Pilot modeling, Modeling techniques, System analysis, Flight test techniques	Unclassified-Unlimited STAR category 08

19. Security Classif. (of this report)	20. Security Classif. (of this page)	21. No. of Pages	22. Price*
Unclassified	Unclassified	125	A06

*For sale by the National Technical Information Service, Springfield, Virginia 22161.